

UCSF

UC San Francisco Electronic Theses and Dissertations

Title

Mechanisms of tumor invasion in the RIP-Tag mouse model of pancreatic neuroendocrine cancer

Permalink

<https://escholarship.org/uc/item/6bj5h4b5>

Author

Chun, Matthew G.H.

Publication Date

2010

Supplemental Material

<https://escholarship.org/uc/item/6bj5h4b5#supplemental>

Peer reviewed|Thesis/dissertation

Mechanisms of Tumor Invasion in the RIP-Tag Mouse Model of
Pancreatic Neuroendocrine Cancer

by

Matthew G.H. Chun

DISSERTATION

Submitted in partial satisfaction of the requirements for the degree of

DOCTOR OF PHILOSOPHY

in

Cell Biology

in the

GRADUATE DIVISION

of the

UNIVERSITY OF CALIFORNIA, SAN FRANCISCO

Copyright (2010)

by

Matthew G.H. Chun

Acknowledgments

As I write this final section of my dissertation, it is difficult to believe that I am finally at the end of graduate school and about to obtain my Ph.D. Without a doubt, grad school has been the most challenging experience I have ever undertaken, and despite the occasional difficulties, it has certainly been the most rewarding experience of my life.

I have learned and accomplished many things during my time at UCSF, some scientific but many that are not related to lab at all. Most obviously, I have learned how to think like a scientist. I now know how to ask an interesting and testable question and can figure out a way to answer that question. More importantly though, I have learned how to keep myself motivated and to persevere, even when things are not going as well as I hoped, and I have also learned how to manage my time effectively, even if I sometimes choose to ignore my well thought out plans. Lastly, I have learned that no matter how talented or smart you are, you cannot know everything. So rather than trying to go it alone, you should ask the people around you who might know better because there are many bright individuals who are willing to help and to give guidance and support if you just ask. In that vein, I would like to thank the many individuals who contributed to my success during grad school and who helped me obtain my Ph.D.

First and foremost, I would like to thank Douglas Hanahan, my thesis advisor. Without a doubt, Doug is a first-class scientist, and I have learned a great deal about how to be a scientist from working with him. His impact on this work should be evident, and I am particularly grateful for his willingness to allow me to develop my own projects and supporting my efforts to pursue my research as I best saw fit.

One of Doug's greatest talents has been his ability to attract top-notch scientists to his lab, and I have been fortunate to have worked with many of them during my Ph.D. I want to thank Chris Chiu, Peter Olson, Oriol Casanovas, Danielle Ulanet, Olivier Nolan-Stevaux, Anny Shai, Liz Allen, Kristian Pietras, Jeff Hager, Johanna Joyce, Enrico Giraudo, Enrique Casado, Sukh Sidhu, Chaity Chaudhury, Morgan Truitt, Neta Erez, Jessica Pahler, and Hiro Nozawa for their support and guidance. I have appreciated all of our conversations and discussions, scientific and otherwise, and I will always value the friendships I have made with this group of talented individuals.

In particular, I would like to thank three of these scientists, who were instrumental in helping me get my Ph.D. Oriol is the unfortunate post-doc who had to mentor me during my rotation in the Hanahan lab. He is incredibly patient and generous, and there was no question I could not ask him or problem that I could not discuss with him. Oriol is a gifted scientist, and he was a major reason that I chose to join the Hanahan lab. I am thankful for our continued friendship, and I look forward to the next time I can visit him in his homeland of Catalonia!

Perhaps the best way to describe my relationship with Chris is to say that he is like the older brother I never had while I am like the younger brother he never wanted. Chris is a talented and rigorous scientist, who was always willing to discuss my experiments with me, teach me a new technique, and help me improve as a scientist. More than the scientific advice, I am grateful for Chris's friendship. I will always remember our conversations about all things geek-related during the times he drove me to play poker, and I will truly miss having him as a lab mate.

Like Oriol and Chris, Peter is as good a scientist as there is. Our conversations about science were some of the most profound and stimulating conversations I had at UCSF and helped make my science substantially better. Peter is also the most optimistic and enthusiastic person I have met in science, and he helped keep me going when things were not going well with my Ph.D. Whether it was talking about sports, taking in an A's game, or going camping, Peter always reminded me that life outside of lab was as important as life in the lab. As with Oriol and Chris, I must admit that I have gained more from my relationship with Peter than he has from me.

Additionally, I want to thank Ehud Drori, Susan Cacacho, Marina Vayner, Ryan Huss, Celeste Rivera, Cherry Concengco, Annie Wang, Katie Gililland, Cristina Guinto, Jhoanna Berrocal, and Memo Peña. Though their names do not always appear on the final publications, they played an important role in making the science possible, and I am grateful for their friendship as well.

I was incredibly fortunate to have had Matthias Hebrok and Martin McMahon as members of my thesis committee and my qualifying committee. Matthias and Martin are incredible scientists who helped refine and improve my science, and I always felt better after my meetings with them. I appreciate Matthias's pragmatic approach to science, and his sense of humor always helped to put things in perspective. Martin was one of the first people I met at UCSF, and I was fortunate to have done a rotation in his lab. To this day, I am in awe of Martin's ability to identify and ask the most important questions in any scientific discussion. Both Martin and Matthias helped shepherd me through my Ph.D. from the beginning to the end, and I am grateful for their encouragement, their support, and their advice.

UCSF was a wonderful place to do a Ph.D., and I have benefited from the many talented faculty and staff that are a part of this community. Allan Balmain and Jian-Hua Mao taught me how to do real mouse genetics and were fantastic collaborators. Mark Anderson and Henry Bourne served on my qualifying committee and always had a positive word for me whenever I saw them in the halls or at seminars. I am grateful to Francis Lynn, Bruce Adams, Juehue Wang, and other members of the German lab for their scientific advice and for sharing reagents. I also want to recognize the Diabetes Center staff, including Karyl Nakamura, Lily Yu, Fred Fermin, and Fran DeNoto, who helped ensure that I was able to do my science and made my time in the Diabetes Center a pleasant one. Sue Adams and Danny Dam kept the Tetrad Program running smoothly and helped me with the many extraneous things that came up during graduate school.

I have been fortunate to have had many colleagues and friends who supported me during my Ph.D., and I would not have succeeded without their support. Yamini Ohol and I first met each other during grad school interviews, and we encouraged each other throughout our time at UCSF. Janet Lau of the Hebrok lab is an incredibly generous person, and I always enjoyed our discussions about our bosses and life outside of science. John Morris, another member of the Hebrok lab, was always a good person with whom to discuss science or baseball.

I would also like to thank my roommates in San Francisco – Brian Goldstein, Nikhil Kacker, Peter Li, and Ben Myers – for being good friends. In particular, Peter, Ben, and I went through the UCSF Ph.D. program at the same time, and it was always nice to have someone to commiserate with.

My old college roommates, Preston Golson, Adam Klein, and Tom Price, encouraged me from afar, and I enjoyed their visits because I got to explore San Francisco with them. I am grateful to my poker buddies, Garrett and Anne Larsson, Dave Gustafson and Jessica Whitten, and Ernie Tedeschi. Seeing them at our poker sessions kept me sane, and I am grateful for their friendship.

I am particularly grateful to my oldest and closest friends, Jim Whitesell and Andrew Love. They helped me to have a life outside of lab, and I always enjoyed the rare times when we could form our three-man wrecking crew. I was incredibly honored to stand beside them at their weddings, and I also want to thank their better halves, Veronica Osetinsky in the case of Jim and Renee Alleman in the case of Andrew, for their friendship as well.

My older sister, Sara, was one of my first teachers (and tormentors), and her sisterly love helped toughen me up and prepare me for the rigors of grad school. We went through graduate school at the same time and could commiserate about the insanity, frustrations, and occasional joys of grad school. I am sure that we fulfilled our parents' wish to produce two doctors who cannot help anyone. Regardless, I am grateful for her friendship and support. To Jerry Hsu, he is a talented scientist, and I have enjoyed our conversations about science and life in general. If nothing else, I would like to thank him for willingly offering himself up as a new target of my sister's harassment. Darwin The Wonder Monkey also deserves special thanks.

Most importantly, I want to thank my mom and dad. My parents, Ann and Robert Chun, have literally been there from the start, and without a doubt, they have been my biggest supporters in everything I have done. They were my first and most important

teachers, and I am indebted to them for their support, their encouragement, and their love. Though they may not know it, they are a major reason why I chose to become a cancer biologist, and I dedicate this work to them. Words cannot adequately describe how much they mean to me so I will just say thank you.

Lastly, I would like to acknowledge the various funding sources that have supported my graduate studies. The National Cancer Institute, the UCSF Department of Biochemistry and Biophysics, the UCSF Helen Diller Family Comprehensive Cancer Center, and the UCSF Diabetes Center provided institutional support. Additionally, I was personally supported by the UCSF Herbert W. Boyer Program in Biological Sciences and by a graduate research fellowship from the National Science Foundation.

Contributions

All data, analyses, interpretations, and conclusions presented in this dissertation are solely the work of Matthew G.H. Chun except as noted below.

Douglas Hanahan (University of California, San Francisco, San Francisco, CA USA) served as the doctoral advisor. He supervised the research and edited the dissertation.

Allan Balmain (University of California, San Francisco, San Francisco, CA USA) assisted in the analysis and interpretation of the results presented in Chapter 3, specifically as they pertain to the linkage analysis and mapping experiments presented in Figures 3.1, 3.7, 3.8, 3.9, and 3.10 and Dataset 3.2. Additionally, he edited sections of Chapter 3.

Jian-Hua Mao (University of California, San Francisco, San Francisco, CA USA) assisted in the analysis and interpretation of the results presented in Chapter 3, specifically as they pertain to the linkage analysis and mapping experiments presented in Figures 3.1, 3.7, 3.8, 3.9, and 3.10 and Dataset 3.2. Additionally, he helped prepare Figures 3.9 and 3.10 and Dataset 3.2 and edited sections of Chapter 3.

Christopher W. Chiu (University of California, San Francisco, San Francisco, CA USA) assisted in the execution of the experiments and the analysis and interpretation of the results presented in Chapter 3, specifically as they pertain to the bone marrow transfer experiments and analysis presented in Figures 3.4 and 3.6. Additionally, he helped prepare Figure 3.6.

At the time of submission of this dissertation, portions of this dissertation had been submitted but not yet accepted for publication. Portions of Chapter 2 were submitted as follows:

“Genetic deletion of the desmosomal component desmoplakin promotes tumor microinvasion in a mouse model of pancreatic neuroendocrine carcinogenesis”

Matthew G. H. Chun and Douglas Hanahan

Portions of Chapter 3 were submitted as follows:

“Polymorphic genetic control of tumor invasion in a mouse model of pancreatic neuroendocrine carcinogenesis”

Matthew G.H. Chun, Jian-Hua Mao, Christopher W. Chiu, Allan Balmain,
and Douglas Hanahan

Mechanisms of tumor invasion in the RIP-Tag mouse model of pancreatic neuroendocrine cancer

by Matthew G.H. Chun

Abstract

My thesis sought to advance our understanding of the genetic, molecular, and cellular factors governing the acquisition of an invasive growth phenotype during tumor development and progression using a genetically engineered mouse model of pancreatic neuroendocrine tumorigenesis (PNET) known as RIP-Tag. In one line of investigation, I compared the genome wide transcriptional profiles of non-invasive and highly invasive PNETs in RIP-Tag mice, which revealed that the expression of multiple genes encoding components of desmosomes, a cell-cell adhesion complex, is downregulated in invasive PNETs. Genetic deletion in RIP-Tag mice of one of these genes, desmoplakin, results in increased local tumor invasion, demonstrating that desmosomes can act as a distinct suppressor of tumor invasion. In a second line of investigation, I show that tumor invasion in the RIP-Tag model can be modified by genetic background. Using genetic mapping analysis, I identify a polymorphic locus on mouse chromosome 17 that is significantly associated with the development of invasive PNETs in RIP-Tag mice. I show that one gene residing in this locus, the anaplastic lymphoma kinase (Alk), is expressed at significantly higher levels in mice inbred into the C57Bl/6 genetic background versus the C3HeB/Fe genetic background and that higher levels of Alk expression are correlated with the development of invasive PNETs in RIP-Tag mice.

Additionally, I demonstrate that pharmacological inhibition of Alk results in reduced tumor invasiveness in RIP-Tag mice. Collectively, my thesis research adds two new functional components to the growing list of factors that affect the hallmark capability of tumor invasion, one component of a malignant tumor phenotype. My thesis work demonstrates that tumor invasion is regulated at both the molecular and genetic levels and establishes desmosomal adhesion and signaling from the anaplastic lymphoma kinase as modulators of invasive tumor growth.

Table of Contents

Chapter 1	Introduction	1
Chapter 2	Genetic deletion of the desmosomal component desmoplakin promotes tumor microinvasion in a mouse model of pancreatic neuroendocrine carcinogenesis	14
	Abstract	15
	Introduction	16
	Results	18
	Discussion	25
	Materials and methods	31
	Acknowledgments	37
Chapter 3	Polymorphic genetic control of tumor invasion in a mouse model of pancreatic neuroendocrine carcinogenesis	80
	Abstract	81
	Introduction	82
	Results	84
	Discussion	91
	Materials and methods	96
	Acknowledgments	102

Chapter 4	Conclusions and future directions	131
References	142
Appendix	Legends for datasets	160

List of Tables

Chapter 2

Table 2.1	38
Table 2.2	39
Table 2.3	40
Table 2.4	41
Table 2.5	43

List of Figures

Chapter 1

Figure 1.1	10
Figure 1.2	12

Chapter 2

Figure 2.1	44
Figure 2.2	46
Figure 2.3	48
Figure 2.4	50
Figure 2.5	52
Figure 2.6	54
Figure 2.7	56
Figure 2.8	58
Figure 2.9	60
Figure 2.10	62
Figure 2.11	64
Figure 2.12	66
Figure 2.13	68
Figure 2.14	70
Figure 2.15	72
Figure 2.16	74

Figure 2.17	76
Figure 2.18	78

Chapter 3

Figure 3.1	103
Figure 3.2	105
Figure 3.3	107
Figure 3.4	109
Figure 3.5	111
Figure 3.6	113
Figure 3.7	115
Figure 3.8	117
Figure 3.9	119
Figure 3.10	121
Figure 3.11	123
Figure 3.12	125
Figure 3.13	127
Figure 3.14	129

Chapter 1.

Introduction

Cancer as a disease

Cancer is a complex disease characterized by the unrestrained proliferation and expansion of abnormal cells. According to the most recent statistics published by the American Cancer Society, nearly 1,500,000 individuals living in the United States were diagnosed with cancer during 2009 while an additional 500,000 persons died from cancer during that same time period (<http://www.cancer.org/>). Additionally, the National Cancer Institute estimates that greater than 11,000,000 Americans currently have cancer or have a history of cancer (<http://www.cancer.org/>), and cancer remains the second leading cause of death in the United States, behind only heart disease. These statistics underscore the continued severity of cancer as a lethal disease and a major health problem in the United States.

Cancer as a science

Due to the significant health consequences resulting from cancer, a considerable effort has been made into understanding and characterizing the basis of cancer in the hopes of developing better therapies for individuals afflicted with this disease. In particular, the field of cancer biology has experienced significant advancements in the past few decades, aided in particular by advances in the fields of genetics and genomics. This work has sought to identify and characterize in a systematic fashion the multitude of genetic, molecular, cellular, and environmental factors that contribute to the initiation and progression of cancer, such that cancer becomes less of a complex and inscrutable disease and more of a manageable, if not predictable, biological process whose outcome can be directed and controlled (Hanahan and Weinberg 2000).

Mice as platforms for cancer research

During the past several decades, the use of animal models has greatly advanced the field of cancer biology. In particular, genetically engineered mouse models (GEMM) of cancer have proven quite powerful in modeling many aspects of tumorigenesis (Tuveson and Jacks 2002; Frese and Tuveson 2007). Indeed, these models have allowed cancer biologists to identify and characterize the underlying genetic and molecular mechanisms that cause and promote cancer at an unprecedented level.

In particular, the ability to model cancer *in vivo* represents the true power of GEMMs. These models give scientists the ability to replicate the *de novo* initiation and development of cancers in the appropriate organ locations and in the context of an intact and completely functioning host system. Furthermore, the recent sequencing and annotation of the mouse genome coupled with advances in mouse genetics allow scientists to study the consequences of adding or subtracting the function of specific genes on cancer initiation and progression through the use of transgenic, knock-in, and knock-out mice. Such research has clear implications for the development of cancer therapeutics and diagnostics (Frese and Tuveson 2007).

Many other practical considerations make mice a powerful system in which to model cancer. The most important is that mice and humans are both mammals with closely related genomes, such that the results obtained using murine systems are often translatable to the human situation. Additionally, the ability to perform many of the same operations in mice that are performed in humans, for example the collection of blood or urine, the ability to image mice using the same modalities used to image humans (Brindle

2008), and the ability to administer both pharmacological- and biological-based therapeutics (Bergers et al. 1999; Casanovas et al. 2005b), make mice an ideal system in which to model cancer. Lastly, the relatively fast reproduction time, the large litter sizes, the ease of use to handle and breed, and the availability of numerous reagents such as murine-specific antibodies and murine-derived cell lines all increase the attractiveness and utility of using mouse models in cancer research.

The RIP-Tag mouse model of pancreatic islet cell carcinogenesis

In the studies presented in this dissertation, I used the genetically engineered mouse model of cancer known as RIP-Tag and specifically the RIP1-Tag2 (RT2) variant of this model. The RT2 mouse model is a transgenic mouse line generated by Doug Hanahan during the early 1980's (Hanahan 1985). These mice harbor a transgene that is composed of the early region of the SV40 virus fused to the rat insulin II promoter (RIP) (Figure 1.1). Consequently, the SV40 oncoproteins large T and small t antigen (Tag) are expressed in all insulin-producing cells, including the β cells found in the pancreatic islets of Langerhans as well as a rare population of cells located in the thymus (Jolicoeur et al. 1994; Smith et al. 1997). Large T antigen inhibits the activity of two well-known tumor suppressors, tumor protein 53 (p53) and the retinoblastoma protein (pRb) (Weinberg 1995; Levine 1997; Ali and DeCaprio 2001), while small t antigen inhibits a third tumor suppressor, the protein phosphatase 2A (PP2A) (Arroyo and Hahn 2005). As a consequence of the concurrent inactivation of these three tumor suppressors, all RIP-Tag mice undergo carcinogenesis of the pancreatic β cells and ultimately develop

multiple pancreatic neuroendocrine tumors (PNET), specifically of the insulinoma subtype (Hanahan 1985).

The power of the RIP-Tag mouse model is that the tumorigenesis pathway occurs in a relatively synchronous and predictable pattern (Figure 1.2). Initially, the islets appear histologically normal despite the expression of the oncogenic transgene. Of the 300-400 islets in the mouse pancreas (Edlund 2002), a fraction develop into hyperplastic/dysplastic lesions, characterized by elevated rates of proliferation and nuclear atypia and increased nuclear/cytoplasmic ratios (Christofori et al. 1994; Casanovas et al. 2005a). This transition occurs in a stochastic manner as the remainder of the islets appears ostensibly normal. Of the islets that develop into hyperplastic/dysplastic lesions, a subset will develop into angiogenic islet dysplasias, characterized by the development of new and often leaky tumor vasculature that causes these lesions to have a dark red appearance (Bergers et al. 1999; Bergers et al. 2000; Inoue et al. 2002). Finally, a fraction of these angiogenic islets will develop into frank insulinomas of varying degrees of invasiveness (Lopez and Hanahan 2002) with the development of distant metastases being infrequent and rare. In the case of the RT2 variant, expression of the RIP-Tag transgene begins during embryogenesis, and all mice develop multiple PNETs by 12–14 weeks of age. RT2 mice ultimately succumb to complications arising from the insulin-secreting tumors by 14–16 weeks of age.

As with all models, there are some limitations with this GEMM, most notably the fact that the RIP-Tag transgene is composed of a powerful promoter and a viral oncogene that does not normally cause cancer in humans. Additionally, the multiplicity of tumors that develop in the pancreas is not typical of the human cancer. Regardless, this model

has proven useful in investigating many aspects of tumorigenesis, including defining the characteristics of the hyperproliferative and angiogenic switches (Christofori et al. 1994; Bergers et al. 2000; Inoue et al. 2002; Casanovas et al. 2005a), identifying suppressors of tumor invasion and metastasis (Perl et al. 1998; Lopez and Hanahan 2002), and assessing the prospects of using anti-angiogenesis therapeutics as effective cancer therapies (Bergers et al. 1999; Casanovas et al. 2005b; Paez-Ribes et al. 2009). Thus, despite its limitations, the RIP-Tag model continues to prove its worth in the field of cancer biology and can be considered a workhorse of this discipline, as well as others (Adams et al. 1987; Skowronski et al. 1990; Geiger et al. 1992; Geiger et al. 1993; Jolicoeur et al. 1994; Forster et al. 1995; Smith et al. 1997).

Tumor invasion is associated with a poor clinical outcome

For my thesis, I sought to use the RT2 mouse model of pancreatic islet cell carcinogenesis to identify and characterize the mechanisms by which cancers acquire an invasive and malignant phenotype. The development of an invasive growth phenotype is associated with poor patient prognosis since this type of growth leads to the destruction of the affected host organ and concomitant disruption of normal organ function. Furthermore, tumor invasion is often considered a precursor to the development of distant metastases, and metastatic growth, and not the primary tumor, is usually the direct cause of death for individuals with cancer (Christofori 2006). As such, understanding the mechanisms governing the development of an invasive growth phenotype is important due to its association with metastatic growth and patient mortality. I have undertaken two independent yet complementary studies, which were focused on understanding the

mechanisms that restrict and/or promote the development of an invasive growth phenotype. The topics are introduced here to set the stage for the chapters that follow, where I describe the discovery and functional characterization of these mechanisms.

Desmosomal adhesion as a distinct barrier to the development of an invasive growth phenotype

In the first study, which is presented in Chapter 2, I used microarray analysis to profile the mRNA transcriptome of the benign, non-invasive islet tumors and the highly invasive carcinomas that develop in RT2 mice. Since these tumor lesions were identified strictly based on their histological appearance and not by any other metric, this screen was intended to identify both pro- and anti-invasive molecules in an unbiased fashion. Of the genes showing differential expression between these two classes of tumor lesions, I observed that multiple genes encoding components of desmosomes were significantly downregulated in the invasive carcinomas as compared to the non-invasive islet tumors of RT2 mice. Desmosomes are complexes dedicated to the maintenance of cell-cell adhesion, and these complexes are composed of transmembrane proteins, namely the desmocollin and desmoglein proteins, that mediate adhesive interactions with neighboring cells as well as intracellular molecules, such as desmoplakin (Dsp) and the plakophilin proteins, that connect these transmembrane proteins to the cytoskeleton (Garrod and Chidgey 2008). Desmosomes are structurally and functionally related to another cell-cell adhesion complex known as adherens junctions, members of which have been shown to be involved in the development of an invasive growth phenotype in the RT2 mouse model and in other models (Perl et al. 1998; Hartsock and Nelson 2008).

Based on the microarray results as well as complementary immunohistochemistry data, I hypothesized that loss of or attenuation of desmosomal adhesion contributes to the development of an invasive growth phenotype. To test this hypothesis, I genetically deleted one of the core desmosomal components, Dsp, in the pancreatic β cells, the same cells that express the RIP-Tag oncogenic transgene. My results suggest that genetic deletion of Dsp leads to an increased incidence of invasive carcinomas. This increase in invasive tumors is due to the development of more of the focally invasive class of RT2 tumors but not of the broadly invasive class of RT2 tumors. Interestingly, deletion of Dsp does not affect tumor growth parameters in RT2 mice nor does it affect the status of adherens junctions. These results demonstrate that desmosomal adhesion can act as an independent barrier to the development of an invasive growth phenotype and that disrupting desmosomal adhesion via the genetic deletion of Dsp increases the likelihood that a tumor will progress to an invasive state.

Genetic background can modify tumor invasion

Genetic background can affect many aspects of tumorigenesis, and a number of studies have identified genetic modifiers that affect multiple parameters of tumorigenesis, including susceptibility to tumor development, tumor progression, and response to therapy (Balmain et al. 2003). In the second study on tumor invasion, which is presented in Chapter 3, I utilized the RT2 mouse line to determine whether genetic background influences the development of an invasive growth phenotype. I observed that RT2 mice inbred into two different genetic backgrounds, the C57Bl/6 (B6) and the C3HeB/Fe (C3H) genetic backgrounds, develop invasive tumors at different rates. RT2 B6 mice

frequently develop both focally invasive and broadly invasive tumors whereas RT2 C3H mice are largely resistant to the development of any invasive tumors. Based on these data, I performed a genome wide association study to identify the genetic locus or loci associated with the invasive phenotype. Using linkage analysis, I identified a region on mouse chromosome 17 that is associated with the development of the widely invasive class of RT2 tumor lesions. Furthermore, I demonstrated that one candidate gene located in this locus, the anaplastic lymphoma kinase (Alk), is more highly expressed in RT2 tumors and normal tissues of the B6 genetic background as compared to the C3H background. I hypothesized that the higher levels of Alk are required for the development of an invasive growth phenotype, and I tested this hypothesis by pharmacologically inhibiting Alk. I found that such inhibition resulted in reduced levels of tumor invasiveness in RT2 B6 mice, which are susceptible to the development of invasive carcinomas. Lastly, I demonstrated that this genetic modifier is unlikely to operate in the bone marrow derived tissue compartment. Collectively, these results suggest that the progression of a tumor to an invasive state is subject to genetic modification and implicate Alk as a regulator of an invasive growth phenotype.

The results presented in this dissertation demonstrate that tumor invasion and the development of an invasive growth phenotype are subject to multiple levels of regulation. I demonstrate that tumor invasion can be affected by alterations to the transcriptional program and by genetic background. Furthermore, I specifically show that the desmosomal cellular adhesion complex restricts tumor invasion while the Alk signaling molecule promotes tumor invasion in a genetically engineered mouse model of pancreatic neuroendocrine tumorigenesis.

Figure 1.1

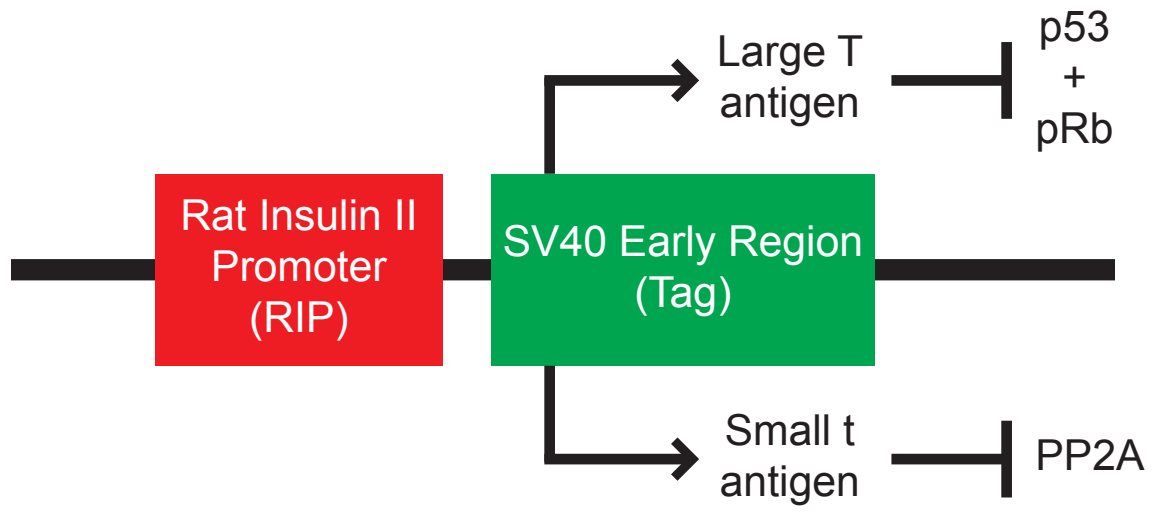


Figure 1.1. Schematic of the RIP-Tag transgene.

The RIP-Tag transgene is composed of two parts, the early region of the SV40 virus (Tag) which is fused to the rat insulin II promoter (RIP) (Hanahan 1985). As a consequence, the viral oncoproteins large T and small t antigen are expressed in all insulin-producing cells, predominantly the pancreatic β cells found in the islets of Langerhans as well as a rare population of cells found in the thymus (Jolicoeur et al. 1994; Smith et al. 1997). Large T antigen can bind and inactivate two well-known tumor suppressors, the tumor protein 53 (p53) and the retinoblastoma protein (pRb) (Weinberg 1995; Levine 1997; Ali and DeCaprio 2001), while small t antigen can bind and inactivate a third tumor suppressor, the protein phosphatase 2A (PP2A) (Arroyo and Hahn 2005).

Figure 1.2

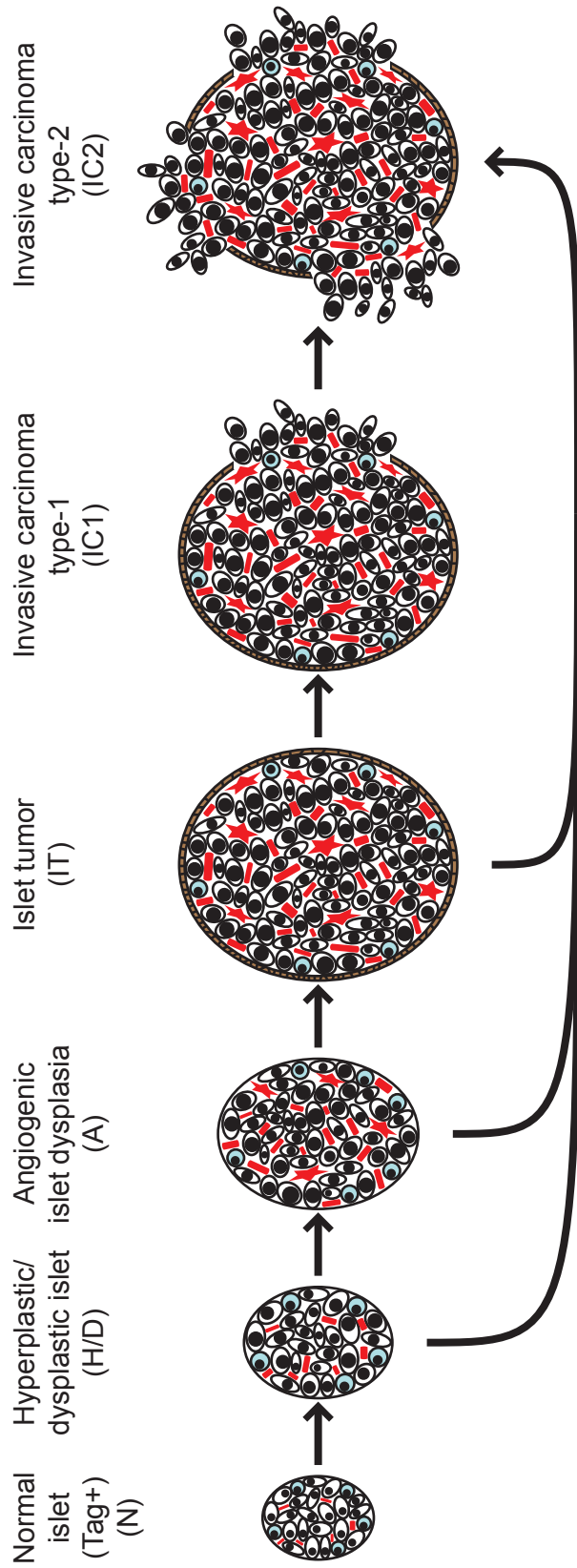


Figure 1.2. Schematic of the RIP-Tag tumorigenesis pathway.

RIP-Tag mice undergo a multistage tumorigenesis pathway composed of distinctive lesional stages, and the transition from one stage to the next occurs in a stochastic process (Hanahan 1985). In the case of the RIP1-Tag2 (RT2) variant of RIP-Tag mice, expression of the oncogenic transgene begins during embryogenesis, around E9.5 (Alpert et al. 1988). Although all of the islets express the oncogenic transgene, they initially have a normal appearance (N). Hyperplastic/dysplastic islets (H/D), characterized by their enlarged size, increased nuclear atypia and nuclear/cytoplasmic ratios, and higher rates of cellular proliferation, begin to appear at ~5 weeks of age, while angiogenic islet dysplasias (A), characterized by the appearance of new tumor vasculature, begin to appear at ~7 weeks of age. Islet tumors of varying degrees of invasiveness begin to develop starting at 10 weeks of age. Non-invasive islet tumors (IT) show no signs of invasion into the surrounding exocrine pancreas while type-1 invasive carcinomas (IC1) and type-2 invasive carcinomas (IC2) show focal and widespread invasion respectively (Lopez and Hanahan 2002). RT2 mice die due to the effects of the insulin-secreting tumors at 14–16 weeks of age.

Chapter 2.

**Genetic deletion of the desmosomal component desmoplakin
promotes tumor microinvasion in a mouse model of pancreatic
neuroendocrine carcinogenesis**

Abstract

We used the RIP1-Tag2 (RT2) mouse model of islet cell carcinogenesis to profile the transcriptome of pancreatic neuroendocrine tumors (PNET) that were either non-invasive or highly invasive, seeking to identify pro- and anti-invasive molecules. Expression of multiple components of desmosomes, structures that help maintain cellular adhesion, was significantly reduced in invasive carcinomas. Genetic deletion of one of these desmosomal components, desmoplakin, resulted in increased local tumor invasion without affecting tumor growth parameters in RT2 PNETs. Expression of cadherin 1, a component of the adherens junction adhesion complex, was maintained in these tumors despite the genetic deletion of desmoplakin. Our results demonstrate that loss of desmoplakin expression and resultant disruption of desmosomal adhesion can promote increased local tumor invasion independent of adherens junction status.

Introduction

The ability of a tumor to invade into the surrounding normal tissue marks a critical step in the transition from benign to malignant tumor growth. The acquisition of this hallmark of cancer is associated with poor prognosis for many human cancers and is often considered a precursor to the development of metastases (Hanahan and Weinberg 2000). As such, considerable effort has been directed towards identifying invasion promoting and suppressing molecules and the mechanisms by which they modulate a tumor's invasive phenotype (Christofori 2006).

Amongst the discernible barriers to the acquisition of an invasive growth phenotype is cell-cell adhesion, and cellular alterations that result in disrupted, reduced, or otherwise functionally altered cellular adhesion are strongly associated with the progression to a malignant tumor phenotype (Hiraki et al. 1996; Hirohashi 1998; Shinohara et al. 1998). The importance of sustaining cellular adhesion for homeostasis, particularly in epithelial tissues, is evident in the number of distinct structures whose primary function is to maintain cell-cell interconnections, which include the adherens junctions (AJs), desmosomes, and tight junctions (Figure 2.1) (Garrod and Chidgey 2008; Hartsock and Nelson 2008). These complexes share many structural similarities, including the presence of transmembrane proteins – typified by the cadherins – that mediate adhesive connections with neighboring cells as well as intracellular molecules – exemplified by the catenin and the plakin families – that connect these transmembrane components to the cytoskeleton (Garrod and Chidgey 2008; Hartsock and Nelson 2008). In particular, changes in the expression and/or function of AJ components have been

associated with malignant cancers, and numerous studies have focused on the role of AJs in restricting invasive growth (Vleminckx et al. 1991; Hirohashi 1998; Perl et al. 1998).

In this study, we utilized the RIP1-Tag2 (RT2) mouse model of cancer to identify the mechanisms by which tumors acquire invasive growth capabilities. RT2 mice develop multiple pancreatic neuroendocrine tumors (PNET) by 12–14 weeks of age due to the expression of the SV40 T antigen oncoprotein (Tag) in the pancreatic β cells (Hanahan 1985). This model has proven useful in characterizing many aspects of tumorigenesis due to its relatively synchronous and predictable progression through distinctive lesional stages that culminate in invasive carcinomas (Christofori et al. 1994; Inoue et al. 2002; Olson et al. 2009). We used this model to identify pro- and anti-invasive molecules in an unbiased fashion by comparing the non-invasive islet tumors to highly invasive carcinomas using microarray profiling of the mRNA transcriptome. We identified several components of desmosomes whose expression was significantly decreased in invasive tumors, implicating attenuation of desmosomal function in malignant progression. To assess this hypothesis, we engineered into the oncogene-expressing cancer cells in RT2 mice a genetic deletion of desmoplakin (Dsp), an intracellular protein critical for desmosomal stability (Gallicano et al. 1998). Loss of Dsp led to an increased incidence of invasive carcinomas providing strong evidence that desmosomal adhesion acts as a distinct barrier to invasive tumor growth.

Results

Expression of desmosomal components is lost in invasive RT2 tumor lesions

We chose to use the RT2 mouse model of cancer to characterize mechanisms governing the switch from benign to invasive tumor growth since a broad spectrum of invasive tumor lesions develop in end-stage RT2 animals. These include the non-invasive islet tumor (IT), the focally invasive carcinoma type-1 (IC1), and the broadly invasive carcinoma type-2 (IC2) (Figure 2.14A–F) (Lopez and Hanahan 2002).

To evaluate potential mechanisms regulating invasive tumor growth in this model, we isolated tissue from IT and IC2 lesions in end-stage RT2 animals by laser capture microdissection and then profiled the mRNA transcriptome (Figure 2.2). The IC2 class showed widespread transcriptional changes as compared to the IT class (Dataset 2.1). We chose to focus our attention on differentially expressed genes encoding components of two cell-cell adhesion structures, namely adherens junctions and desmosomes (Table 2.1), since elements of each were prominently downregulated. The expression of cadherin 1 (Cdh1, also known as E-cadherin), a molecule previously demonstrated to restrict invasive growth in this and other models (Perl et al. 1998; Jeanes et al. 2008), was decreased in IC2 lesions as expected. Interestingly, Cdh1 was the only member of AJs that was significantly altered in IC2 lesions (Table 2.1). In contrast, multiple genes encoding components of desmosomes were significantly reduced in IC2 lesions (Table 2.1). Moreover, the expression of several desmosomal genes in addition to Cdh1 was progressively reduced in the distinctive stages of PNET tumorigenesis in RT2 mice as well as in human PNET tumors as compared to normal human pancreatic islets, when total lesional stages, in particular ungraded tumors, were analyzed (Figure 2.3) (Olson et

al. 2009). Although the expression of these genes was reduced in ungraded whole tumors in comparison to normal islets, their levels were further reduced in the microdissected invasive IC2 lesions (Table 2.1). Based on these results, we sought to determine what role desmosomal adhesion might play in regulating invasive tumor growth in this mouse model of cancer.

To confirm the microarray results, we performed immunohistochemistry for multiple desmosomal components. Staining for Dsp and for one of the desmosomal cadherins, desmoglein 2 (Dsg2), as well as for Cdh1 demonstrated that these molecules are expressed in the pancreatic islets as well as in the pancreatic ducts and the exocrine pancreas of wild-type animals (Figures 2.4, 2.5). In tumors of end-stage RT2 animals, the expression of all three molecules was maintained in IT lesions and was completely extinguished in IC2 lesions (Figures 2.4, 2.5). In contrast to Cdh1, expression of catenin beta 1 (Ctnnb1), another component of AJs, was maintained in both IT and IC2 lesions, comparable to wild-type islets (Figure 2.6). This result is consistent both with the microarray result demonstrating that Cdh1 was the only AJ component to show any change in expression and with a previous study suggesting that Ctnnb1 does not contribute to RT2 tumorigenesis (Herzig et al. 2007). Collectively, these data confirm the microarray results and suggest the hypothesis that loss of desmosomal adhesion might contribute to the development of an invasive phenotype.

β cell specific deletion of Dsp in RT2 animals

To address the hypothesis raised by the microarray and immunohistochemistry results, we asked whether functionally disrupting desmosomal activity *in vivo* would

promote invasive tumor growth in RT2 mice. To accomplish this, we chose to genetically delete Dsp since there is a single Dsp gene as compared to other components of desmosomes for which there are multiple non-allelic genes (Garrod and Chidgey 2008). Furthermore, ablation of Dsp *in vivo* has previously been shown to impair desmosome function (Gallicano et al. 1998). Since the Dsp whole body knockout is embryonic lethal (Gallicano et al. 1998), we employed the Cre/loxP system to ablate the Dsp gene specifically in the pancreatic β cells, the same cells that express the Tag oncogene in RT2 mice. In combination with a Dsp^{Flox} allele (Vasioukhin et al. 2001b), we used a mouse line in which a tamoxifen-regulatable Cre recombinase is controlled by the pancreatic duodenal homeobox gene 1 promoter (Pdx1-Cre^{ER}) (Gu et al. 2002). Pdx1 is expressed in all pancreatic lineages during development and is variably expressed in the adult pancreas, in particular being widely expressed in β cells (Offield et al. 1996; Gidekel Friedlander et al. 2009).

We intercrossed RT2+; Dsp^{Flox/WT} with Pdx1-Cre^{ER+}; Dsp^{Flox/WT} mice to generate the appropriate genotypes, and all expected genotypes and genders were observed in approximate Mendelian ratios (Figure 2.7, Tables 2.2, 2.3). To induce Cre activity, all Pdx1-Cre^{ER} positive mice were given tamoxifen for five consecutive days beginning at 10 weeks of age when incipient tumors are first observed in RT2 mice (Figure 2.8) (Bergers et al. 1999). In the absence of the RT2 transgene, genetic ablation of Dsp resulted in uniform loss of Dsp expression in the pancreatic islets, as determined by immunohistochemistry (Figure 2.9). Deletion of Dsp did not cause any change in Cdh1 expression or in the gross morphological appearance of the non-oncogene-expressing islets (Figure 2.9). Loss of Dsp was accompanied by the concomitant loss of Dsg2

expression in the pancreatic islets whereas the expression of insulin (Ins), the hormone produced by β cells, did not appear to be affected (Figure 2.10). These results are consistent with compromised desmosomal adhesion, although we cannot strictly rule out the possibility that some residual desmosomal function persists in the absence of Dsp. Ablation of Dsp in normal pancreatic islets did not affect multiple physiological parameters, such as body mass and fasting glucose levels, and its expression in this tissue compartment is apparently dispensable in adult mice (Figure 2.11), setting the stage to assess the impact of its loss on PNETs arising from such islets. Lastly, the tamoxifen induction regimen by itself had no obvious effect on any aspect of RT2 tumorigenesis examined, including tumor invasion, when tamoxifen was applied to RT2 mice that lacked the Pdx1-Cre^{ER} and Dsp^{Flox} alleles (Figure 2.12).

Loss of Dsp does not affect tumor growth parameters in RT2 mice

Induced loss of Dsp at 10 weeks of age did not affect any of the tumor growth parameters in RT2 mice that were sacrificed 4 weeks later. No significant changes were observed in the number of tumors that developed nor in the collective tumor burden when comparing RT2+; Pdx1-Cre^{ER}+; Dsp^{Flox/Flox} mice and littermate controls (Figure 2.13A–B). Furthermore, the rates of tumor proliferation and tumor apoptosis, as judged by the levels of the proliferation marker Ki67 and the TUNEL assay respectively, were indistinguishable between groups (Figure 2.13C–J). Thus, we conclude that the loss of Dsp does not affect tumor growth in this model.

Loss of Dsp leads to increased local tumor invasion in RT2 mice

While conditional genetic ablation of Dsp in the angiogenic islet dysplasias and incipient solid tumors of RT2 mice had no discernible effects on tumor formation and subsequent tumor growth parameters, it did lead to an increase in tumor invasion. RT2 mice develop a spectrum of tumor lesions, including non-invasive (IT), focally invasive (IC1), and broadly invasive (IC2) lesions (Figure 2.14A–F) (Lopez and Hanahan 2002). Loss of Dsp resulted in a greater frequency of invasive tumors and a concomitant reduction in the percentage of non-invasive IT tumors in mice analyzed four weeks after genetic ablation of Dsp in incipient solid tumors (Figure 2.14G–H). Whereas ~40% of total tumors could be classified as invasive carcinomas in control mice, greater than 60% of all tumors fell into this category in RT2+; Pdx1-Cre^{ER+}; Dsp^{Flox/Flox} mice (Figure 2.14G). Interestingly, this shift appears to result from selective progression to the focally invasive IC1 but not to the widely invasive IC2 tumors. Indeed, while there is no significant change in the development of IC2 lesions (approximately 10% of all tumors fall into this class regardless of Dsp status), more than 50% of tumors can be classified as IC1 lesions in RT2+; Pdx1-Cre^{ER+}; Dsp^{Flox/Flox} mice versus ~30% in control mice (Figure 2.14H).

We confirmed that Dsp was in fact lost in these tumors by examining the recombination status of the Dsp allele by PCR. Tumors that were genotypically Dsp^{Flox/Flox} showed near universal recombination of the Dsp allele, confirming that Dsp was lost in these tumors (Figure 2.14I). Tumors isolated from control Dsp^{WT/WT} or Dsp^{Flox/WT} mice showed no recombination or were heterozygous for the recombined and wild-type Dsp alleles respectively. Thus, we conclude that the conditional genetic ablation of Dsp in incipient tumors of RT2 mice leads to increased local tumor invasion.

Cdh1 expression is maintained in IC1 tumor lesions regardless of Dsp status

We were intrigued that loss of Dsp led to an increase in the IC1 class but not in the IC2 class of invasive tumors. Since Cdh1 also acts as a dominant invasion suppressor in this model, we examined its status in the tumors from RT2+; Pdx1-Cre^{ER+}; Dsp^{Flox/Flox} mice and littermate controls by immunohistochemistry. We found that Cdh1 expression was maintained in the IT and IC1 tumors that developed regardless of Dsp status (Figure 2.15I–L). Tumor margins and regions of invasion were identified by staining for the Tag oncprotein (Figure 2.15E–H). Indeed, Cdh1 appeared to be expressed at comparable levels in IT and IC1 tumor lesions regardless of Dsp status (Figure 2.15M–T). Expression in IT and IC1 lesions of a second component of AJs, junction plakoglobin (Jup, also known as gamma catenin), was also unaffected by Dsp status (Figure 2.16) consistent with AJ function being maintained in these lesions despite the absence of Dsp and impaired/ablated desmosomal function. Lastly, cadherin 2 (Cdh2, also known as N-cadherin), a marker of epithelial-mesenchymal transition (EMT), was expressed at readily detectable and comparable levels in IT and IC1 tumors regardless of Dsp status, as well as in the IC2 tumors that did not express Cdh1 (Figure 2.17), consistent with the results of a previous study investigating determinants of progression to invasive carcinoma (Perl et al. 1998); notably, there is no indication that activation of the invasive growth capability in this pathway involves an EMT, as reflected in differential expression of Cdh2 or other markers of EMT. Given that the expression of both Dsp and Cdh1 was lost in IC2 lesions, the most invasive class of RT2 tumors, both in unmodified RT2 mice and in tamoxifen-treated RT2+; Pdx1-Cre^{ER+}; Dsp^{Flox/Flox} mice (Figure 2.4 and data not

shown), we infer that loss of Dsp by itself is sufficient to promote the development of focally invasive tumors while the additional loss of Cdh1 is required to develop a more aggressive invasive tumor phenotype.

Discussion

To date, much of the work on desmosomes in human disease has focused on their role in maintaining heart and skin integrity, where desmosomal defects are associated with cardiomyopathy and skin blistering conditions respectively (Bazzi and Christiano 2007). More recently, a potential role for desmosomes in cancer progression has been suggested based on a variety of experimental clues (Chidgey and Dawson 2007). For example, *in vitro* cell culture assays demonstrated that inhibiting desmosomal adhesion via blocking peptides caused morphological disorganization (Runswick et al. 2001) while introduction of desmosomal components into a nonadhesive cell line resulted in increased cell aggregation and reduced cellular invasion *in vitro* (Tselepis et al. 1998). These studies suggested that loss of desmosomal function might contribute to tumor invasion and malignancy, consistent with their role in maintaining cellular adhesion. (Our attempts to perform similar *in vitro* experiments using cell lines derived from RT2 tumors [β TCs] were hindered by the fact that β TC cell lines express desmosomal components at low levels, presumably due to adaptations to culture, and generally perform poorly in migration/invasion assays – data not shown). In further support of the proposed role of desmosomes as a barrier to malignant progression, several pathology studies characterizing human cancers have shown that decreased or altered expression of desmosomal components, including Dsp, correlates with increased tumor invasion, advanced tumor grade, and poor patient prognosis, particularly in oral cancers where desmosomal components are highly expressed in the normal oral mucosa (Hiraki et al. 1996; Shinohara et al. 1998; Papagerakis et al. 2009). Additionally, our bioinformatic analysis of human cancer databases confirmed that the expression of desmosomal genes

is often decreased in human epithelial cancers as compared to normal tissues and is occasionally further decreased in more advanced grades of tumors (Table 2.4). The present study substantively extends this current state of knowledge by demonstrating that desmosomal adhesion can indeed act as a distinct barrier to the development of an invasive tumor phenotype in the *in vivo* setting of a genetically engineered mouse model of cancer.

We identified several components of desmosomes – Dsp, Dsg2, desmocollin 2 (Dsc2), and plakophilin 2 (Pkp2) – whose expression was significantly downregulated in the highly invasive tumor lesions that develop in the RT2 mouse model of PNET. These changes were reflected at the protein level as determined by immunostaining of non-invasive IT lesions and broadly invasive IC2 lesions. The simultaneous decrease in expression for multiple desmosomal genes suggests that there may be coordinated transcriptional regulation of desmosomal components. Prime candidates for such regulation include the transcription factors that regulate EMT, such as the Snail and Twist families of transcription factors (Peinado et al. 2007). Notably, however, we did not detect significant differential expression of such transcription factors in our microarray analysis comparing non-invasive IT and highly invasive IC2 PNETs (Dataset 2.1), and the expression of one prominent marker of EMT, Cdh2, was not obviously different between IT and IC2 lesions, consistent with the results of a previous study investigating determinants of the invasive phenotype using this same model of PNET (Perl et al. 1998). Thus, the current evidence suggests that the acquisition of an invasive phenotype in this tumor type does not involve a classical EMT. Our results clearly demonstrate that the conditional genetic deletion of a single core desmosomal component, Dsp, promotes

increased local tumor invasion in RT2 mice, producing a phenocopy of such inferred transcriptional regulation in the normal circumstances of tumor progression.

While desmosomes play an integral role in maintaining epithelial integrity, they are by no means the only structure involved in cellular adhesion. In addition to desmosomes, several related structures, including AJs, contribute to maintaining cell-cell adhesion (Hartsock and Nelson 2008). However, while desmosomes and AJs play related biological roles in terms of maintaining cellular adhesion and have similar structural compositions, it is worth noting that there are clear differences in the consequences of impaired desmosome adhesion versus impaired AJ adhesion on tumor phenotypes. An elegant functional genetic study demonstrated that Cdh1, a core member of AJs, acts as an invasion suppressor *in vivo*; targeting a transgene encoding a dominant-negative Cdh1 molecule to the oncogene-expressing pancreatic β cells markedly accelerated tumor progression and led to significantly increased frequencies of invasive carcinomas and to the development of lymph node metastasis in this same RT2 mouse model of PNET (Perl et al. 1998). In comparison, deletion of Dsp only led to an increase in the frequency of the focally invasive IC1 grade of islet carcinomas but not the more widely aggressive IC2 carcinomas, and distant metastases were not observed (data not shown). One possible explanation for the differences in these phenotypic outcomes is the different roles that Dsp and Cdh1 play within their respective adhesion complex. While Cdh1 is a transmembrane protein that directly links cells together by forming homotypic interactions with other Cdh1 molecules on neighboring cells (Halbleib and Nelson 2006), Dsp is an intracellular molecule that contributes to the overall stability of the desmosomal plaque and links this plaque to the intermediate filaments (Gallicano et al. 1998).

Therefore, deletion of Dsp may attenuate but not totally abolish desmosomal function; if so, then the specific deletion of one of the desmosomal cadherins, Dsc2 or Dsg2, might have a more pronounced effect on invasiveness. An additional explanation for the increase in the focally invasive IC1 fraction but not the broadly invasive IC2 fraction of invasive tumors following ablation of Dsp involves the observed maintenance of Cdh1 and AJs. Expression of Cdh1 as well as a second component of AJs, Jup, was retained in both the non-invasive IT tumors and in the now more prevalent focally invasive IC1 tumors following genetic deletion of Dsp. It would seem likely, in light of the aforementioned functional study in this same mouse model of cancer (Perl et al. 1998), that the preservation of Cdh1 expression and of AJ function serves to maintain an additional, stronger brake on tumor invasion. Thus, while loss of Dsp and impairment of desmosomal adhesion leads to the focal invasion observed in IC1 lesions, the development of the broadly invasive phenotype found in IC2 lesions evidently requires the concomitant loss of Cdh1. Indeed, the IC2 tumor lesions that normally develop in RT2 mice show a coordinated reduction in the expression of Cdh1 and multiple desmosomal components (Table 2.1, Figures 2.4, 2.5). The apparently independent regulation of desmosomal and AJ adhesion is notable since AJ stability has been proposed to affect desmosomal stability and vice versa in other contexts (Lewis et al. 1994; Lewis et al. 1997; Vasioukhin et al. 2001b), whereas Cdh1 and Jup are evidently not affected by the deletion of Dsp during PNET tumorigenesis in RT2 mice.

Interestingly, the genetic deletion of Dsp had no consequential effects on the other parameters of RT2 tumorigenesis beyond invasion. Although it has been suggested that Dsp and other desmosomal components can affect cellular proliferation and apoptosis

(Nava et al. 2007; Wan et al. 2007), we did not observe any changes in tumor growth parameters following the genetic deletion of Dsp (Figure 2.13). Our results are consistent with one of the earliest studies to examine the role of Dsp *in vivo*, wherein a skin-specific deletion of catenin alpha 1 (Cttna1), the AJ homologue of Dsp, led to increased skin proliferation and hyperplasia whereas ablation of Dsp did not (Vasioukhin et al. 2001a). Thus, with regards to the RT2 model of PNET and possibly other forms of cancer, it appears that desmosomes primarily serve to maintain cell-cell adhesion and hence suppress the acquisition of an invasive growth capability such that the observed downregulation of desmosomal genes results in the impairment of desmosomal function and a concomitant weakening in cellular adhesion without affecting other parameters of tumorigenesis.

Finally, it is important to set these results into the broader context of knowledge about malignant progression to an invasive growth state in this stereotypical pathway of multistep tumorigenesis. While disrupted cell-cell adhesion caused by the reduced expression of Cdh1 (Perl et al. 1998) and/or desmosomal genes (this report) clearly promotes invasive tumor growth, other factors are involved as well. Thus for example, increased expression of the type-1 insulin-like growth factor receptor (Igf1r) can drive these PNETs to acquire a highly invasive phenotype (Lopez and Hanahan 2002). Additionally, the recruitment of immune cells to the margins of these PNETs has been shown to promote invasiveness, in part by supplying cathepsin proteases and heparanase (Joyce et al. 2005; Gocheva et al. 2006; Gocheva et al. 2010). As such, multiple factors can impact the progression to invasiveness by varying degrees (Figure 2.18), and future research may well identify additional components. Irrespective, our results demonstrate

that loss of desmosomal adhesion, as exemplified by the genetic deletion of Dsp, can enable a tumor to acquire an invasive phenotype. The functional study presented herein establishes desmosomal adhesion as a distinct and ostensibly independent suppressor of invasive tumor growth. This knowledge will likely contribute to a better understanding of the mechanisms governing tumor progression to an invasive growth state and may prove useful in evaluating invasive states of human cancers.

Material and methods

Genetically engineered mice

The generation and characterization of the RIP1-Tag2 (RT2) (Hanahan 1985), Dsp^{Flox} (Vasioukhin et al. 2001b), and Pdx1-Cre^{ER} (Gu et al. 2002) mouse lines have been previously reported. All mice were backcrossed a minimum of six generations into the C57Bl/6 (B6) background (Charles River, Wilmington, MA) and then intercrossed to generate the specified genotypes. To induce Cre^{ER} activity, mice were injected intraperitoneally with 100 μ l of 10 mg/ml tamoxifen (Sigma, St. Louis, MO) suspended in peanut oil for five consecutive days beginning at 10 weeks of age. To relieve the effects of hypoglycemia induced by the insulin-secreting tumors, all RT2 mice received 50% sugar food (Harlan Teklad, Madison, WI) beginning at 10 weeks of age. All mice used in this study were housed and maintained in accordance with the University of California, San Francisco (UCSF) institutional guidelines governing the care of laboratory mice.

Tissue preparation, tumor analysis, and histology

Pancreata were isolated from 14-week-old mice and embedded in OCT (Sakura Finetek, Torrance, CA) on dry ice. Tumor number and tumor volume were quantified as previously described (Inoue et al. 2002). For histological analysis, frozen tissues were sectioned at 10 μ m thickness, and every tenth section was stained with hematoxylin and eosin (Surgipath Medical Industries, Richmond, IL) using standard methods. Tumors were classified as a non-invasive islet tumor (IT), a focally invasive carcinoma type-1

(IC1), or a broadly invasive carcinoma type-2 (IC2) using a previously defined grading scheme (Lopez and Hanahan 2002).

Laser capture microdissection and RNA purification and amplification

Fresh-frozen pancreatic sections (10 μ m) from 14-week-old RT2 B6 mice were fixed in cold 70% ethanol for 16 hours prior to laser capture microdissection (LCM). Sections were stained using a modified hematoxylin and eosin stain that preserves RNA integrity while allowing for the microscopic visualization of pancreatic structures (Lawlor et al. 2006). LCM was performed using an Arcturus PixCell II laser capture microscope system (Molecular Devices, Sunnyvale, CA). Total RNA was isolated using the Arcturus PicoPure RNA Isolation kit (Molecular Devices, Sunnyvale, CA) and DNase I treated (Qiagen, Valencia, CA). Equal amounts of RNA (8 ng/lesion) from three independent IT or IC2 tumor lesions were pooled, and then cDNA was generated, amplified, and biotinylated using the Ovation Biotin System (NuGen, San Carlos, CA). Three independent pools per tumor class were generated for subsequent microarray analysis.

Microarray analysis

Labeled cDNA was hybridized to Affymetrix Mouse Genome 430 2.0 arrays (Affymetrix, Santa Clara, CA) according to the manufacturer's specifications. Data were analyzed by the UCSF Helen Diller Family Comprehensive Cancer Center Biostatistics and Computational Biology Core. The data were normalized using a robust multi-chip averaging method utilizing the freely available R language. Linear models were fit for

each pair of groups to be compared with log₂ expression as the response and the tumor phenotype indicator as the independent variable using the limma package in Bioconductor. Moderated t-statistics were used, and p-values were adjusted by controlling the false discovery rate. A change in gene expression was identified as significant if the false discovery rate was less than 0.05, meaning that fewer than 5% of false findings would be expected among the genes declared to be differentially expressed.

Immunohistochemical staining and analysis

Frozen tissues were sectioned at 10 µm thickness. For immunofluorescence staining, sections were fixed in cold acetone. For colorimetric staining, sections were fixed in 10% Zn-buffered formalin (Medical Chemical Corporation, Torrance, CA), subjected to antigen retrieval using the Antigen Unmasking Solution (Vector Laboratories, Burlingame, CA), and blocked for endogenous peroxidase activity. Antibodies used in this study were as follows: rat anti-cadherin 1 (Invitrogen, Carlsbad, CA); mouse anti-desmoplakin I/II, mouse anti-desmoglein 1/2 (Fitzgerald, Concord, MA); mouse anti-catenin beta 1, mouse anti-cadherin 2, mouse anti-junction plakoglobin (BD Biosciences, San Jose, CA); rabbit anti-T-antigen (Hanahan laboratory preparation); rabbit anti-Ki67 (Novus Biologicals, Littleton, CO); rhodamine red-X-conjugated donkey anti-mouse IgG, rhodamine red-X-conjugated donkey anti-rabbit IgG, FITC-conjugated donkey anti-rat IgG, biotin-conjugated donkey anti-rabbit IgG (Jackson ImmunoResearch Laboratories, West Grove, PA). For mouse antibodies, non-specific binding was blocked using the Mouse on Mouse Blocking Reagent (Vector Laboratories, Burlingame, CA). Fluorescently labeled tissues were mounted with Vectashield mounting medium

containing 4',6-diamidino-2-phenylindole (DAPI) (Vector Laboratories, Burlingame, CA) to visualize cell nuclei. The TdT-mediated dUTP-digoxigenin nick-end labeling (TUNEL) assay was used to assess tumor apoptosis as previously described (Lopez and Hanahan 2002). For colorimetric staining, signal was amplified using the Vectastain Elite ABC kit (Vector Laboratories, Burlingame, CA), visualized using Nova Red substrate (Vector Laboratories, Burlingame, CA), and counterstained with hematoxylin. For Ki67 and TUNEL quantification, two to three random fields were obtained using a 40X objective lens from at least two tumors per mouse and at least five mice per group. The proliferation or apoptosis index was calculated as the percentage of total cells per field that were Ki67- or TUNEL-positive respectively using the MetaMorph software package (Molecular Devices, Sunnyvale, CA). For all other immunohistochemical analysis, two to three tumors per mouse from a minimum of five mice per indicated group were analyzed per staining condition. All images were captured using an Axio Imager bright field microscope or an Axio Scope fluorescence microscope and the AxioVision LE software package (Carl Zeiss, Thornwood, NY).

Statistical analysis

Fisher's exact test and the chi-square test were used to compare tumor invasion metrics. The Mann-Whitney test was used to compare tumor burden, tumor number, tumor proliferation rates, tumor apoptosis rates, and body mass metrics. The Mann-Whitney and the Wilcoxon matched pairs test was used to compare fasting glucose metrics. For all statistical tests, a p-value of $p \leq 0.05$ was considered significant. All

statistics were performed using the Prism software package (GraphPad Software, La Jolla, CA).

Fasting glucose measurements

Animals were fasted overnight for 14–16 hours prior to the first tamoxifen injection and one week following the final tamoxifen injection. Fasting glucose levels were measured using a FreeStyle Freedom glucose meter (Abbott Laboratories, Abbott Park, IL).

Tumor genotype analysis by polymerase chain reaction (PCR)

Tumor tissue was isolated directly from OCT embedded tissues, and genomic DNA was isolated using the QIAmp DNA Micro kit (Qiagen, Valencia, CA). PCR was performed using standard methods. Primers used were as follows: Cre (forward: 5'-CATG TTCAGGGATCGCCAGG-3' and reverse: 5'-TGCGGTGCTAACCAGCGTTTT-3'); β 2 microglobulin (forward: 5'-CACCGGAGAATGGGAAGCCGAA-3' and reverse: 5'-TCCACACAGATGGAGCGTCCAG-3'); Dsp-WT/Flox (forward: 5'-GGTTGGGCCTCTCGAATCATGAGTGTCTAGCG-3' and reverse: 5'-TGTCTGTTGCCATGTGATGCC-3'); Dsp-Recombined/Non-Recombined (forward: 5'-ACAGGCCAGATGAGATCACC-3' and reverse: 5'-TGTCTGTTGCCATGTGATGCC-3').

Real-time quantitative PCR

Normal islets were isolated from six-week-old wild-type B6 mice, and hyperplastic islets were isolated from six-week-old RT2 B6 mice as previously described (Parangi et al. 1995). Angiogenic islets were isolated from nine-week-old RT2 B6 mice by selection based on their red, hemorrhagic appearance following collagenase digestion of pancreata (Parangi et al. 1995). Islet tumors were excised from the surrounding exocrine pancreas from 14-week-old RT2 B6 mice. Total RNA was purified using the RNeasy Mini kit (Qiagen, Valencia, CA) and DNase I treated (Qiagen, Valencia, CA). cDNA was synthesized using the iScript cDNA Synthesis kit (Bio-Rad Laboratories, Hercules, CA). Real-time quantitative PCR was performed using a 7900HT system (Applied Biosystems, Foster City, CA) (see Table 2.5 for a complete list of primers used in this study) according to the manufacturer's specifications.

Acknowledgments

We thank: Elaine Fuchs (Howard Hughes Medical Institute, Rockefeller University, New York, NY) and Douglas Melton (Howard Hughes Medical Institute, Harvard University, Boston, MA) for the Dsp^{Flox} mice and the Pdx1-Cre^{ER} mice respectively; Eric Nakakura (UCSF, San Francisco, CA) for the human PNET RNA samples; The J. David Gladstone Institute Genomics Core (Chris Barker, director) for assistance with the microarrays; the UCSF Helen Diller Family Comprehensive Cancer Center Genomics Core; the UCSF Diabetes Center Microscopy and Islet Isolation Cores; Susan Cacacho, Ehud Drori, Marina Vayner, and Annie Wang for superior technical support; Johanna Joyce for critically reviewing the manuscript; and Matthias Hebrok, Martin McMahon, and members of the Hanahan laboratory for advice and encouragement at all stages of this project. D.H. is an American Cancer Society Research Professor. This work was supported by a grant from the National Cancer Institute (to D.H.) and by a graduate research fellowship from the National Science Foundation (to M.G.H.C).

Table 2.1. Summary of microarray results for components of desmosomes and adherens junctions.

P-value	Fold-change^a	Affymetrix probe ID^b	Gene symbol	Gene name	Synonyms	Complex
0.017	-7.81	1426911_at	Dsc2	Desmocollin 2		Desmosome
0.027	-7.52	1439476_at	Dsg2	Desmoglein 2		Desmosome
0.053	-12.61	1435494_s_at	Dsp	Desmoplakin		Desmosome
0.019	-14.03	1449799_s_at	Pkp2	Plakophilin 2		Desmosome
0.029	-12.99	1448261_at	Cdh1	Cadherin 1	E-cadherin	Adherens junction
0.181	-1.33	1437807_x_at	Ctnna1	Catenin alpha 1	Alpha E catenin	Adherens junction
0.795	-1.09	1430533_a_at	Ctnnb1	Catenin beta 1	Beta catenin	Adherens junction
0.444	1.29	1445830_at	Ctnnd1	Catenin delta 1	P120 catenin	Adherens junction
0.852	1.30	1426873_s_at	Jup	Junction plakoglobin	Gamma catenin	Adherens junction; desmosome

^a Fold-change represents the widely invasive carcinoma type-2 (IC2) class as compared to the non-invasive islet tumor (IT) class of RIP1-Tag2 (RT2) tumor lesions

^b Affymetrix probe ID corresponds to the Mouse Genome 430 2.0 Array

Table 2.2. Genotyping of pups resulting from intercross between RIP1-Tag2+; Dsp^{Flox/WT} and Pdx1-Cre^{ER+}; Dsp^{Flox/WT} mice.

Genotype	Expected	Observed
RIP1-Tag2-; Pdx1-Cre ^{ER-} ; Dsp ^{WT/WT}	6.25%	6.9% (14)
RIP1-Tag2-; Pdx1-Cre ^{ER-} ; Dsp ^{Flox/WT}	12.5%	17.2% (35)
RIP1-Tag2-; Pdx1-Cre ^{ER-} ; Dsp ^{Flox/Flox}	6.25%	6.4% (13)
RIP1-Tag2+; Pdx1-Cre ^{ER-} ; Dsp ^{WT/WT}	6.25%	7.4% (15)
RIP1-Tag2+; Pdx1-Cre ^{ER-} ; Dsp ^{Flox/WT}	12.5%	12.8% (26)
RIP1-Tag2+; Pdx1-Cre ^{ER-} ; Dsp ^{Flox/Flox}	6.25%	6.4% (13)
RIP1-Tag2-; Pdx1-Cre ^{ER+} ; Dsp ^{WT/WT}	6.25%	6.4% (13)
RIP1-Tag2-; Pdx1-Cre ^{ER+} ; Dsp ^{Flox/WT}	12.5%	10.8% (22)
RIP1-Tag2-; Pdx1-Cre ^{ER+} ; Dsp ^{Flox/Flox}	6.25%	5.9% (12)
RIP1-Tag2+; Pdx1-Cre ^{ER+} ; Dsp ^{WT/WT}	6.25%	4.9% (10)
RIP1-Tag2+; Pdx1-Cre ^{ER+} ; Dsp ^{Flox/WT}	12.5%	9.4% (19)
RIP1-Tag2+; Pdx1-Cre ^{ER+} ; Dsp ^{Flox/Flox}	6.25%	5.4% (11)

The expected and observed frequency of each genotype is shown as a percentage, with the absolute numbers of individuals shown in parentheses.

Table 2.3. Gender distribution of pups resulting from intercross between RIP1-Tag2+; Dsp^{Flox/WT} and Pdx1-Cre^{ER+}; Dsp^{Flox/WT} mice.

Gender	Expected	Observed
Female	50%	48.8% (99)
Male	50%	51.2% (104)

The expected and observed frequency of each genotype is shown as a percentage, with the absolute numbers of individuals shown in parentheses.

Table 2.4. Bioinformatic assessment of desmosomal gene expression in human cancers.

Gene	Class 1 ^a	Class 2 ^a	Fold-change ^b	P-value	Oncomine category	Platform	Source	Citation
Dsc2	Fetal kidney (3)	Clear cell sarcoma of the kidney (14)	-2.353	6.77E-04	Cancer versus normal	Human genome U133A array	Cutcliffe renal	Clinical Cancer Research 2005/11/15
Dsc2	Skin (7)	Cutaneous melanoma (45)	-1.911	4.00E-03	Cancer versus normal	Human genome U133A array	Talantov melanoma	Clinical Cancer Research 2005/10/15
Dsc2	Breast (3)	Lobular breast carcinoma (21)	-2.207	8.93E-05	Cancer versus normal	Undefined on Oncomine	Zhao breast	Molecular Biology of the Cell 2004/06/01
Dsg2	Fetal kidney (3)	Clear cell sarcoma of the kidney (14)	-16.174	3.36E-06	Cancer versus normal	Human genome U133A array	Cutcliffe renal	Clinical Cancer Research 2005/11/15
Dsg2	Brain (23)	Oligodendroglioma (50)	-1.519	8.00E-03	Cancer versus normal	Human genome U133 Plus 2.0 array	Sun brain	Cancer Cell 2006/04/01
Dsg2	Skin (7)	Cutaneous melanoma (45)	-11.919	8.82E-07	Cancer versus normal	Human genome U133A array	Talantov melanoma	Clinical Cancer Research 2005/10/15
Dsp	Fetal kidney (3)	Clear cell sarcoma of the kidney (14)	-17.869	1.82E-08	Cancer versus normal	Human genome U133A array	Cutcliffe renal	Clinical Cancer Research 2005/11/15
Dsp	Brain (23)	Glioblastoma (81)	-1.820	1.79E-05	Cancer versus normal	Human genome U133 Plus 2.0 array	Sun brain	Cancer Cell 2006/04/01
Dsp	Brain (23)	Oligodendroglioma (50)	-1.824	1.41E-05	Cancer versus normal	Human genome U133 Plus 2.0 array	Sun brain	Cancer Cell 2006/04/01
Dsp	Skin (7)	Cutaneous melanoma (45)	-66.700	6.06E-18	Cancer versus normal	Human genome U133A array	Talantov melanoma	Clinical Cancer Research 2005/10/15
Dsp	Breast (3)	Lobular breast carcinoma (21)	-1.545	3.50E-02	Cancer versus normal	Undefined on Oncomine	Zhao breast	Molecular Biology of the Cell 2004/06/01
Pkp2	Brain (23)	Glioblastoma (81)	-2.553	2.05E-06	Cancer versus normal	Human genome U133 Plus 2.0 array	Sun brain	Cancer Cell 2006/04/01
Pkp2	Brain (23)	Oligodendroglioma (50)	-1.808	5.83E-04	Cancer versus normal	Human genome U133 Plus 2.0 array	Sun brain	Cancer Cell 2006/04/01
Pkp2	Skin (7)	Cutaneous melanoma (45)	-6.005	1.43E-11	Cancer versus normal	Human genome U133A array	Talantov melanoma	Clinical Cancer Research 2005/10/15
Dsc2	Esophageal cancer precursor (8)	Esophageal carcinoma (8)	-3.804	7.00E-03	Cancer histology	Human genome U133A array	Kimchi esophagus	Cancer Research 2005/04/15
Dsc2	Melanoma precursor (18)	Cutaneous melanoma (45)	-1.956	3.33E-05	Cancer histology	Human genome U133A array	Talantov melanoma	Clinical Cancer Research 2005/10/15
Dsg2	Melanoma precursor (18)	Cutaneous melanoma (45)	-2.777	4.80E-06	Cancer histology	Human genome U133A array	Talantov melanoma	Clinical Cancer Research 2005/10/15
Dsp	Colorectal adenoma (17)	Colorectal carcinoma (313)	-1.645	2.41E-04	Cancer histology	Human genome U133A	Bittner colon	Not published 2005/01/15

Dsp	Esophageal cancer precursor (8)	Esophageal carcinoma (8)	-2.114	3.00E-03	Cancer histology	array Human genome U133A array	Kimchi esophagus	Cancer Research 2005/04/15
Dsp	Melanoma precursor (18)	Cutaneous melanoma (45)	-51.746	6.20E-20	Cancer histology	Human genome U133A array	Talantov melanoma	Clinical Cancer Research 2005/10/15
Pkp2	Colorectal adenoma (17)	Colorectal carcinoma (313)	-1.564	1.00E-02	Cancer histology	Human genome U133A array	Bittner colon	Not published 2005/01/15
Pkp2	Esophageal cancer precursor (8)	Esophageal carcinoma (8)	-1.639	2.80E-02	Cancer histology	Human genome U133A array	Kimchi esophagus	Cancer Research 2005/04/15
Pkp2	Melanoma precursor (18)	Cutaneous melanoma (45)	-1.590	1.50E-02	Cancer histology	Human genome U133A array	Talantov melanoma	Clinical Cancer Research 2005/10/15

^a Number in parentheses indicates number of samples profiled per class

^b Fold-change represents Class 2 as compared to Class 1

All data presented were obtained from the Oncomine online database (<https://www.oncomine.org/resource/login.html>)

Table 2.5. List of primers used for quantitative PCR.

Gene symbol	Gene name	Manufacturer	Assay ID ^a	Primer/Probe Sequences ^b
Dsc2 (mouse)	Desmocollin 2	Applied Biosystems	Mm01130569_m1	
Dsg2 (mouse)	Desmoglein 2	Applied Biosystems	Mm00514609_m1	
Dsp (mouse)	Desmoplakin	Applied Biosystems	Mm01351874_m1	
Pkp2 (mouse)	Plakophilin 2	Applied Biosystems	Mm00503159_m1	
Cdh1 (mouse)	Cadherin 1	Applied Biosystems	Mm00486906_m1	
Ctnna1 (mouse)	Catenin alpha 1	Applied Biosystems	Mm00486752_m1	
Ctnnb1 (mouse)	Catenin beta 1	Applied Biosystems	Mm00483039_m1	
Ctnd1 (mouse)	Catenin delta 1	Applied Biosystems	Mm00483042_m1	
Jup (mouse)	Junction plakoglobin	Applied Biosystems	Mm00550249_m1	
Igf2 (mouse)	Insulin-like growth factor 2	Applied Biosystems	Mm00439565_g1	
Dsg2 (human)	Desmoglein 2	Applied Biosystems	Hs00170071_m1	
Dsp (human)	Desmoplakin	Applied Biosystems	Hs00189422_m1	
Cdh1 (human)	Cadherin 1	Applied Biosystems	Hs00170423_m1	
Rpl19 (mouse)	Ribosomal protein L19	UCSF Helen Diller Cancer Center Genome Core		Forward: 5'-CCAAGAAGATTGACCGCCATA-3' Reverse: 5'-GTCAGCCAGGAGCTTCTTGC-3' Probe: 5'-CATCCTCATGGAGCACATCCACAAGC-3'
Gusb (human)	Glucuronidase beta	UCSF Helen Diller Cancer Center Genome Core		Forward: 5'-CTCATTGGAAATTTGCCGATT-3' Reverse: 5'-CCGAGTGAAGATCCCTTTTITA-3' Probe: 5'-TGAACAGTCACCGACGAGAGTGCTGG-3'

^a Assay IDs are provided for primers obtained from Applied Biosystems

^b Primer/probe sequences are provided for primers designed by the UCSF Helen Diller Family Comprehensive Cancer Center Genomics Core

Figure 2.1

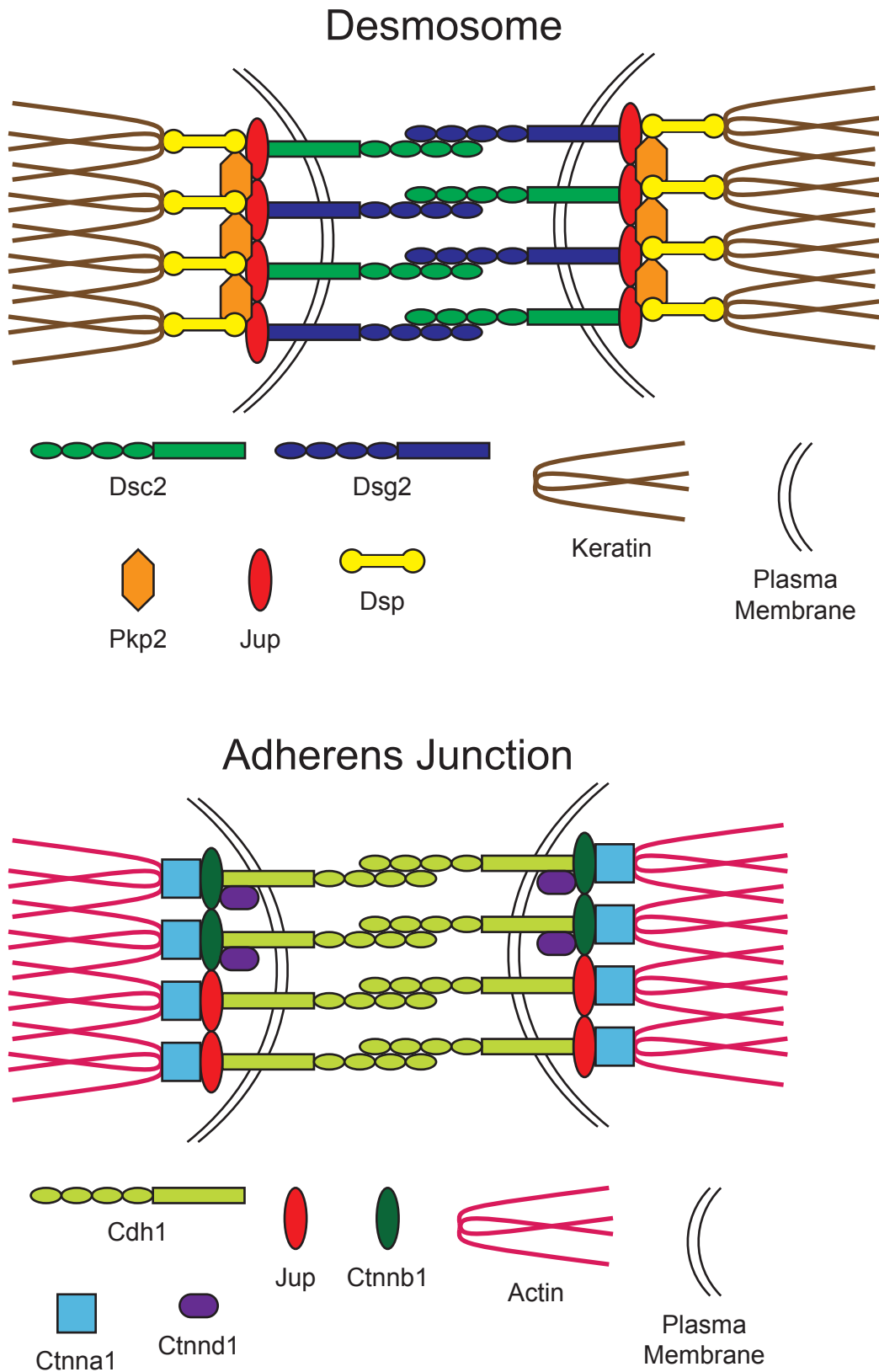


Figure 2.1. Structure of desmosomes and adherens junctions.

Desmosomes and adherens junctions (AJ) are cell-cell adhesion complexes that share a similar structure (Garrod and Chidgey 2008; Hartsock and Nelson 2008). Transmembrane proteins, the desmocollin (Dsc) and desmoglein (Dsg) proteins in the case of desmosomes and the cadherin (Cdh) proteins in the case of AJs, make interconnections between cells. These transmembrane proteins are connected to various intracellular proteins, desmoplakin (Dsp) and the plakophilin (Pkp) proteins in the case of desmosomes and the catenin (Ctnn) proteins in the case of AJs, which in turn form connections with the cytoskeleton. Desmosomes are linked to the keratin filaments while AJs are linked to the actin cytoskeleton. Schematics for desmosomes and AJs were adapted from (Cavallaro and Christofori 2004; Bazzi and Christiano 2007).

Figure 2.2

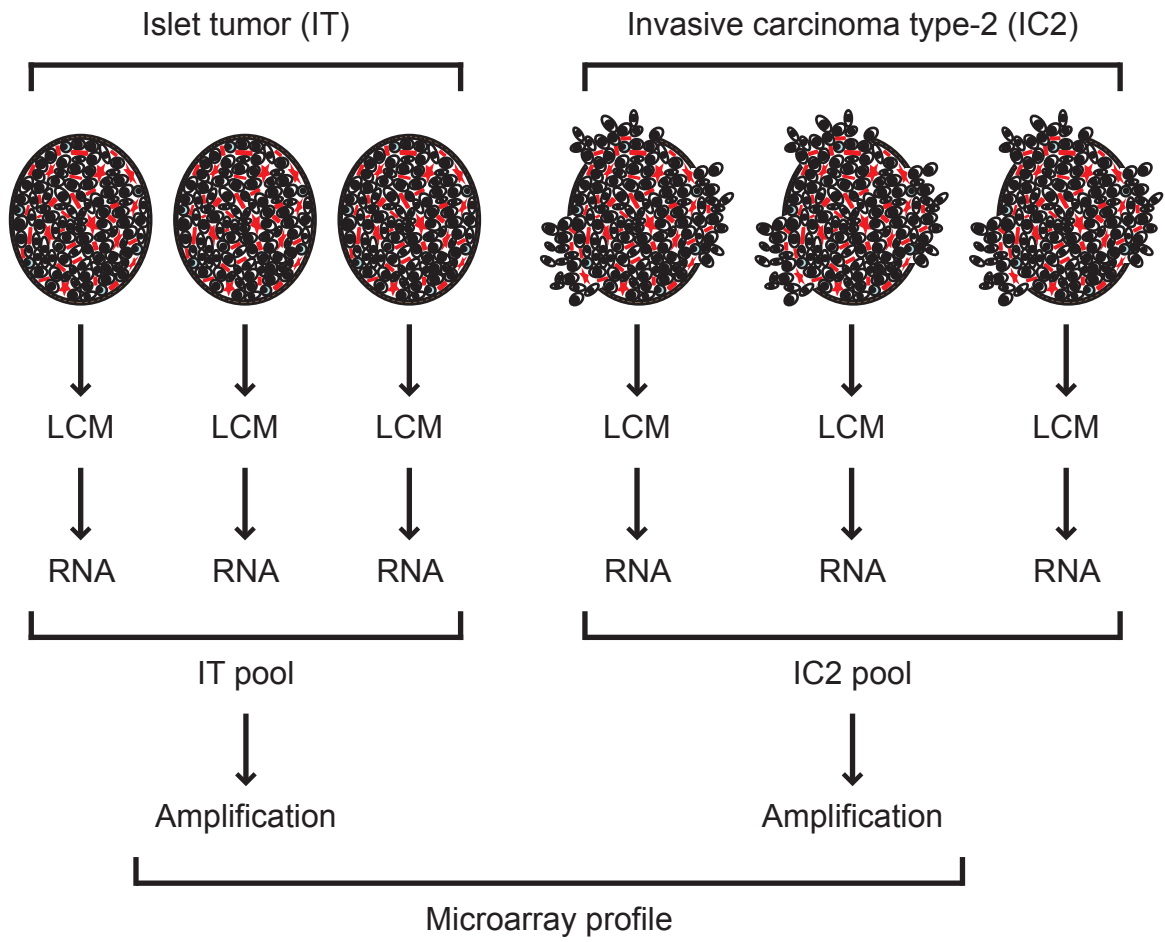


Figure 2.2. Laser capture microdissection of RT2 PNETs.

The non-invasive islet tumor (IT) class and the highly invasive carcinoma type-2 (IC2) class of RIP1-Tag2 (RT2) tumor lesions were transcriptionally profiled. IT and IC2 tumors were identified histologically, and then tissue was isolated by laser capture microdissection (LCM). RNA from individual tumors was pooled, and these pools were amplified and subsequently analyzed by microarray profiling of the mRNA transcriptome using Affymetrix microarrays.

Figure 2.3

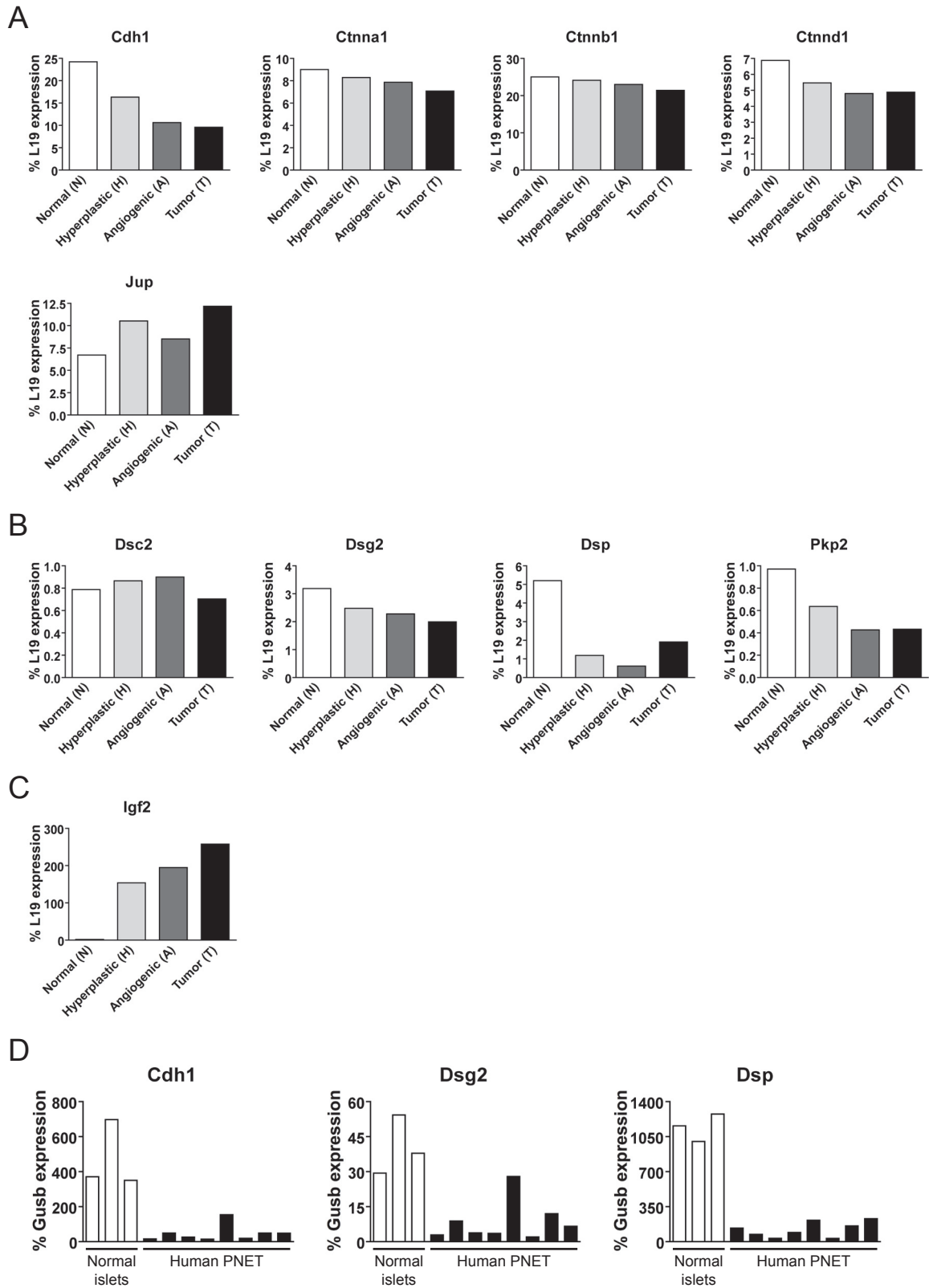


Figure 2.3. Expression of adherens junction and desmosomal components is decreased during PNET tumorigenesis in RT2 mice and in human pancreatic neuroendocrine tumors.

(A) Real-time quantitative PCR values for AJ components (cadherin 1 [Cdh1], catenin alpha 1 [Ctnna1], catenin beta 1 [Ctnnb1], catenin delta 1 [Ctnd1], junction plakoglobin [Jup]) during the stages of RT2 tumorigenesis – normal, hyperplastic, angiogenic, and tumor stage. Notably, in this analysis, whole ungraded RT2 PNETs were analyzed without knowledge of their invasiveness in contrast to the analysis presented in Table 2.1, which involved microdissected tissue from either widely invasive IC2 tumors or from non-invasive IT tumors. (B) Same as A except for desmosomal components (desmocollin 2 [Dsc2], desmoglein 2 [Dsg2], desmoplakin [Dsp], plakophilin 2 [Pkp2]). (C) Same as A except for the insulin-like growth factor 2 (Igf2), a gene whose expression is known to increase at the mRNA level during the later stages of RT2 tumorigenesis. (D) Real-time quantitative PCR values for Cdh1, Dsg2, and Dsp in pools of normal human pancreatic islets and individual human pancreatic neuroendocrine tumors (PNET). PNETs include ungraded primary and metastatic insulinomas, glucagonomas, and non-functional neuroendocrine tumors. Values are shown as the percent expression of the housekeeping genes ribosomal protein L19 (L19) (A–C) or glucuronidase beta (Gusb) (D).

Figure 2.4

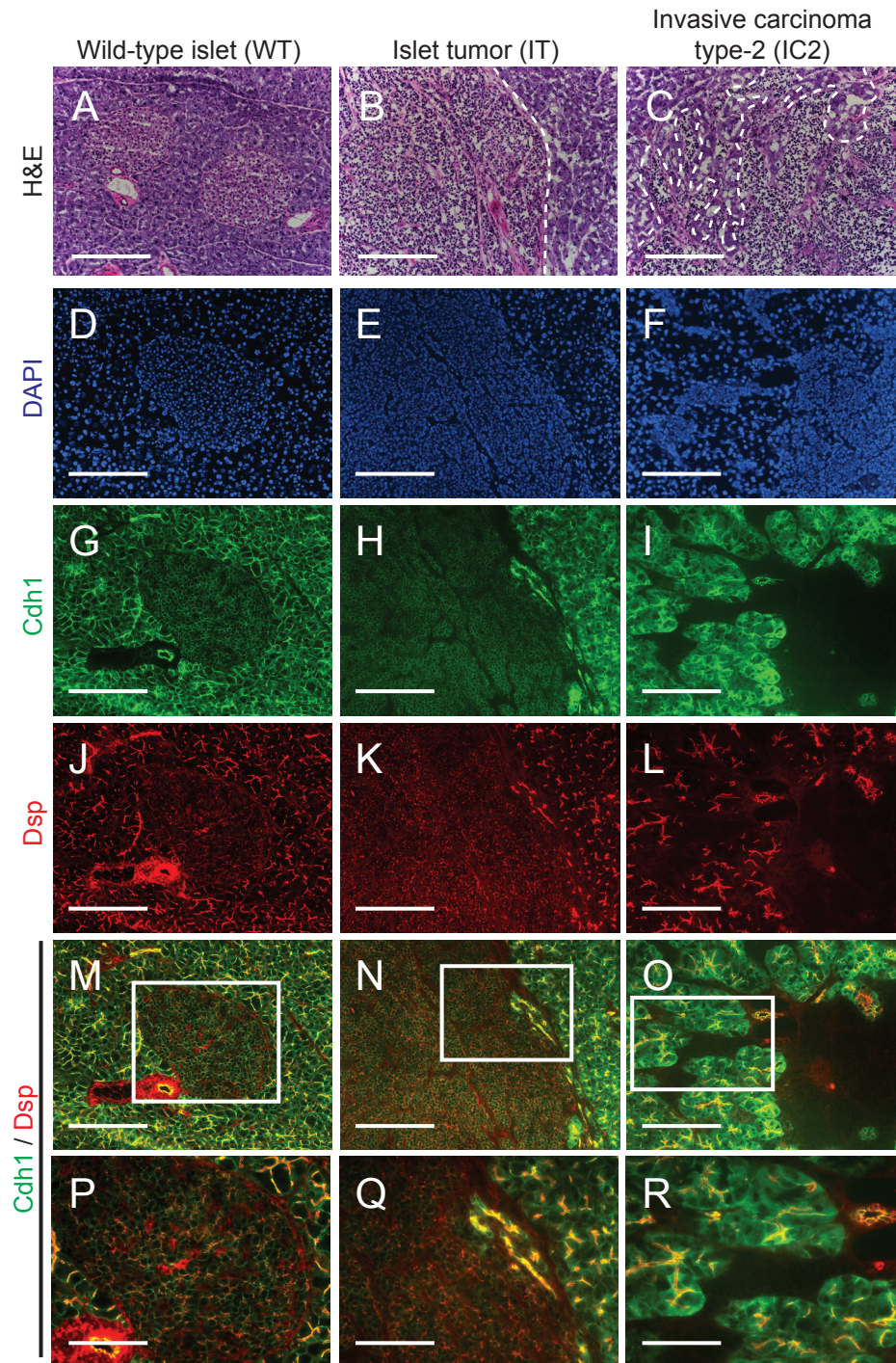


Figure 2.4. Desmoplakin and cadherin 1 expression in wild-type islets and RT2 PNETs.

Expression of desmoplakin (Dsp) and cadherin 1 (Cdh1) is lost in the IC2 but not the IT grade of PNET in RT2 mice. (A–C) H&E staining of a normal islet from a wild-type B6 mouse and of an IT and an IC2 tumor from an end-stage RT2 mouse. Dashed lines demarcate tumor margins. (D–F) Immunofluorescence staining with DAPI to visualize cellularity. (G–I) Immunofluorescence staining for Cdh1. (J–L) Immunofluorescence staining for Dsp. (M–O) Merge of Cdh1 and Dsp immunofluorescence staining (G–L). (P–R) Higher magnification of the boxed regions in M–O. Scale bars represent 200 μm (A–O) and 100 μm (P–R).

Figure 2.5

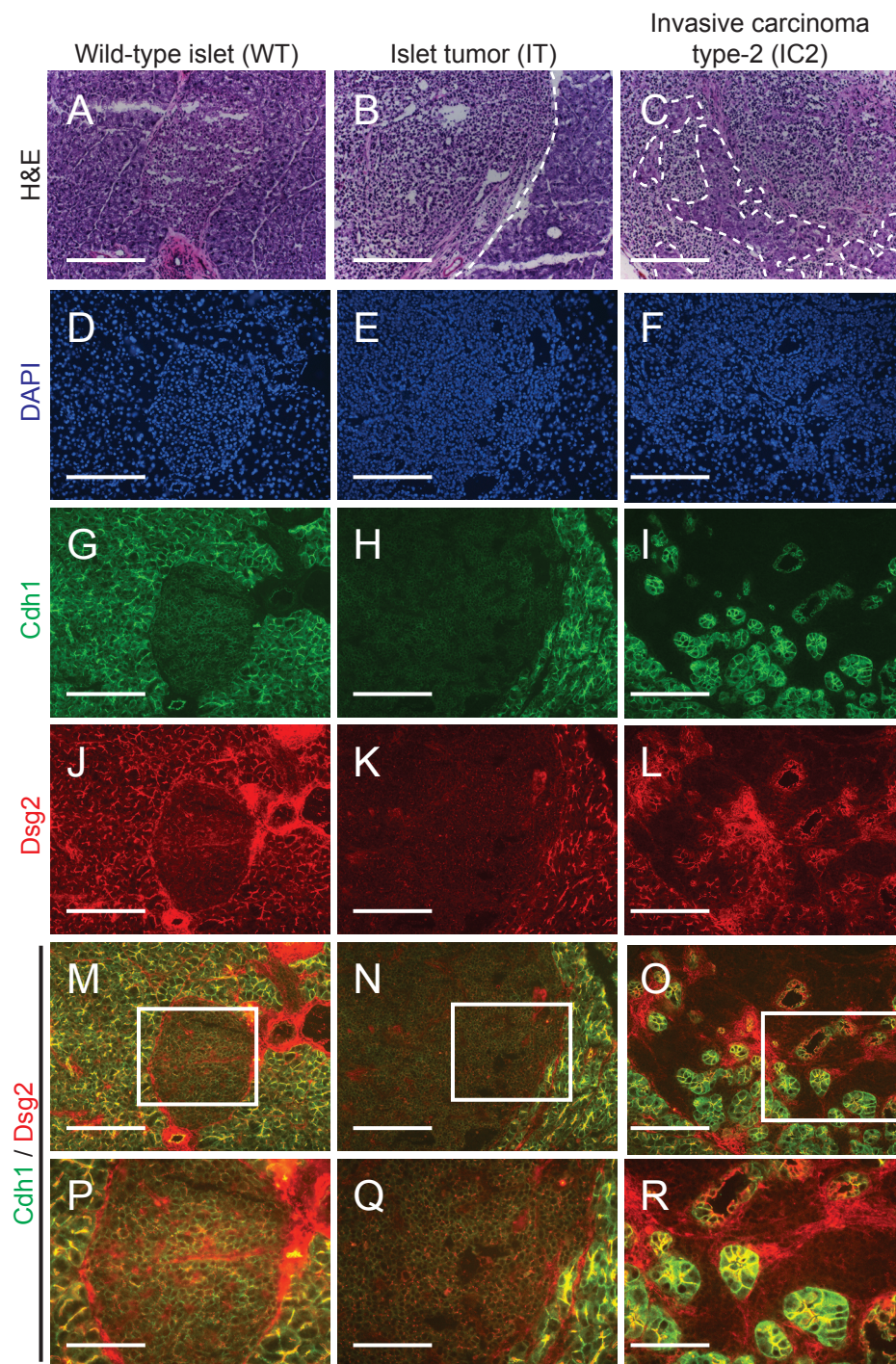


Figure 2.5. Desmoglein 2 expression in RT2 PNETs.

Expression of desmoglein 2 (Dsg2) is lost in the IC2 but not the IT grade of PNET in RT2 mice. (A–C) H&E staining of a normal islet from a wild-type B6 mouse and an IT and IC2 lesion from an end-stage RT2 mouse. Dashed lines demarcate tumor margins. (D–F) Immunofluorescence staining with DAPI to reveal cellularity. (G–I) Immunofluorescence staining for Cdh1. (J–L) Immunofluorescence staining for Dsg2. (M–O) Merge of Cdh1 and Dsg2 immunofluorescence staining (G–L). (P–R) Higher magnification of the boxed regions in M–O. Scale bars represent 200 μm (A–O) and 100 μm (P–R).

Figure 2.6

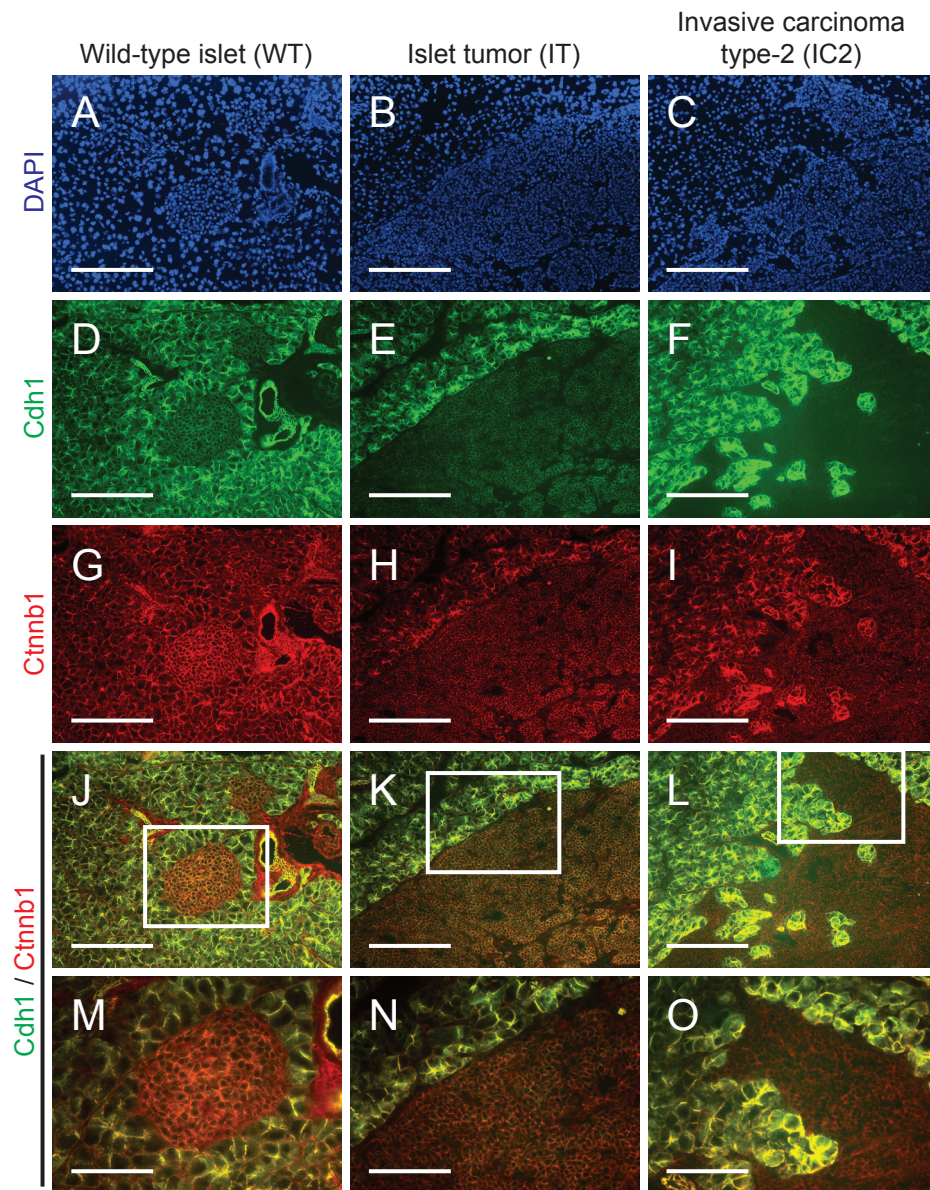


Figure 2.6. Catenin beta 1 expression in RT2 PNETs.

Expression of catenin beta 1 (Ctnnb1) is maintained in both the IT and IC2 grades of PNET in RT2 mice. (A–C) Immunofluorescence staining with DAPI to reveal cellularity of a normal islet from a wild-type B6 mouse and an IT and IC2 tumor from an end-stage RT2 mouse. (D–F) Immunofluorescence staining for Cdh1. (G–I) Immunofluorescence staining for Ctnnb1. (J–L) Merge of Cdh1 and Ctnnb1 immunofluorescence staining (D–I). (M–O) Higher magnification of the boxed regions in J–L. Scale bars represent 200 μm (A–L) and 100 μm (M–O).

Figure 2.7

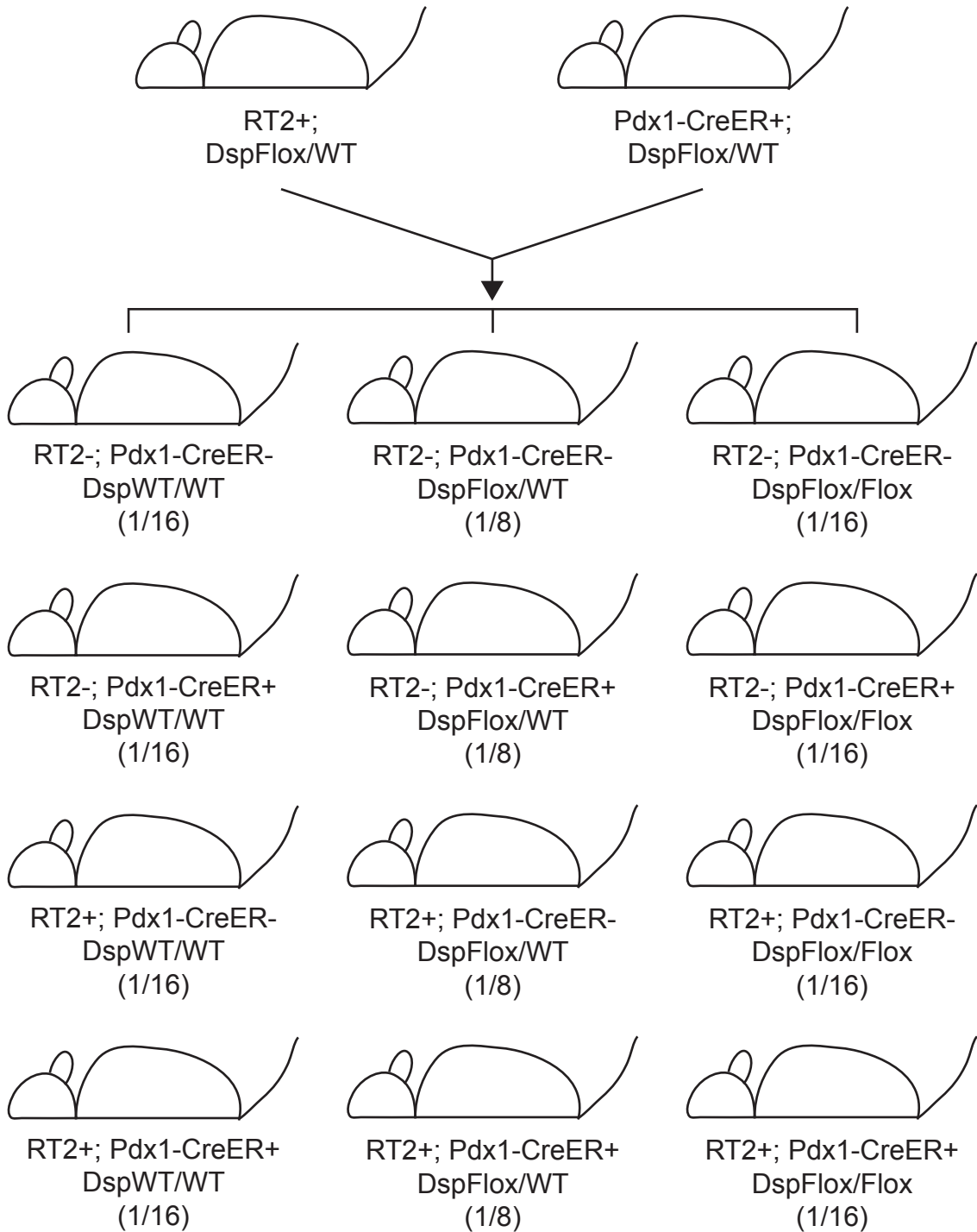


Figure 2.7. Breeding scheme to produce RT2+; Pdx1-Cre^{ER+}; Dsp^{Flox/Flox} mice.

Schematic of the intercross to produce RIP1-Tag2 (RT2) mice in which the desmoplakin (Dsp) gene was genetically deleted in the pancreatic β cells. RT2+; Dsp^{Flox/WT} mice were intercrossed with Pdx1-Cre^{ER+}; Dsp^{Flox/WT} mice to produce RT2+; Pdx1-Cre^{ER+}; Dsp^{Flox/Flox} mice and littermate control mice. Pdx1-Cre^{ER+}-positive mice carry a transgene in which a tamoxifen-inducible Cre recombinase is under the control of the pancreatic duodenal homeobox gene 1 promoter (Pdx1), which is expressed in all pancreatic lineages during embryogenesis and is variably expressed in the adult pancreas, in particular being widely expressed in the β cells (Offield et al. 1996; Gidekel Friedlander et al. 2009). All possible genetic combinations for this intercross are shown.

Figure 2.8

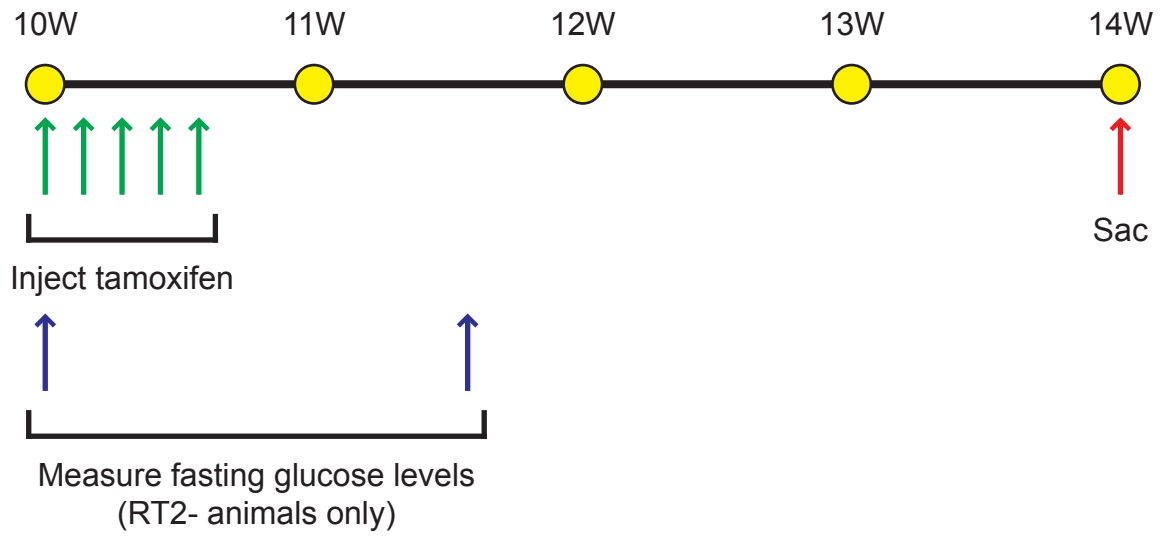


Figure 2.8. Tamoxifen dose regimen used to induce Pdx1-Cre^{ER} activity.

Schematic of the tamoxifen dosing regimen used to induce Cre activity in Pdx1-Cre^{ER}-positive mice. All Pdx1-Cre^{ER}-positive mice were injected with five consecutive doses of tamoxifen suspended in oil beginning at 10 weeks of age, when incipient tumors are first observed in RIP1-Tag2 (RT2) mice (Bergers et al. 1999), and all mice were sacrificed at 14 weeks of age. The fasting glucose levels were measured in the RT2-negative population immediately prior to the first tamoxifen injection and one week after the final tamoxifen injection. A similar dosing regimen was employed with unmanipulated RT2 mice to assess any effects of tamoxifen on RT2 tumorigenesis.

Figure 2.9

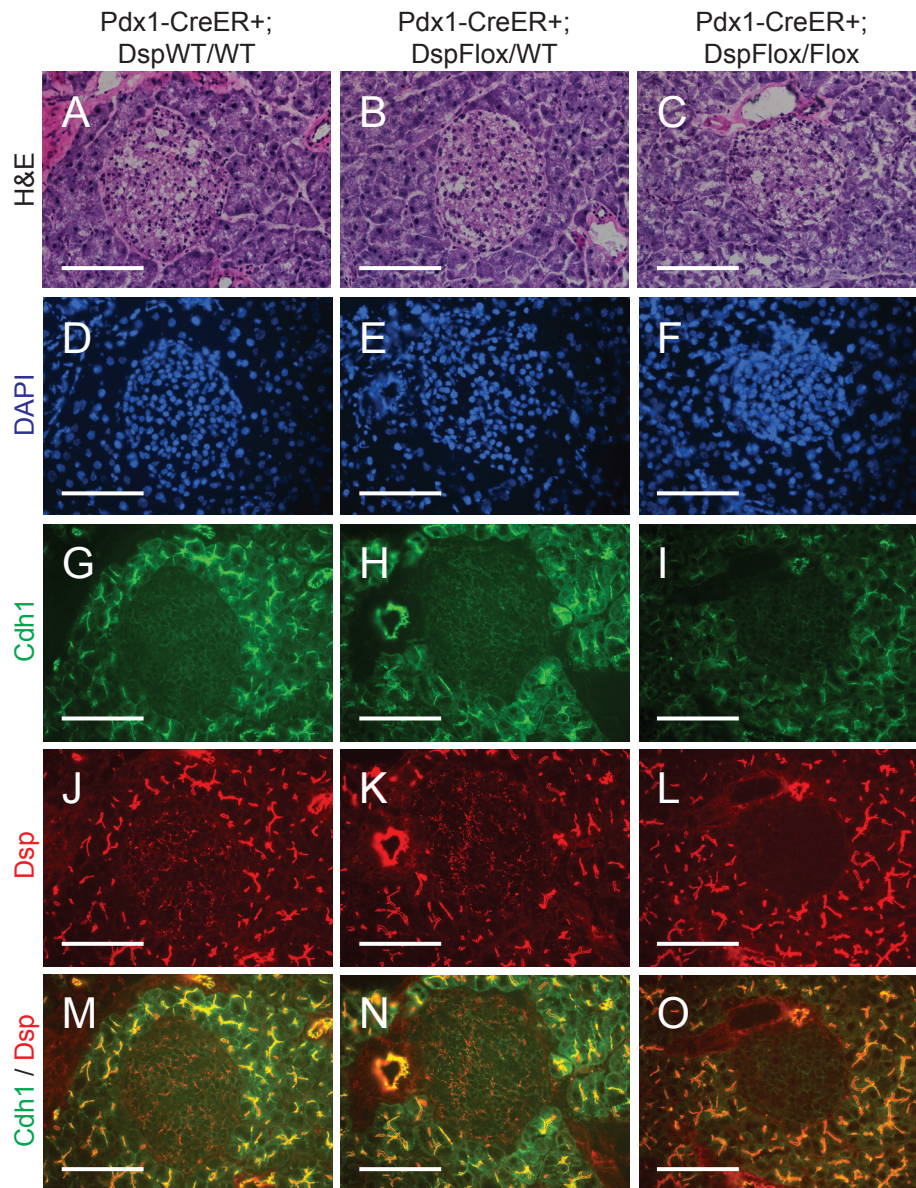


Figure 2.9. Genetic deletion of desmoplakin does not affect cadherin 1 expression in the pancreatic islets.

Expression of Cdh1 is maintained following conditional genetic deletion of Dsp in the pancreatic islets of control mice lacking the RT2 oncogenic transgene. (A–C) H&E staining of pancreatic islets in Pdx1-Cre^{ER+}; Dsp^{WT/WT}, Pdx1-Cre^{ER+}; Dsp^{Flox/WT}, and Pdx1-Cre^{ER+}; Dsp^{Flox/Flox} mice at 14 weeks. Cre activity was induced at 10 weeks. (D–F) Immunofluorescence staining with DAPI to reveal cellularity. (G–I) Immunofluorescence staining for Cdh1. (J–L) Immunofluorescence staining for Dsp. (M–O) Merge of Cdh1 and Dsp immunofluorescence staining (G–L). Scale bars represent 100 μm (A–O).

Figure 2.10

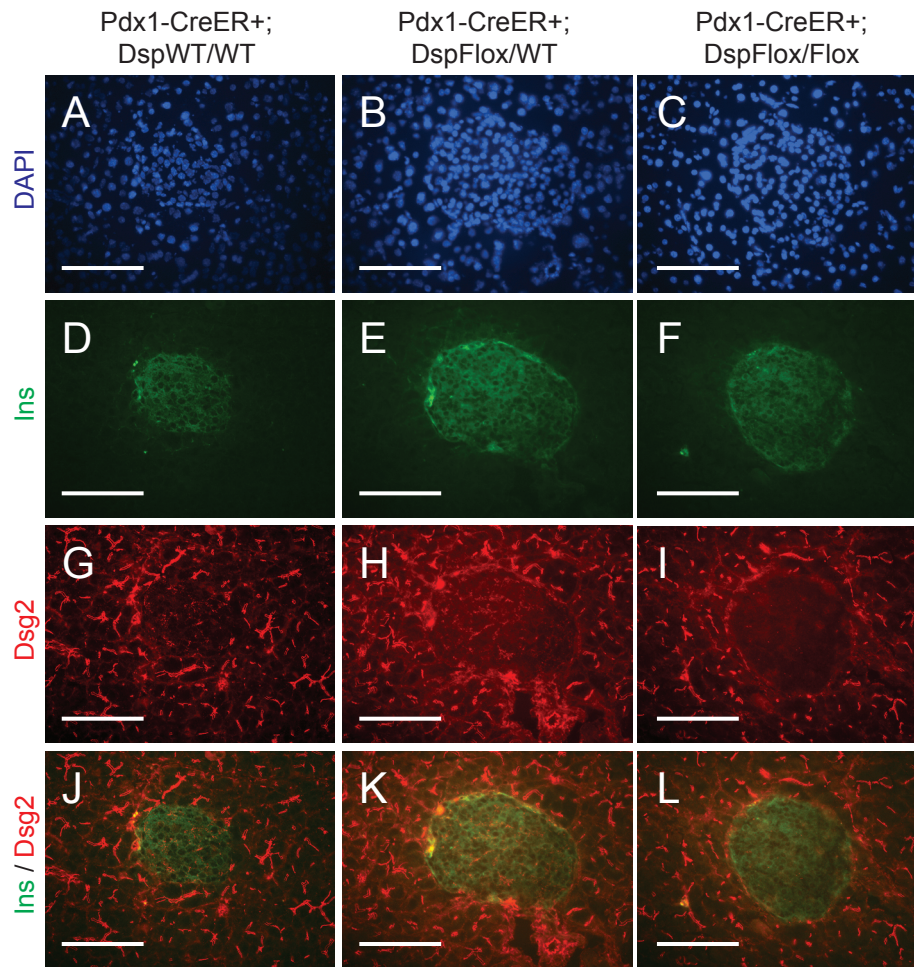
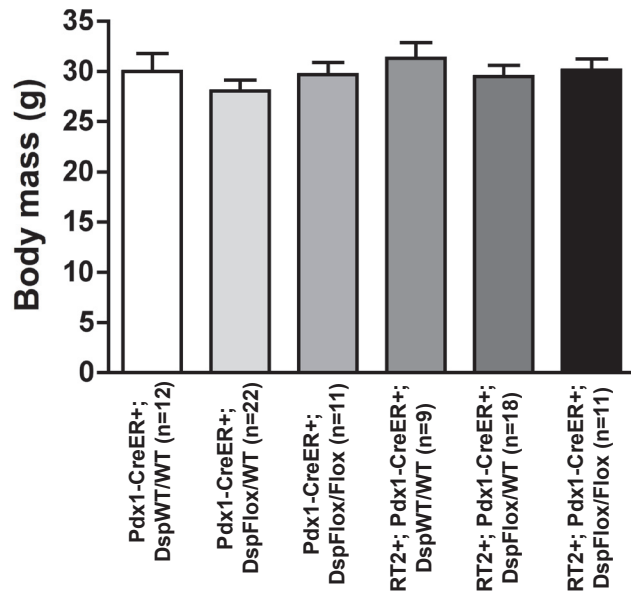


Figure 2.10. Genetic deletion of desmoplakin leads to decreased desmoglein 2 expression but not insulin expression in the pancreatic islets.

Expression of Dsg2 but not insulin (Ins) is concomitantly lost in the adult pancreatic islets following conditional genetic deletion of Dsp in mice lacking the RT2 oncogenic transgene. (A–C) Immunofluorescence staining with DAPI to reveal cellularity in pancreatic islets in Pdx1-Cre^{ER+}; Dsp^{WT/WT}, Pdx1-Cre^{ER+}; Dsp^{Flox/WT}, and Pdx1-Cre^{ER+}; Dsp^{Flox/Flox} mice at 14 weeks. Cre activity was induced at 10 weeks. (D–F) Immunofluorescence staining for Ins. (G–I) Immunofluorescence staining for Dsg2. (J–L) Merge of Ins and Dsg2 immunofluorescence staining (D–I). Scale bars represent 100 μ m (A–L).

Figure 2.11

A



B

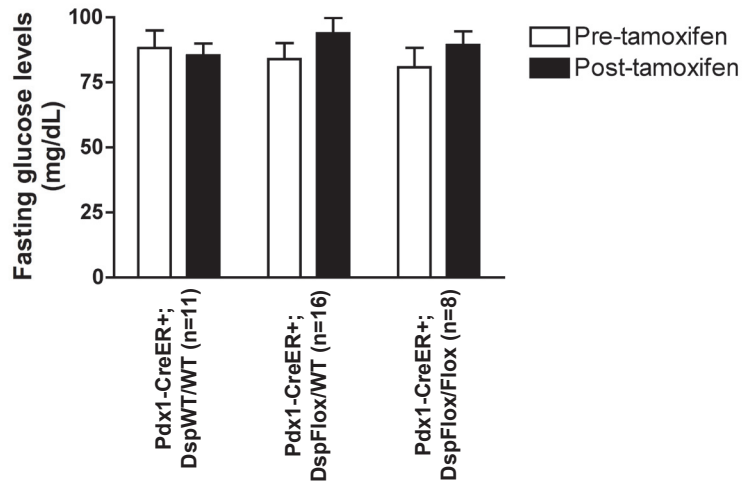


Figure 2.11. Genetic deletion of desmoplakin in the pancreatic islets does not affect multiple physiological parameters.

Conditional genetic deletion of Dsp has no effect on the physiological parameters of body mass and islet function in regulating glucose levels. (A) Body mass of Pdx1-Cre^{ER+}; Dsp^{WT/WT}, Pdx1-Cre^{ER+}; Dsp^{Flox/WT}, Pdx1-Cre^{ER+}; Dsp^{Flox/Flox}, RT2+; Pdx1-Cre^{ER+}; Dsp^{WT/WT}, RT2+; Pdx1-Cre^{ER+}; Dsp^{Flox/WT}, and RT2+; Pdx1-Cre^{ER+}; Dsp^{Flox/Flox} mice at 14 weeks. Cre activity was induced at 10 weeks. Groups are not statistically different. (B) Fasting glucose levels in Pdx1-Cre^{ER+}; Dsp^{WT/WT}, Pdx1-Cre^{ER+}; Dsp^{Flox/WT}, and Pdx1-Cre^{ER+}; Dsp^{Flox/Flox} mice. Cre activity was induced at 10 weeks. Mice were fasted for 14–16 hours. Glucose levels were measured immediately prior to the first tamoxifen dose and one week following the last tamoxifen dose. Pre- and post-tamoxifen glucose levels within and between groups are not statistically different.

Figure 2.12

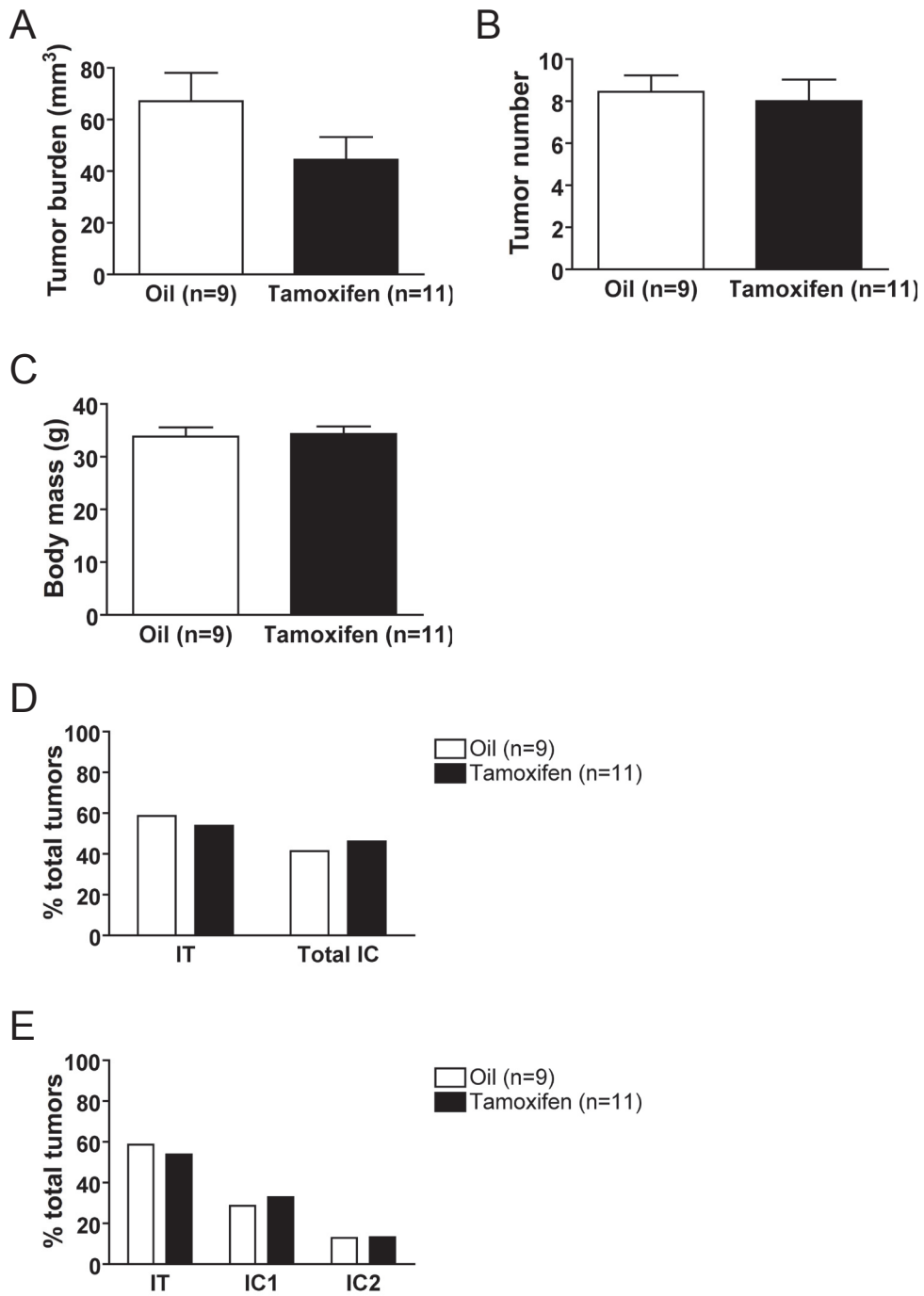


Figure 2.12. Tamoxifen does not affect the parameters of RT2 tumorigenesis.

Tamoxifen does not affect PNET tumorigenesis in unmodified RT2 transgenic mice. Cohorts of male RT2 mice that were $Dsp^{WT/WT}$ and that lacked the $Pdx1-Cre^{ER}$ allele were treated with five consecutive daily doses of tamoxifen or vehicle at 10 weeks of age and sacrificed 4 weeks later. (A–C) Tumor burden, tumor number, and body mass at time of sacrifice for RT2 mice treated with tamoxifen or vehicle. Data shown are mean plus standard error. Groups are not statistically different for these metrics. (D) Quantification of tumor invasiveness represented as the percentage of IT lesions or total IC lesions (IC1+IC2) in RT2 mice treated with tamoxifen or vehicle. A minimum of 76 tumors per group was graded. Groups are not statistically different. (E) Same as D except IC lesions are separated into the IC1 and IC2 subclasses. Groups are not statistically different.

Figure 2.13

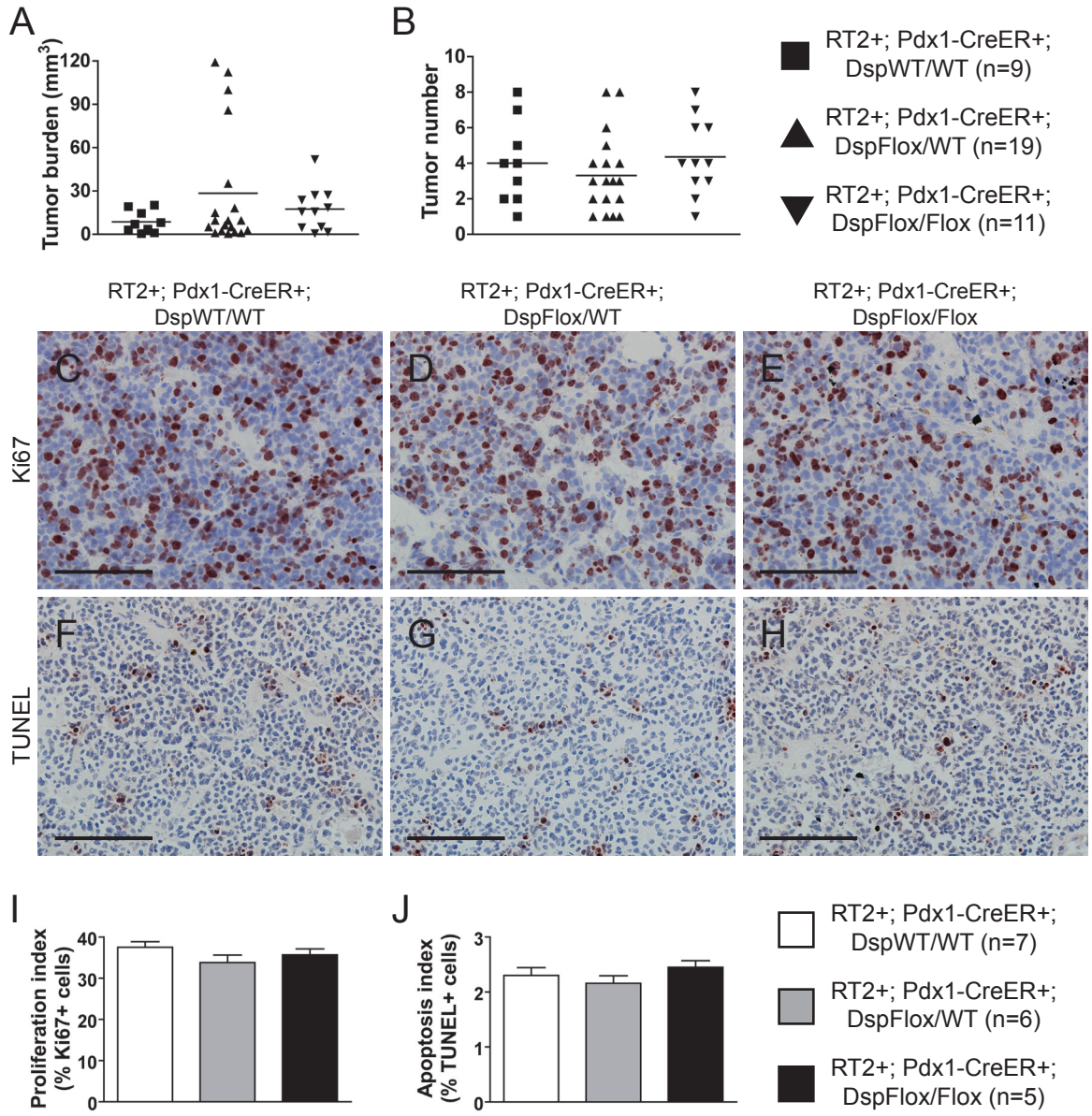


Figure 2.13. Genetic deletion of desmoplakin does not affect tumor growth parameters in RT2 PNETs.

Conditional genetic deletion of *Dsp* in angiogenic islet dysplasias and incipient solid tumors does not affect tumor formation or tumor growth parameters in RT2 mice. (A–B) Tumor burden and tumor number in RT2+; Pdx1-Cre^{ER+}; *Dsp*^{WT/WT}, RT2+; Pdx1-Cre^{ER+}; *Dsp*^{Flox/WT}, and RT2+; Pdx1-Cre^{ER+}; *Dsp*^{Flox/Flox} mice. Cre activity was induced at 10 weeks, and mice were sacrificed at 14 weeks. Data shown are individual values plus mean. Groups are not statistically different for these metrics. (C–E) Ki67 staining on tumors from RT2+; Pdx1-Cre^{ER+}; *Dsp*^{WT/WT}, RT2+; Pdx1-Cre^{ER+}; *Dsp*^{Flox/WT}, and RT2+; Pdx1-Cre^{ER+}; *Dsp*^{Flox/Flox} mice. (F–H) TUNEL staining on tumors from RT2+; Pdx1-Cre^{ER+}; *Dsp*^{WT/WT}, RT2+; Pdx1-Cre^{ER+}; *Dsp*^{Flox/WT}, and RT2+; Pdx1-Cre^{ER+}; *Dsp*^{Flox/Flox} mice. (I) Quantification of C–E. Data shown are mean plus standard error. Groups are not statistically different. (J) Quantification of F–H. Data shown are mean plus standard error. Groups are not statistically different. Scale bars represent 100 μ m (C–H).

Figure 2.14

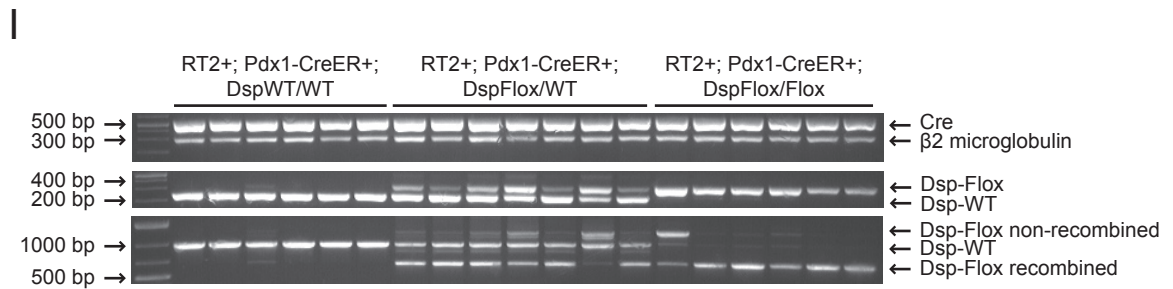
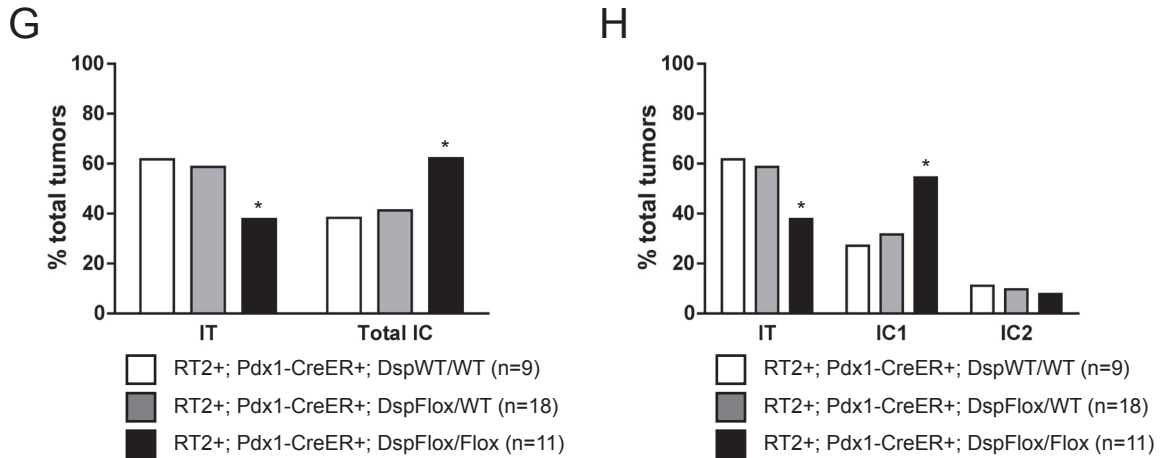
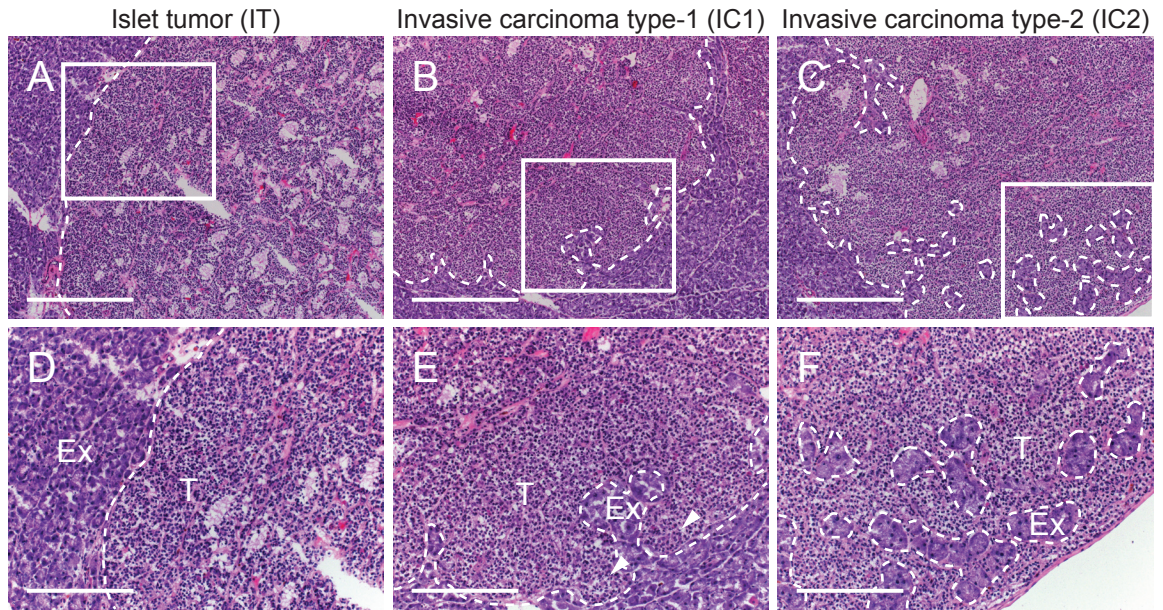


Figure 2.14. Genetic deletion of desmoplakin leads to increased local tumor invasion in RT2 mice.

Conditional genetic deletion of Dsp in angiogenic islet dysplasias and incipient solid tumors increases the rate of progression to focally invasive IC1 tumors in RT2 mice. (A–C) H&E staining of a non-invasive IT tumor lesion, a focally invasive IC1 tumor lesion, and a broadly invasive IC2 tumor lesion from RT2+; Pdx1-Cre^{ER+}; Dsp^{WT/WT}, RT2+; Pdx1-Cre^{ER+}; Dsp^{Flox/WT}, and RT2+; Pdx1-Cre^{ER+}; Dsp^{Flox/Flox} mice. (D–F) Higher magnification of the boxed regions in A–C. T indicates tumor region and Ex indicates exocrine pancreas. Dashed lines demarcate tumor margins. Arrowheads indicate regions of tumor invasion. (G) Quantification of tumor invasiveness represented as the percentage of IT lesions or total IC lesions (IC1+IC2) in RT2+; Pdx1-Cre^{ER+}; Dsp^{WT/WT}, RT2+; Pdx1-Cre^{ER+}; Dsp^{Flox/WT}, and RT2+; Pdx1-Cre^{ER+}; Dsp^{Flox/Flox} mice at 14 weeks of age. A minimum of 36 tumors per group was graded. * p<0.01 by Fisher's exact test. (H) Same as G except IC lesions are separated into the IC1 and IC2 subclasses. * p<0.01 by the Chi-square test. (I) Tumors from RT2+; Pdx1-Cre^{ER+}; Dsp^{WT/WT}, RT2+; Pdx1-Cre^{ER+}; Dsp^{Flox/WT}, and RT2+; Pdx1-Cre^{ER+}; Dsp^{Flox/Flox} mice were genotyped for the presence of the Cre recombinase (~530 bp), β 2 microglobulin (~290 bp), and the floxed (~360 bp) or wild-type Dsp allele (~230 bp). These same tumors were assessed for the recombination status of Dsp: wild-type allele (~960 bp), non-recombined floxed allele (~1200 bp), recombined floxed allele (~650 bp). Scale bars represent 400 μ m (A–C) and 200 μ m (D–F).

Figure 2.15

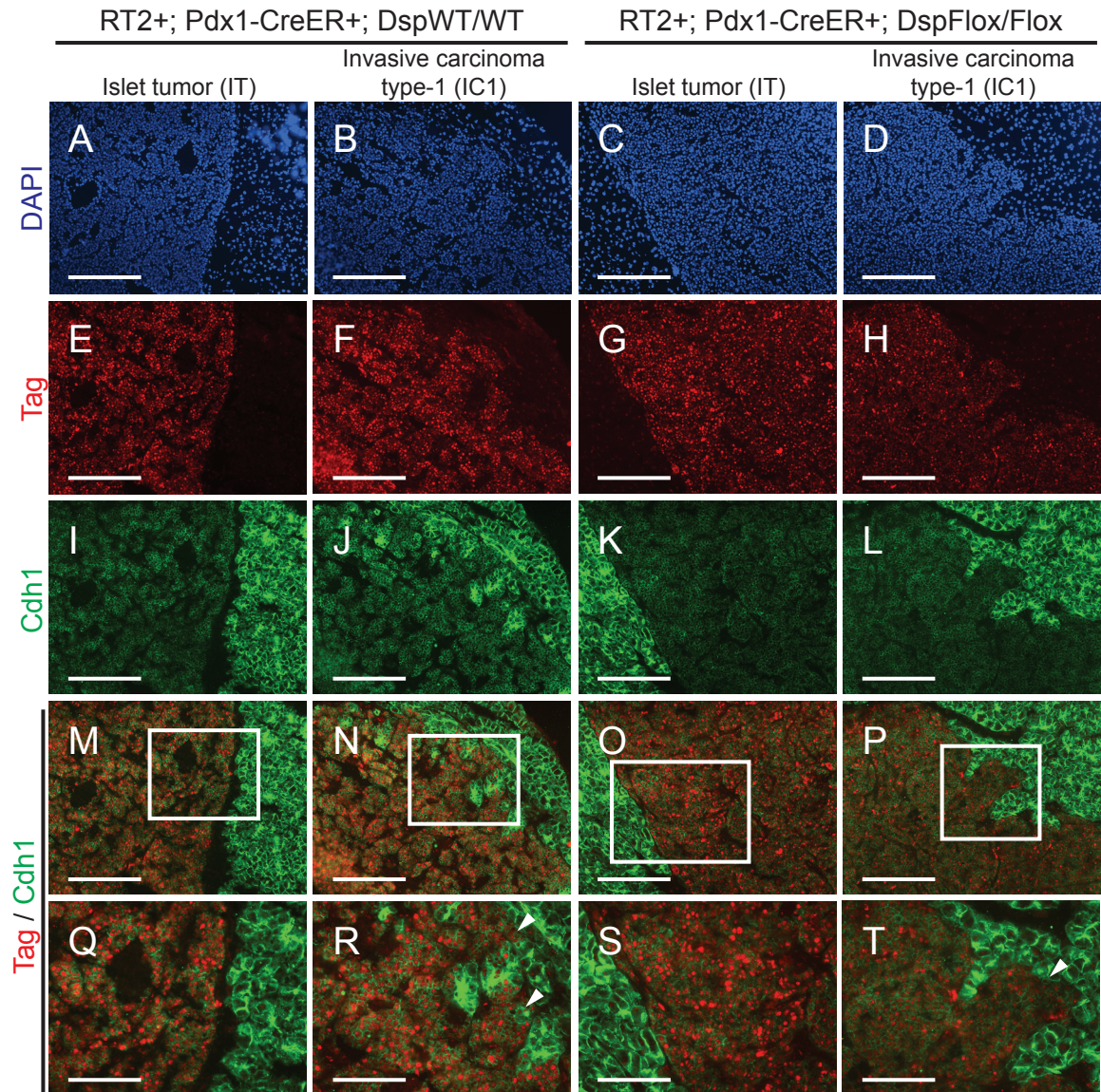


Figure 2.15. Genetic deletion of desmoplakin does not affect cadherin 1 expression in RT2 PNETs.

Cdh1 expression is maintained in the IC1 grade of tumors in both RT2+; Pdx1-Cre^{ER+}; Dsp^{WT/WT} and RT2+; Pdx1-Cre^{ER+}; Dsp^{Flox/Flox} mice. (A–D) Immunofluorescence staining with DAPI to reveal cellularity in IT and IC1 tumors in RT2+; Pdx1-Cre^{ER+}; Dsp^{WT/WT} and RT2+; Pdx1-Cre^{ER+}; Dsp^{Flox/Flox} mice. (E–H) Immunofluorescence staining for the oncoprotein T antigen (Tag). (I–L) Immunofluorescence staining for Cdh1. (M–P) Merge of Tag and Cdh1 immunofluorescence staining (E–L). (Q–T) Higher magnification of the boxed regions in M–P. Arrowheads indicate regions of tumor invasion. Scale bars represent 200 μm (A–P) and 100 μm (Q–T).

Figure 2.16

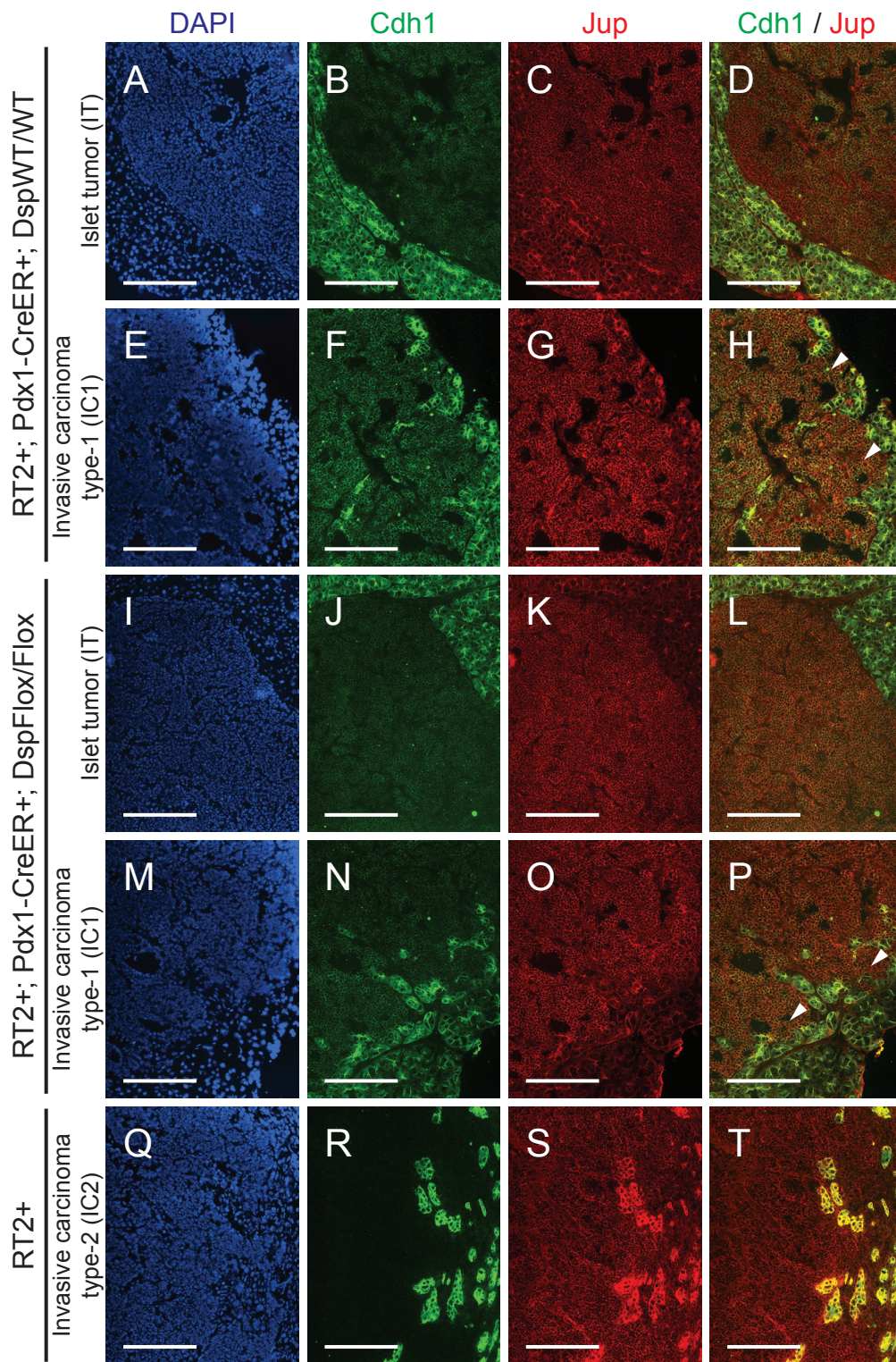


Figure 2.16. Genetic deletion of desmoplakin does not affect junction plakoglobin expression in RT2 PNETs.

Junction plakoglobin (Jup, also known as gamma catenin) expression is maintained in the IC1 grade of tumors in both RT2+; Pdx1-Cre^{ER+}; Dsp^{WT/WT} and RT2+; Pdx1-Cre^{ER+}; Dsp^{Flox/Flox} mice. (A–D) Immunofluorescence staining for DAPI to reveal cellularity, Cdh1, Jup, and merge of Cdh1 and Jup staining in an IT PNET from a RT2+; Pdx1-Cre^{ER+}; Dsp^{WT/WT} mouse. (E–H) Same as A–D except for an IC1 PNET from a RT2+; Pdx1-Cre^{ER+}; Dsp^{WT/WT} mouse. (I–L) Same as A–D except for an IT PNET from a RT2+; Pdx1-Cre^{ER+}; Dsp^{Flox/Flox} mouse. (M–P) Same as A–D except for an IC1 PNET from a RT2+; Pdx1-Cre^{ER+}; Dsp^{Flox/Flox} mouse. (Q–T) Same as A–D except for an IC2 PNET from an unmanipulated RT2+ mouse. Arrowheads indicate regions of tumor invasion. Scale bars represent 200 μm .

Figure 2.17

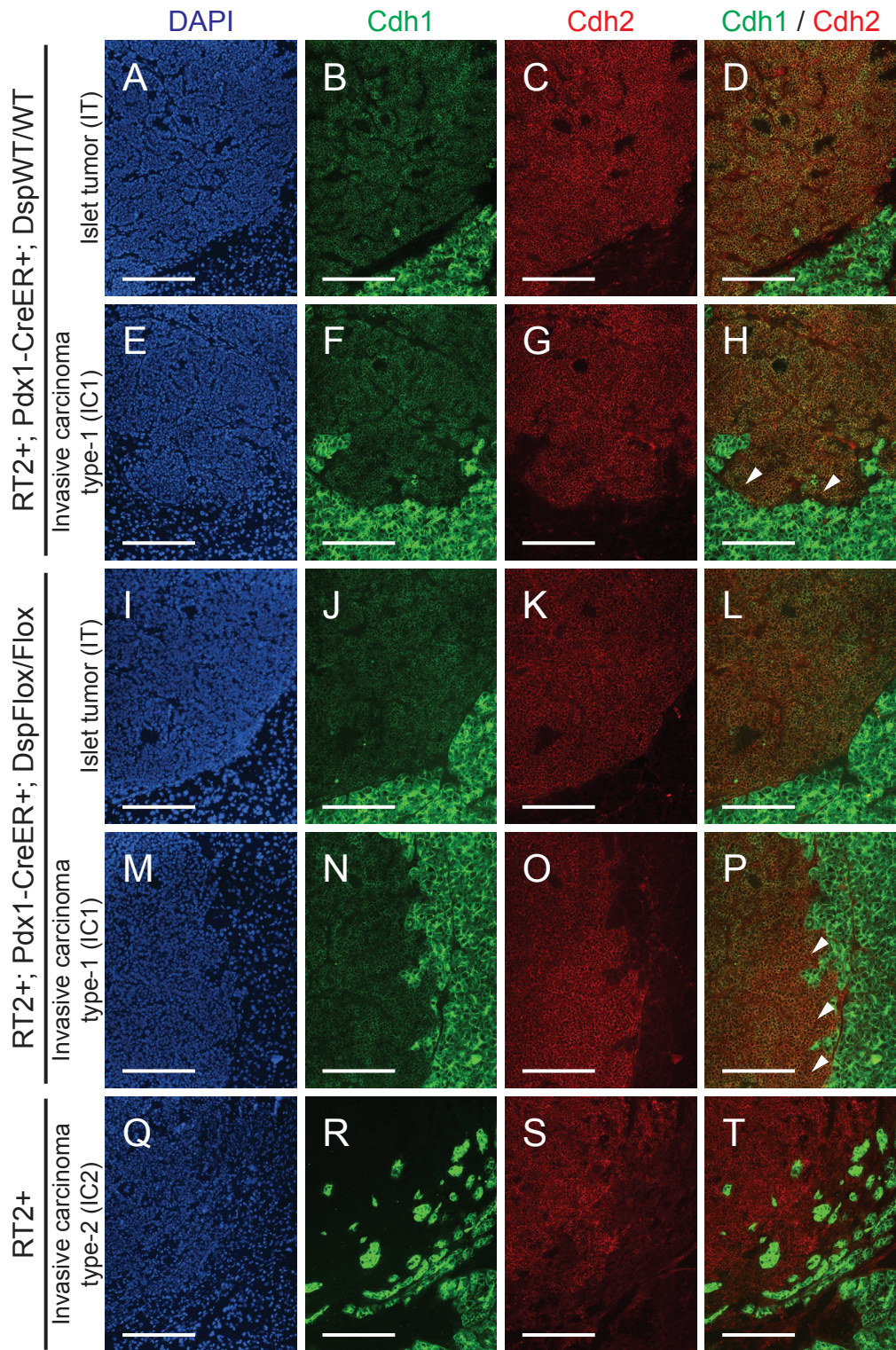


Figure 2.17. Genetic deletion of desmoplakin does not affect cadherin 2 expression in RT2 PNETs.

Cadherin 2 (Cdh2, also known as N-cadherin) expression is maintained in the IC1 grade of tumors in both RT2+; Pdx1-Cre^{ER+}; Dsp^{WT/WT} and RT2+; Pdx1-Cre^{ER+}; Dsp^{Flox/Flox} mice. (A–D) Immunofluorescence staining for DAPI to reveal cellularity, Cdh1, Cdh2, and merge of Cdh1 and Cdh2 staining in an IT PNET from a RT2+; Pdx1-Cre^{ER+}; Dsp^{WT/WT} mouse. (E–H) Same as A–D except for an IC1 PNET from a RT2+; Pdx1-Cre^{ER+}; Dsp^{WT/WT} mouse. (I–L) Same as A–D except for an IT PNET from a RT2+; Pdx1-Cre^{ER+}; Dsp^{Flox/Flox} mouse. (M–P) Same as A–D except for an IC1 PNET from a RT2+; Pdx1-Cre^{ER+}; Dsp^{Flox/Flox} mouse. (Q–T) Same as A–D except for an IC2 PNET from an unmanipulated RT2+ mouse. Arrowheads indicate regions of tumor invasion. Scale bars represent 200 μm .

Figure 2.18

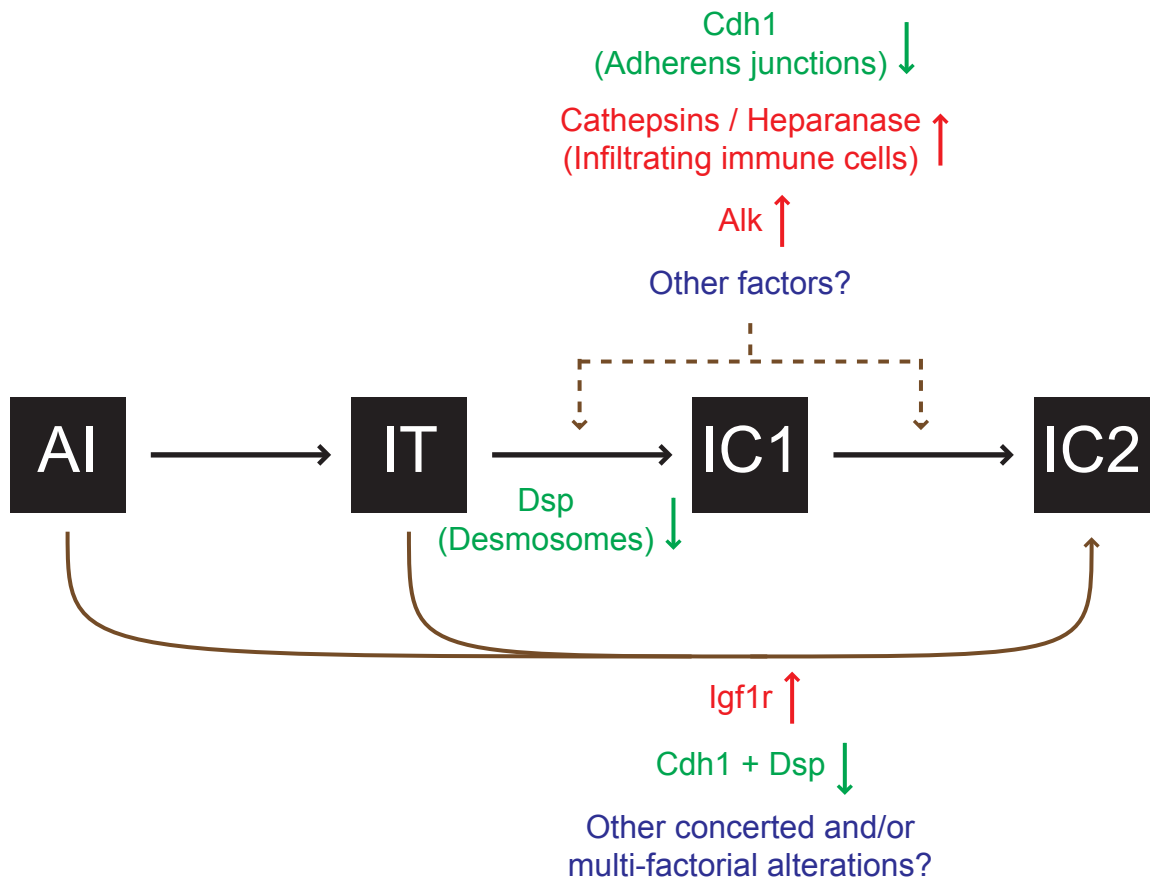


Figure 2.18. Progression to an invasive growth state is governed by multiple factors in the RT2 model of PNET.

Multiple factors impact the progression to an invasive phenotype as illustrated by the RIP1-Tag2 (RT2) mouse model of pancreatic neuroendocrine tumorigenesis (PNET). This study demonstrates that the genetic deletion of desmoplakin (Dsp) and concomitant loss/attenuation of desmosomal adhesion can promote local tumor invasion, specifically to a focally invasive type typified by the IC1 tumor class. Other factors have also been demonstrated to affect tumor invasion in this model. Activation of heparanase and cathepsin proteases (Joyce et al. 2005; Gocheva et al. 2006; Gocheva et al. 2010) supplied by infiltrating immune cells or suppression of cadherin 1 (Cdh1, also known as E-cadherin) (Perl et al. 1998) can each contribute to invasion. Upregulation of the type-1 insulin-like growth factor receptor (Igf1r) preferentially promotes progression to the IC2 stage, in part via a branched pathway from earlier neoplastic stages such as angiogenic islet dysplasias (AI), bypassing the canonical AI→IT→IC1→IC2 progression (Lopez and Hanahan 2002). Future research may well identify additional factors that impact tumor invasion.

Chapter 3.

**Polymorphic genetic control of tumor invasion in a mouse
model of pancreatic neuroendocrine carcinogenesis**

Abstract

Cancer is a disease subject to both genetic and environmental influences. In this study, we used the RIP1-Tag2 (RT2) mouse model of islet cell carcinogenesis to identify a genetic locus that influences tumor progression to an invasive growth state. RT2 mice inbred into the C57Bl/6 (B6) background develop both non-invasive pancreatic neuroendocrine tumors (PNET) as well as invasive carcinomas with varying degrees of aggressiveness. In contrast, RT2 mice inbred into the C3HeB/Fe (C3H) background are comparatively resistant to the development of invasive tumors as are RT2 C3HB6(F1) hybrid mice. Using linkage analysis, we identified a 13 Mb locus on mouse chromosome 17 with significant linkage to the development of highly invasive PNETs. A gene residing in this locus, the anaplastic lymphoma kinase (Alk), was expressed at significantly lower levels in PNETs from invasion-resistant C3H mice versus invasion-susceptible B6 mice, and pharmacological inhibition of Alk led to reduced tumor invasiveness in RT2 B6 mice. Collectively, our results demonstrate that tumor invasion is subject to polymorphic genetic control and identify Alk as a genetic modifier of invasive tumor growth.

Introduction

Cancer is a complex disease governed by environmental and genetic factors, including genetic mutations and polymorphisms that modulate cancer susceptibility (Balmain et al. 2003). While many investigations have focused on identifying factors that affect initial tumor development (Easton et al. 2007; Tomlinson et al. 2008), data from both human and mouse studies have demonstrated that genetic polymorphisms can modulate multiple aspects of tumorigenesis, such as tumor progression (Nagase et al. 1995; Lifsted et al. 1998; Park et al. 2005) and response to therapy (Sequist et al. 2007).

In this study, we investigated the effects of genetic background on tumor progression to an invasive growth state, motivated by a provocative observation that mice carrying the same oncogenic transgene but differing in genetic background developed tumors that were markedly distinctive in their invasiveness. This model, the RIP1-Tag2 (RT2) mouse model of islet cell carcinogenesis, develops multiple pancreatic neuroendocrine tumors (PNET) in a relatively synchronous and predictable multistage progression pattern by 12–14 weeks of age due to the expression of the SV40 T antigen oncoprotein (Tag) in the pancreatic β cells (Hanahan 1985). The tumorigenesis pathway has predominantly been studied in RT2 mice inbred into the C57Bl/6 (B6) background, and the PNETs that arise in this genetic context display a spectrum of invasive phenotypes and can be classified as non-invasive islet tumors (IT), focally invasive type-1 carcinomas (IC1), and broadly invasive type-2 carcinomas (IC2) (Lopez and Hanahan 2002). Surprisingly, we observed that when RT2 mice were inbred into a second strain, C3HeB/Fe (C3H), the tumors that arose were predominantly non-invasive, despite being otherwise similar in their tumorigenesis phenotype. The implication that the invasive

phenotype was influenced by genetic background prompted our investigation, which was aimed at assessing the hypothesis that a polymorphic modifier locus (or loci) mediated the susceptibility or resistance to the acquisition of the hallmark capability for invasive growth in the RT2 mouse model of cancer.

Results

PNET progression to invasive carcinoma is modulated by genetic background

Following anecdotal observations that PNETs developing in RT2 mice inbred into the C3H background were predominantly non-invasive, we carefully examined the distribution of the distinctive invasive phenotypes in *de novo* PNETs arising in RT2 mice inbred into either the B6 or C3H genetic backgrounds as well as in C3HB6(F1) hybrids (F1) to determine whether the parameter of tumor invasiveness was indeed affected by genetic background (Figure 3.1A–F).

The development of invasive carcinoma lesions (IC) was strongly suppressed in RT2 C3H mice. Whereas IC lesions constitute more than half of all tumors in RT2 B6 animals at 14 weeks, less than 15% of all tumors could be classified as invasive in RT2 C3H mice (Figure 3.1G). This reduction occurred in both the focally invasive IC1 and the widely invasive IC2 subclasses of invasive RT2 tumor lesions (Figure 3.1H). The development of IC lesions was also suppressed in RT2 F1 mice, and the overall distribution of invasive lesions in RT2 F1 mice was similar to RT2 C3H mice (Figure 3.1G–H). These data indicate that the C3H genetic background is resistant to the development of invasive RT2 PNETs, while the F1 phenotype demonstrates that the resistant C3H background is dominant over the susceptible B6 background.

We also examined other parameters of PNET tumorigenesis in the B6 and C3H backgrounds to determine whether additional phenotypes were similarly affected by genetic background. The average tumor burden per animal was significantly higher in both RT2 C3H and RT2 F1 mice as compared to RT2 B6 mice while the average number of macroscopic tumors per animal was higher in RT2 C3H mice as compared to RT2 B6

and RT2 F1 mice (Figure 3.2). However, there were no significant differences with regards to either the rate of tumor proliferation or tumor apoptosis (Figure 3.2). There was no indication that the driving oncogene was responsible for these phenotypic differences as the levels of the Tag oncoprotein were similar in tumors isolated from RT2 mice in the different genetic backgrounds (Figure 3.3), consistent with a previous assessment (Hager et al. 2004). Additionally, the expression of cadherin 1 (Cdh1, also known as E-cadherin), a known regulator of invasion in the RT2 model as well as other cancers (Perl et al. 1998), was not obviously different (Figure 3.3).

The invasive modifier does not act in the bone marrow derived tissue compartment

Since bone marrow derived (BMD) inflammatory cells that supply matrix-degrading enzymes such as cathepsin proteases and heparanase are functionally implicated in the invasive phenotype in this model (Joyce et al. 2005; Gocheva et al. 2006; Gocheva et al. 2010), we examined the possibility that the reduced invasiveness in RT2 C3H and RT2 F1 mice was due to deficiencies in the invasion-promoting functionality of BMD cells. We transferred bone marrow from B6 or F1 donor mice into RT2 F1 animals with the rationale that B6 but not F1 bone marrow would “rescue” the invasive phenotype in recipient RT2 F1 mice if the invasive modifier operated in this tissue compartment (Figure 3.4). RT2 F1 mice were chosen as recipients since they develop invasive PNETs at a reduced frequency (Figure 3.1G–H) and should also be capable of receiving bone marrow from either B6 or F1 donors without host/donor incompatibility complications. In brief, we did not observe any differences in the invasive phenotype or in any other parameter of RT2 tumorigenesis in RT2 F1 mice

whose immune systems had been rendered B6 (Figures 3.5, 3.6). These results suggest that the polymorphic difference is operative in the cancer cells themselves or possibly in other cellular compartments of the stroma.

In light of the evident genetic differences in the frequency of developing invasive carcinomas in RT2 mice, we next sought to map the putative polymorphic locus/loci associated with susceptibility versus resistance to the invasive phenotype using standard genetic linkage analysis.

Linkage analysis identifies a region on chromosome 17 that is associated with the development of invasive carcinomas in RT2 mice

To identify the genetic locus/loci that modify the invasive phenotype in RT2 mice, we performed a genome wide linkage study. 143 RT2 N2 backcrossed mice, resulting from crossing RT2 F1 male mice with B6 female mice (Figure 3.7), were scored for the incidence of IT, IC1, and IC2 tumor lesions in addition to the other parameters of RT2 tumorigenesis (Dataset 3.1). Constitutional tail DNA was genotyped across 561 single nucleotide polymorphisms (SNP) that cover the mouse genome and discriminate between the B6 and C3H backgrounds (Figure 3.8, Dataset 3.1). Statistical analysis was subsequently performed using R/qtl to determine whether there was evidence of linkage to the development of invasive lesions or to any of the other RT2 tumor phenotypes. LOD scores of $\text{LOD} \geq 1.9$ and $\text{LOD} \geq 3.0$ were considered suggestive and significant linkage respectively (Lander and Kruglyak 1995).

Using the development of IT, IC1, or IC2 PNETs as quantitative traits, we observed significant linkage to four SNPs on chromosome 17 for the development of IC2

lesions, with a peak LOD score of 3.52 (Figure 3.9C, Dataset 3.2). The 95% confidence interval was located from 63.7–76.4 Mb, a 13 Mb region that contains over 50 annotated genes (Figure 3.9D). Interestingly, we did not identify any locus that was linked to the IC1 phenotype, despite the different frequencies in the development of this class of tumors in RT2 B6 and RT2 C3H mice (Figure 3.9B, Dataset 3.2).

Additionally, we observed significant linkage to the X chromosome to the development of IT lesions (Figure 3.9A, Dataset 3.2) and to the metric of tumor number (Figure 3.10, Dataset 3.2). In both situations, the linked region essentially spanned the entire chromosome, which complicated our efforts to analyze this region in further detail. We therefore proceeded to investigate the genes in the minimal region of chromosome 17 that showed significant linkage to the development of IC2 tumors.

The anaplastic lymphoma kinase resides in the chromosome 17 minimal region and is differentially expressed in the B6 and C3H genetic backgrounds

It has previously been suggested that genetic polymorphisms can influence the levels of gene expression in the context of phenotypic modifiers of complex traits (Hubner et al. 2005; Quigley et al. 2009). We therefore asked whether any of the genes located within the minimal chromosome 17 region might be differentially expressed between the parental strains and therefore contribute to the observed differences in the invasion phenotypes.

RNA from RT2 B6 and RT2 C3H tumors were profiled by quantitative PCR for the genes located within the minimal region on chromosome 17. This analysis revealed that a small subset of the resident genes – *Alk*, *Dlgap1*, *Emilin2*, *Lbh*, *Ltbp1*, *Rab31*, and

Spdya – showed significant differential expression between the B6 and C3H genetic backgrounds at the mRNA level (Figures 3.9D, 3.11A, Dataset 3.3).

We were particularly intrigued by the *Alk* gene, which encodes the anaplastic lymphoma kinase. *Alk* mRNA levels were ~60% lower in RT2 C3H tumors versus RT2 B6 tumors, which was also reflected at the protein level (Figure 3.11A, C). *Alk* expression was also reduced in wild-type islets from C3H mice as compared to B6 mice, consistent with *Alk* being expressed at higher levels in the B6 background versus the C3H background regardless of the neoplastic state of this tissue (Figure 3.11B). *Alk* levels were higher in tumors compared to wild-type islets in both genetic backgrounds, and *Alk* expression showed a progressive increase during the course of RT2 tumorigenesis (Figure 3.11B, D). Notably, there are no polymorphisms in the exonic regions of the *Alk* gene that differentiate the B6 allele from the C3H allele (data not shown), and therefore the *Alk* protein is not intrinsically different in structure or function in these different genetic backgrounds. Interestingly, *Alk* belongs to the insulin-receptor superfamily of receptor tyrosine kinases (Chiarle et al. 2008), members of which are known to influence PNET tumorigenesis in RT2 mice, including tumor invasion (Lopez and Hanahan 2002; Ulanet et al. 2010). Given this association and our observation that *Alk* expression levels were significantly different between the B6 and C3H backgrounds, we sought to explore the potential role that *Alk* might play in the development of invasive RT2 tumors.

A pharmacological inhibitor of *Alk* inhibits invasion and other parameters of PNET tumorigenesis

We used a small molecule inhibitor of Alk kinase activity, NVP-TAE684 (TAE684) (Galkin et al. 2007), in an experimental therapeutic trial in RT2 mice aiming to assess the effects of reduced Alk activity on RT2 tumorigenesis, particularly with regards to the parameter of tumor invasion.

Male RT2 B6 mice were treated for four weeks with TAE684 or vehicle using a previously defined dose regimen (Galkin et al. 2007) beginning at 10 weeks of age when incipient tumors are first observed in RT2 mice (Figure 3.12) (Bergers et al. 1999). RT2 B6 mice were used since they develop IC lesions at significantly higher levels than RT2 C3H mice, and they also express Alk in the pancreatic islets and PNETs at significantly higher levels than RT2 C3H mice (Figures 3.1G–H, 3.11A–C). This is also the stage of RT2 tumorigenesis when there is an appreciable increase in Alk expression levels (Figure 3.11D). TAE684 was well tolerated, and 13 of 14 treated mice and 12 of 13 control mice survived until the end of the trial (Figure 3.13 and data not shown).

At the defined endpoint of the trial, TAE684-treated mice proved to have developed ~25% fewer macroscopic tumors than control mice (Figure 3.14B); there was a concomitant trend towards reduced tumor burden in TAE684-treated mice, which, however, was not statistically significant (Figure 3.14A).

Notably, TAE684-treated mice developed significantly fewer invasive lesions than control mice. There was a clear reduction in the frequency of total IC tumors (49.7% versus 33.3% of total tumors in control versus treated mice), which was accompanied by a concomitant increase in the frequency of IT tumors (50.3% versus 66.7% of total tumors in control versus treated mice), in TAE684-treated mice (Figure

3.14C). This shift was due to a reduction in the frequencies of both the IC1 and IC2 subclasses of invasive RT2 PNETs (Figure 3.14D).

TAE684 functions by interfering with Alk kinase activity (Galkin et al. 2007), and tumors from treated RT2 mice showed reduced levels of phosphorylated Alk (Figure 3.14E). We also observed a modest but appreciable reduction in the levels of phosphorylated Akt, one downstream Alk target, compared to controls (Figure 3.14E), confirming that TAE684 inhibited Alk activity in the tumors of RT2 mice.

Discussion

A considerable body of research has identified polymorphic modifier loci scattered across the mouse genome that affect multiple aspects of cancer susceptibility and development (Balmain et al. 2003; Demant 2003; Quan et al. 2010). Our data demonstrate that tumor progression, specifically to an invasive growth state, is also subject to polymorphic genetic control. We identify a polymorphic locus on mouse chromosome 17 (syntenic to human chromosomes 2 [107.5–110 Mb], 5 [2.5–10 Mb], and 18 [29–34 Mb]), which influences the susceptibility of PNETs to progress from solid adenomatous tumors to invasive carcinomas.

Using a prototypical mouse model of multistage tumorigenesis, we observed that the propensity to develop an invasive phenotype is affected by genetic background. RT2 mice inbred into the B6 background develop PNETs of varying degrees of invasiveness whereas RT2 mice inbred into the C3H background are largely resistant to the development of invasive tumors. Furthermore, RT2 F1 hybrid mice are also resistant, indicating that the C3H genetic background is dominant-suppressive over the invasion-prone B6 background. Linkage analysis of RT2 N2 backcross mice, produced from backcrossing RT2 F1 mice once to the susceptible B6 background, identified a locus on chromosome 17 that correlated with susceptibility (when the locus is homozygous B6) versus resistance (when a C3H allele is present). Previous studies have documented that tumors isolated from RT2 mice undergo chromosomal gains and losses at different frequencies dependent on genetic background (Hodgson et al. 2001; Hager et al. 2004). Notably, chromosome 17 is not affected by copy number abnormalities in either the B6

or C3H backgrounds, suggesting that this locus is of a class of genetic modifiers that is not altered during tumorigenesis.

The invasion modifier locus on chromosome 17 (63.7–76.4 Mb) contains more than 50 annotated genes. Of these, 7 were found to be differentially expressed in the PNETs isolated from RT2 mice inbred into the B6 and C3H backgrounds. As a first step towards auditing candidate invasion modifier genes in this locus, we focused on the Alk receptor tyrosine kinase, motivated in part by a series of studies demonstrating that Alk is activated by mutation or chromosomal translocation in human hematopoietic and solid cancers, evidently converting it into an initiating oncogene (Morris et al. 1994; Chiarle et al. 2008; George et al. 2008; Mosse et al. 2008). Based on these and previous studies implicating Alk as an oncogene, several small molecule inhibitors specific to Alk have been developed as potential therapeutics for these diseases (Galkin et al. 2007; Li and Morris 2008). Our use of one such kinase inhibitor to probe the possible roles of Alk in PNET tumorigenesis demonstrated that Alk promoted both tumor growth and progression; most notably, pharmacological inhibition of Alk activity reduced tumor invasiveness in RT2 B6 mice. These results are consistent with our observation that Alk is expressed at lower levels in the tumors of RT2 C3H mice, which are rarely invasive, as compared to the tumors of RT2 B6 mice, which consistently develop invasive PNETs. In comparing the B6 and C3H sequences, we did not identify any polymorphism in either the protein-coding or untranslated portions of the Alk mRNA that might suggest a basis for Alk's invasion modifier effects and/or differential expression. However, there are four polymorphisms located within 10 kbp of the 5'-flanking region and two within 10 kbp of the 3'-flanking region, in addition to ~300 polymorphisms residing in the large

intron 2 of the Alk gene, that distinguish the B6 and C3H alleles (data not shown), and one or more of these polymorphisms may account for the observed differences in allelic expression. Our results associating Alk with invasion are also congruent with a previous study demonstrating that anti-Alk antibodies can reduce tumor cell invasion in an *in vitro* setting (Stylianou et al. 2009). Additionally, pharmacological inhibition of Alk hindered tumor formation in RT2 mice, in accordance with earlier studies examining the oncogenic properties of Alk (Piva et al. 2006; Galkin et al. 2007; George et al. 2008; Mosse et al. 2008). Importantly and in contrast to the aforementioned studies where Alk was the driving oncogene, our results demonstrate that Alk can also act as a tumor progression factor, being upregulated during multi-step tumorigenesis to collaborate with an initiating oncogene (in this case the SV40 Tag oncogene that abrogates the tumor suppressing activities of pRb and p53). Thus, Alk inhibition may prove to be a useful therapy even in situations where Alk is not the initiating oncogene, either as a result of mutation or other means.

While our data implicate Alk levels as a determinant of RT2 tumor invasion, we envision that other polymorphic invasion modifier genes may reside in the chromosome 17 locus. The Alk inhibitor reduced tumor invasiveness, but not to the degree seen in the C3H background, which could reflect incomplete Alk inhibition or additional genetic components to the modifier effect. Indeed, several other genes residing in this locus also showed significant differential expression in RT2 tumors from the B6 and C3H genetic backgrounds (Figure 3.11A), and one of these genes, *Ltbp1*, contains a nonsynonymous coding change between the B6 and C3H backgrounds (data not shown). As such, other genes in this locus merit future investigation.

Although BMD inflammatory cells have been shown to contribute to the invasiveness of RT2 PNETs (Gocheva et al. 2006; Gocheva et al. 2010), it does not appear that their activity is modulated by the invasion modifier gene(s). Thus, invasive PNETs were still rare in RT2 F1 mice that received bone marrow from an invasion-permissive B6 donor. Although we cannot rule out the possibility that this modifier locus operates in other stromal cell types or in another tissue compartment, it seems most likely that the invasive modifier acts in the cancer cells.

In addition to pro-invasive inflammatory cells, other factors are known to influence progression to an invasive growth state in this prototypical model of multistage tumorigenesis. Loss of cell-cell adhesion complexes, including the adherens junctions mediated by Cdh1 (Perl et al. 1998) and desmosomes (M.G.H.C. and D.H., in preparation), are associated with the development of more invasive tumors. Signaling through the type-1 insulin-like growth factor receptor (Igf1r) can also drive progression to an invasive state (Lopez and Hanahan 2002). The present study now establishes a new dimension to this multifactorial invasive growth phenotype, involving a polymorphic genetic modifier that can alternatively override or allow these other functional effectors of invasive growth. It remains to be determined whether the chromosome 17 invasion modifier locus identified in this study modulates any of these functionalities or acts in a completely independent fashion.

Finally, it is pertinent to consider the translational implications of this newly identified invasion modifier. First, we suspect that this polymorphic modifier will prove operative in other cancer types but most likely not in all. Notably, the development of squamous carcinoma is under distinctive polymorphic control in mice. In this case, the

B6 background is largely resistant to the development of invasive squamous carcinomas in three different oncogenic contexts – an activated Hras oncogene (Wakabayashi et al. 2007), the HPV16 oncogenes (Coussens et al. 1996), and chemical carcinogens (Hennings et al. 1993). Thus, the B6 background is permissive for invasive cancers in the pancreas but resistant for Hras-induced cancers in the skin. A major determinant of skin tumor resistance is a polymorphism in the Patched gene (Ptc1), located on mouse chromosome 13, that introduces a non-conservative coding sequence change at the C-terminus of the protein (Wakabayashi et al. 2007). This polymorphism was not detected in the present linkage analysis of invasive pancreatic tumors. Therefore, both tumor types are governed by polymorphic modifiers of invasive cancer, albeit distinctive ones. Additionally, yet other phenotypic modifiers of metastasis are implicated in mouse models of breast cancer (Winter and Hunter 2008) and in human breast cancer (Hsieh et al. 2009).

Assessing the existence of polymorphic invasion modifiers in human cancers will be challenging. The availability of increasingly cost-effective DNA sequencing of individual genomes (both normal and cancerous) may afford inroads to identifying polymorphisms correlating with progression to invasive carcinomas, particularly in organs where both non-invasive adenomas and invasive carcinomas are prevalent, such as the colon. Elucidation of such polymorphic modifiers could well contribute to the future of personalized medicine, where susceptibility versus resistance alleles of invasion modifiers might be factored into the treatment for patients diagnosed with early-stage cancers.

Materials and methods

Genetically engineered mice

The generation and characterization of the RIP1-Tag2 (RT2) mouse line has been previously described (Hanahan 1985). The RT2 line has been backcrossed into the C57Bl/6 (B6) (Charles River Laboratories, Wilmington, MA) and the C3HeB/Fe (C3H) (The Jackson Laboratory, Bar Harbor, ME) genetic backgrounds more than 20 times and is effectively inbred into these backgrounds. RT2 C3HB6(F1) hybrid mice (F1) and RT2 N2 mice were generated as described (Figure 3.7). Beginning at 10 weeks of age, all RT2 mice received 50% sugar food (Harlan Teklad, Madison, WI) to relieve the effects of hypoglycemia caused by the insulin-secreting tumors. CAG-EGFP B6 mice were purchased from The Jackson Laboratory (Bar Harbor, ME). All mice used in this study were housed and maintained in accordance with the University of California, San Francisco (UCSF) institutional guidelines governing the care of laboratory mice.

Tissue preparation and tumor analysis

Pancreata were isolated from 14-week-old RT2 mice. Tumor burden and tumor number were analyzed as previously described (Inoue et al. 2002). Fresh frozen tissues were embedded in OCT (Sakura Finetek, Torrance, CA) on dry ice. Fixed tissues were incubated overnight at 4°C in 10% Zn-buffered formalin (Medical Chemical Corporation, Torrance, CA) and then dehydrated through a series of graded alcohols before embedding in paraffin (Paraplast) (Thermo Fisher Scientific, Waltham, MA).

Histological and immunohistochemical staining and analysis

Both frozen and paraffin tissues were sectioned at 10 μm thickness. For histological analysis, every tenth section was stained with hematoxylin and eosin (Surgipath Medical Industries, Richmond, IL) using standard methods. Tumors were classified as a non-invasive islet tumor (IT), a focally invasive carcinoma type-1 (IC1), or a broadly invasive carcinoma type-2 (IC2) using a previously defined grading scheme (Lopez and Hanahan 2002). For immunohistochemistry, frozen sections were fixed in cold acetone while paraffin sections were deparaffinized, rehydrated in a series of graded alcohols, subjected to antigen retrieval in Antigen Unmasking Solution (Vector Laboratories, Burlingame, CA), and blocked for endogenous peroxidase activity. Antibodies used in this study were as follows: rabbit anti-T-antigen (Hanahan laboratory preparation), rat anti-cadherin 1 (Invitrogen, Carlsbad, CA), rabbit anti-Ki67 (Novus Biologicals, Littleton, CO), rhodamine red-X-conjugated donkey anti-rabbit IgG, FITC-conjugated donkey anti-rat IgG, biotin donkey anti-rabbit IgG (Jackson ImmunoResearch Laboratories, West Grove, PA). Fluorescently labeled tissues were mounted with Vectashield mounting medium containing 4',6-diamidino-2-phenylindole (DAPI) (Vector Laboratories, Burlingame, CA) to visualize cell nuclei. The TdT-mediated dUTP-digoxigenin nick-end labeling (TUNEL) assay was used to detect tumor apoptosis as previously described (Lopez and Hanahan 2002). For colorimetric staining, signal was amplified using the Vectastain Elite ABC kit (Vector Laboratories, Burlingame, CA), visualized using Fast DAB (Sigma, St. Louis, MO), and counterstained with methyl green (Sigma, St. Louis, MO). For Ki67 and TUNEL quantification, two to three random fields were obtained using a 40X objective lens from at least three tumors per mouse and at least five mice per group. The proliferation or apoptosis index was calculated as the

percentage of total cells per field that were Ki67- or TUNEL-positive respectively using the MetaMorph software package (Molecular Devices, Sunnyvale, CA). For all other immunohistochemical analysis, a minimum of five mice per indicated group was analyzed per staining condition. All images were captured using an Axio Imager bright field microscope or an Axio Scope fluorescence microscope and the AxioVision LE software package (Carl Zeiss, Thornwood, NY).

Genomic DNA preparation, SNP genotyping, and linkage analysis

Genomic DNA (gDNA) was isolated from mouse tails by proteinase K (Qiagen, Valencia, CA) digestion followed by phenol-chloroform extraction using standard methods (Sambrook and Russell 2001). 4 µg of gDNA per animal was SNP genotyped using the Illumina platform according to the manufacturer's specifications (Illumina, San Diego, CA), and 143 RT2 N2 mice for which tumor phenotype data were available were genotyped by this method. A panel of primers that discriminate between the B6 and C3H genetic backgrounds across all 19 somatic chromosomes and the X chromosome was employed (see Dataset 3.1 for a complete list of SNPs used in this study). Statistical analysis was performed using R/qtl (<http://www.rqtl.org/>) for the IT, IC1, IC2, tumor number, and tumor burden metrics. Because these metrics were not normally distributed, non-parametric tests were chosen in R/qtl. A LOD score of $\text{LOD} \geq 3.0$ was considered significant (Lander and Kruglyak 1995).

Lethal irradiation and bone marrow transfer

Five-week-old RT2 F1 mice were lethally irradiated (950 rad) using a cesium source. Mice were injected via the tail vein with 1.5×10^6 bone marrow derived cells from B6 or F1 donor mice 24 hours post-irradiation as previously described (Gocheva et al. 2010). Donor mice were CAG-EGFP positive. Mice were maintained on antibiotics (1.1 g/L neomycin sulfate [Sigma, St. Louis, MO] and 1×10^6 units/L polymyxin B sulfate [Sigma, St. Louis, MO]) for four weeks post-irradiation. Successful bone marrow engraftment was confirmed by flow cytometry of blood four weeks post-irradiation looking at GFP expression in CD4-positive cells, a bone marrow derived cell type.

RNA isolation and preparation and quantitative PCR

Normal islets were isolated from six-week-old wild-type B6 and C3H mice, and hyperplastic islets were isolated from six-week-old RT2 B6 mice as previously described (Parangi et al. 1995). Angiogenic islets were isolated from nine-week-old RT2 B6 mice by selection based on their red, hemorrhagic appearance following collagenase digestion of pancreata (Parangi et al. 1995). Islet tumors were excised from the surrounding exocrine pancreas from 14-week-old RT2 B6 and RT2 C3H mice. Total RNA was isolated using the RNeasy Mini kit (Qiagen, Valencia, CA) and DNase I treated (Qiagen, Valencia, CA). cDNA was synthesized using the iScript Synthesis kit (Bio-Rad, Hercules, CA). Quantitative PCR was performed using TaqMan primers and TaqMan Custom Arrays (Applied Biosystems, Foster City, CA) (see Dataset 3.3 for a complete list of primers used in this study) and a 7900HT Fast Real-Time PCR System (Applied Biosystems, Foster City, CA) according to the manufacturer's specifications.

TAE684 inhibitor trial

The characterization of the Alk inhibitor NVP-TAE684 (TAE684) has been previously described (Galkin et al. 2007). TAE684 was resuspended in 10% 1-methyl-2-pyrrolidinone/90% PEG 300 (volume/volume) (Sigma, St. Louis, MO), and male RT2 B6 mice were administered a 10 mg/kg dose once daily or vehicle solution alone by oral gavage from 10–14 weeks of age. Body mass was monitored twice weekly to adjust dosing levels and to assess any toxicity caused by the treatment.

Western analysis

Whole RT2 tumors were lysed in protein extraction buffer (10 mM Tris, pH 8.0; 1% NP-40; 0.5% Triton X-100) containing protease inhibitors (Roche, Indianapolis, IN) and phosphatase inhibitors (Sigma, St. Louis, MO) on ice for 30 minutes and then centrifuged at 16,000g for 30 minutes at 4°C. The resulting supernatants were used for immunoblotting. Equivalent amounts of protein from individual tumors were pooled and then loaded onto a 7.5% Tris-HCl gel (Bio-Rad, Hercules, CA) and transferred to a PVDF membrane (Bio-Rad, Hercules, CA). Membranes were blocked with 5% bovine serum albumin in 10 mM Tris pH 8.0; 150 mM NaCl; 0.1% Tween-20, probed with primary antibodies in block overnight at 4°C, incubated with secondary antibodies in block, and developed with enhanced chemiluminescence reagents (Amersham Biosciences, Pittsburgh, PA). Prior to re-probing, blots were stripped with Restore Buffer (Thermo Scientific, Rockford, IL). Antibodies used in this study were as follows: rabbit anti-T-antigen (Hanahan laboratory preparation), rat anti-cadherin 1 (Invitrogen, Carlsbad, CA), mouse anti-Alk-c, rabbit anti-phospho-Alk (Y1507), mouse anti- β -actin

(Abcam, Cambridge, MA), rabbit anti-total-Akt, rabbit anti-phospho-Akt (S473) (Cell Signaling Technology, Beverly, MA), HRP-goat anti-rabbit IgG, HRP-goat anti-rat IgG, HRP-goat anti-mouse IgG (Jackson ImmunoResearch Laboratories, West Grove, PA).

Statistical analysis

Fisher's exact test and the chi-square test were used to compare tumor invasion metrics. The Mann-Whitney test was used to compare tumor burden, tumor number, tumor proliferation, tumor apoptosis, body mass, and mRNA expression level metrics. For all statistical tests, a p-value of $p \leq 0.05$ was considered significant. All statistics were performed using the Prism software package (GraphPad Software, La Jolla, CA).

Acknowledgments

We thank: the Mutation Mapping and Developmental Analysis Project (Harvard Medical School, Boston, MA; NICHD grant U01-HD43430), the Partners Healthcare Center for Genetics and Genomics (Harvard Medical School, Boston, MA), and the Helen Diller Family Comprehensive Cancer Center Genomics Core (University of California, San Francisco, San Francisco, CA) for genotyping and genomics services; the Diabetes Center Microscopy and Islet Isolation Cores (University of California, San Francisco, San Francisco, CA); Nathanael Gray (Dana-Farber Cancer Institute, Boston, MA) for the TAE684; Stefan Morris (St. Jude Children's Research Hospital, Memphis, TN) for advice on Alk antibodies; Anguraj Sadanandam (Swiss Federal Institute of Technology Lausanne, Lausanne, CH) for bioinformatic analysis of the modifier locus; Susan Cacacho, Ehud Drori, I. Celeste Rivera, Marina Vayner, and Annie Wang for superior technical support; and Matthias Hebrok, Martin McMahon, and members of the Hanahan laboratory for advice and encouragement at all stages of this project. D.H. is an American Cancer Society Research Professor. This work was supported by a grant from the National Cancer Institute (5R01CA45234-24; to D.H.) and by a graduate research fellowship from the National Science Foundation (to M.G.H.C). A.B. and J.-H.M. were supported by grants from the National Cancer Institute (U01-CA84244) and the Department of Energy (DE-FG02-03ER63630).

Figure 3.1

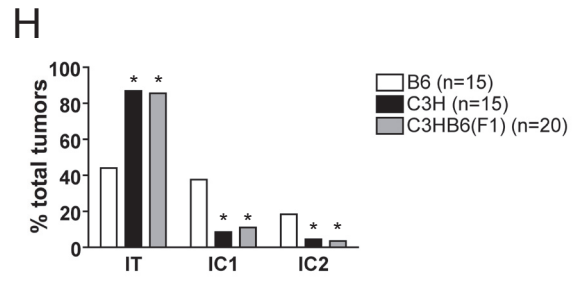
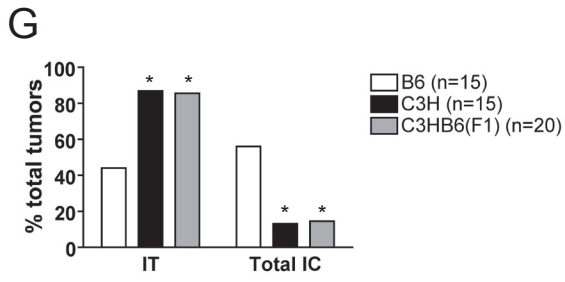
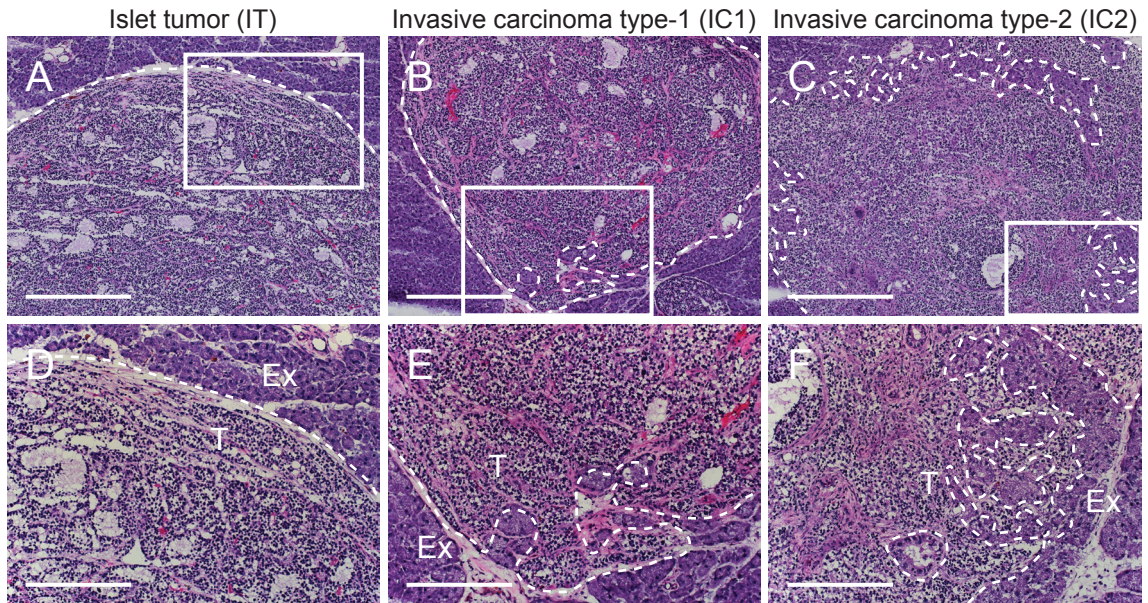


Figure 3.1. PNET invasion is dependent on genetic background.

(A–C) H&E staining of a non-invasive IT PNET, a focally invasive IC1 PNET, and a broadly invasive IC2 PNET from a RT2 B6 mouse. (D–E) Higher magnification of boxed regions in A–C. T indicates tumor region and Ex indicates exocrine pancreas. Dashed lines demarcate tumor margins. (F) Quantification of tumor invasiveness represented as the percentage of IT tumors or total IC tumors (IC1+IC2) in RT2 mice on the B6, C3H, and F1 genetic backgrounds at 14 weeks of age. A minimum of 117 tumors per group was graded. * $p < 0.001$ by Fisher's exact test. (G) Same as F except IC lesions are separated into the IC1 and IC2 subclasses. * $p < 0.001$ by the Chi-square test. Scale bars represent 400 μm (A–C) and 200 μm (D–F).

Figure 3.2

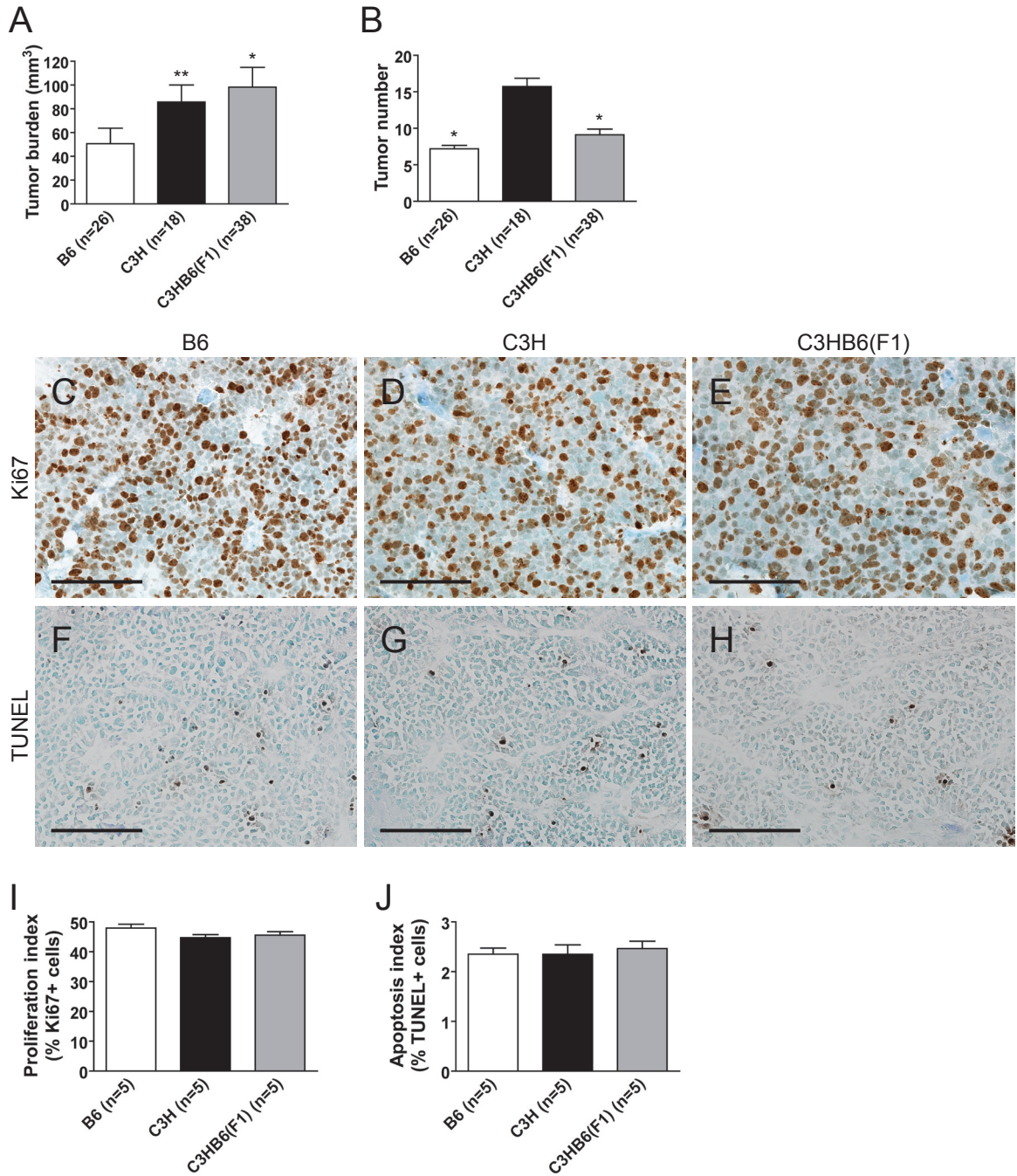


Figure 3.2. Tumor burden and tumor number but not rates of tumor proliferation or tumor apoptosis are affected by genetic background in RT2 mice.

(A) Tumor burden for RT2 mice on the B6, C3H, and F1 genetic backgrounds at 14 weeks of age. Data shown are mean plus standard error. * $p < 0.05$ and ** $p < 0.01$ by the Mann-Whitney test. (B) Tumor number for RT2 mice on the B6, C3H, and F1 genetic backgrounds at 14 weeks of age. Data shown are mean plus standard error. * $p < 0.001$ by the Mann-Whitney test. (C–E) Ki67 staining on tumors from RT2 mice on the B6, C3H, and F1 genetic backgrounds at 14 weeks of age. (F–H) TUNEL staining on tumors from RT2 mice on the B6, C3H, and F1 genetic backgrounds at 14 weeks of age. (I) Quantification of C–E. Data shown are mean plus standard error. Groups are not statistically different. (J) Quantification of F–H. Data shown are mean plus standard error. Groups are not statistically different. Scale bars represent 100 μm (C–H).

Figure 3.3

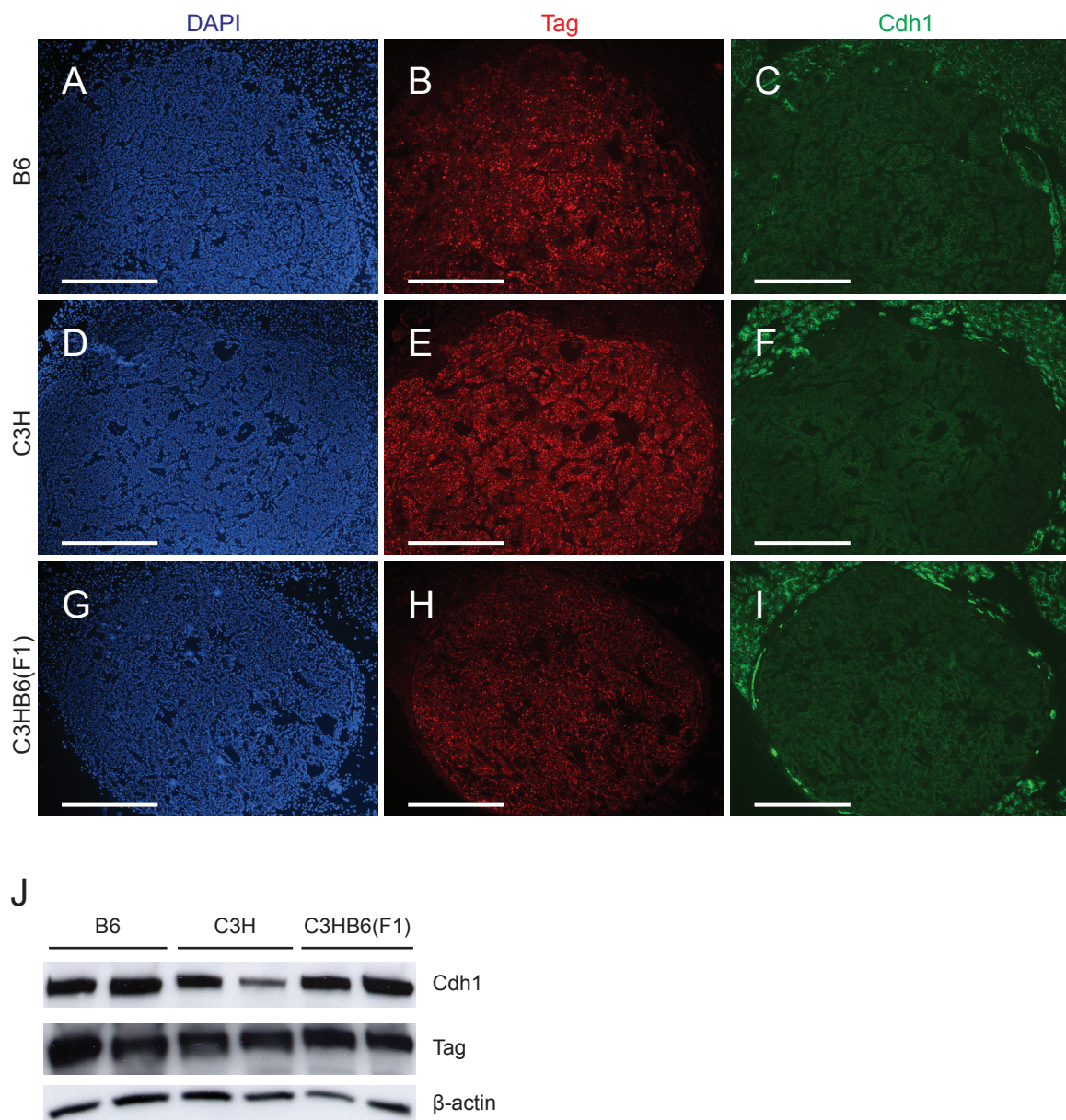


Figure 3.3. Expression levels of the oncoprotein T antigen (Tag) and the adhesion molecule cadherin 1 (Cdh1) are unaffected by genetic background.

(A–C) Immunofluorescence staining for DAPI to visualize cell nuclei, Tag, and Cdh1 on a RT2 B6 tumor. (D–F) Same as A–C except for a RT2 C3H tumor. (G–I) Same as A–C except for a RT2 F1 tumor. (J) Western analysis for Tag, Cdh1, and β -actin on lysates from individual tumors isolated from RT2 mice on the B6, C3H, and F1 genetic backgrounds. Scale bars represent 400 μ m.

Figure 3.4

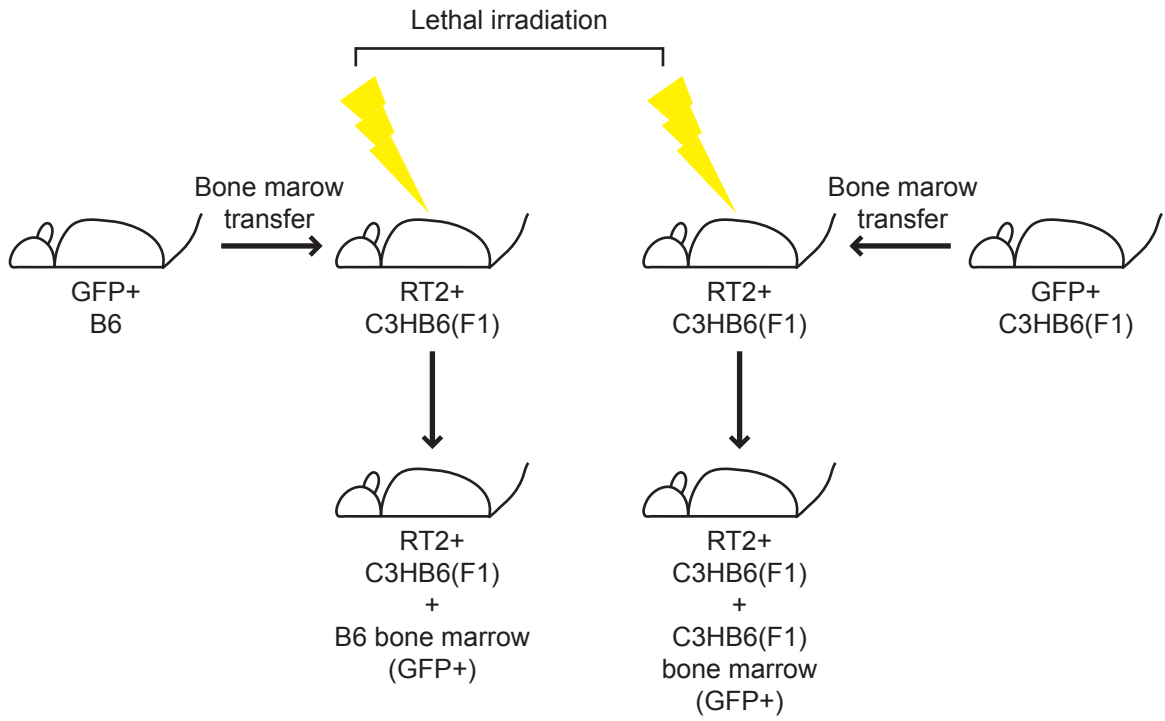


Figure 3.4. Schematic for bone marrow transfer into RT2 F1 mice.

RT2 C3HB6(F1) (F1) mice were lethally irradiated at five weeks of age. 24 hours post-irradiation, these mice were reconstituted with bone marrow from C57Bl/6 (B6) or F1 donor mice. Donor mice were GFP-positive to enable the assessment of the degree of bone marrow engraftment in the recipient mice.

Figure 3.5

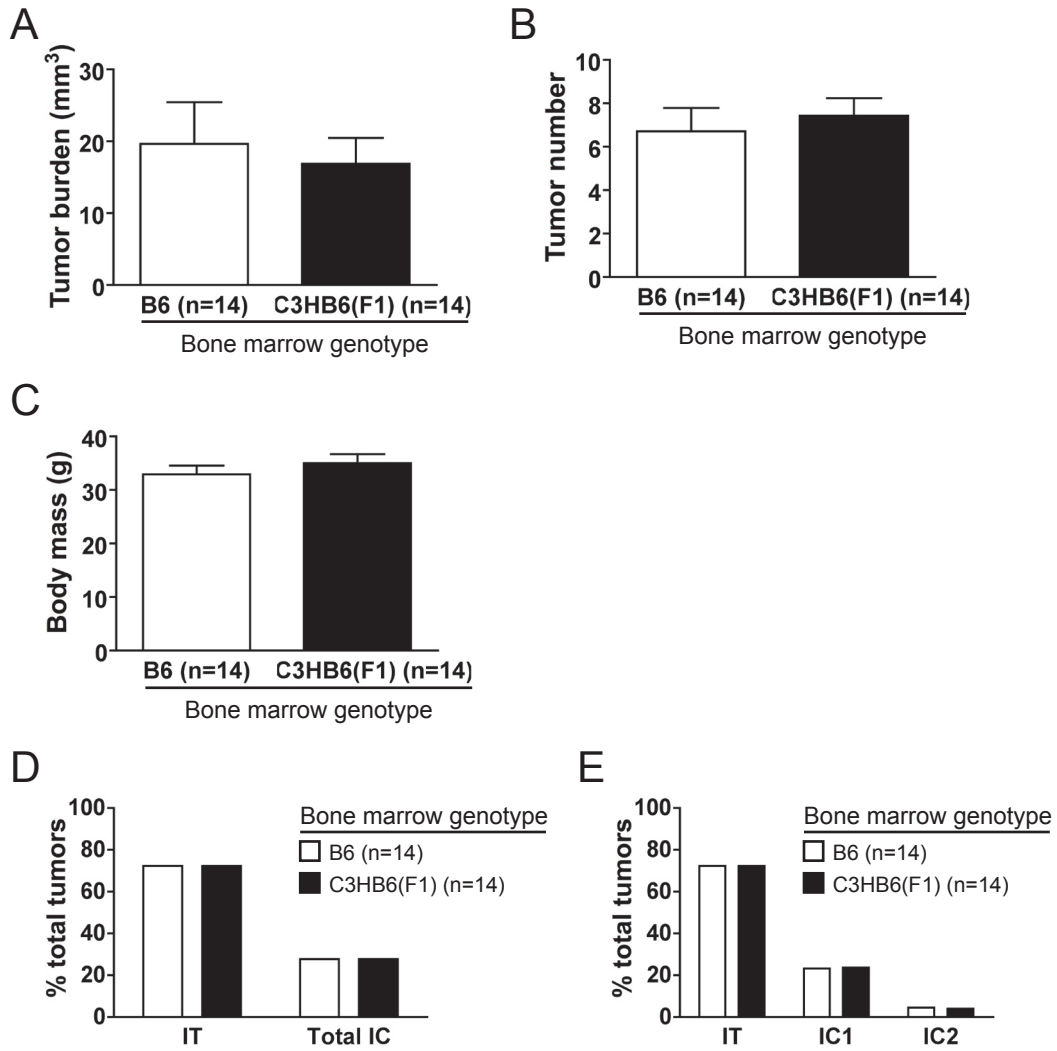


Figure 3.5. The invasive modifier does not act in the bone marrow derived tissue compartment.

(A–C) Tumor burden, tumor number, and body mass for RT2 F1 mice reconstituted with bone marrow derived from B6 or F1 donors at five weeks of age and sacrificed at 14 weeks of age. Data shown are mean plus standard error. Groups are not statistically different for these metrics. (D) Quantification of tumor invasiveness represented as the percentage of IT tumors or total IC tumors (IC1+IC2) in RT2 F1 mice reconstituted with bone marrow derived from B6 or F1 donors. A minimum of 94 tumors per group was graded. Groups are not statistically different. (E) Same as D except IC lesions are separated into the IC1 and IC2 subclasses. Groups are not statistically different.

Figure 3.6

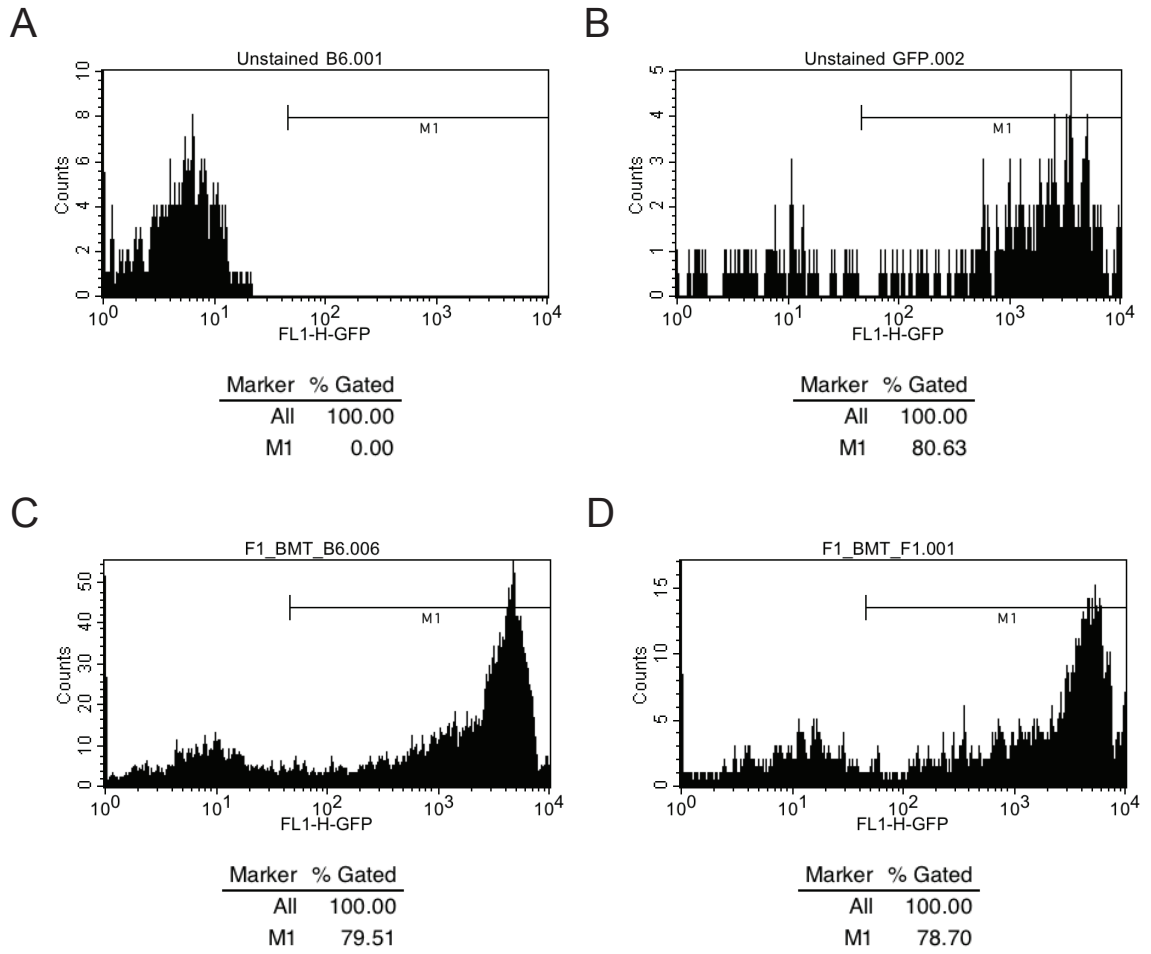


Figure 3.6. RT2 F1 mice successfully received bone marrow from GFP-labeled B6 or F1 donors.

Flow cytometry analysis of blood from recipient RT2 F1 mice looking at GFP positivity (M1 population) in CD4-positive cells, a bone marrow derived cell population (All population). (A) Flow cytometry plot from a control, non-reconstituted wild-type B6 mouse. (B) Flow cytometry plot from a control, non-reconstituted CAG-EGFP B6 mouse. (C) Flow cytometry plot from a RT2 F1 mouse reconstituted with bone marrow derived from a CAG-EGFP B6 donor 5 weeks post-transfer. (D) Flow cytometry plot from a RT2 F1 mouse reconstituted with bone marrow derived from a CAG-EGFP F1 donor 5 weeks post-transfer.

Figure 3.7

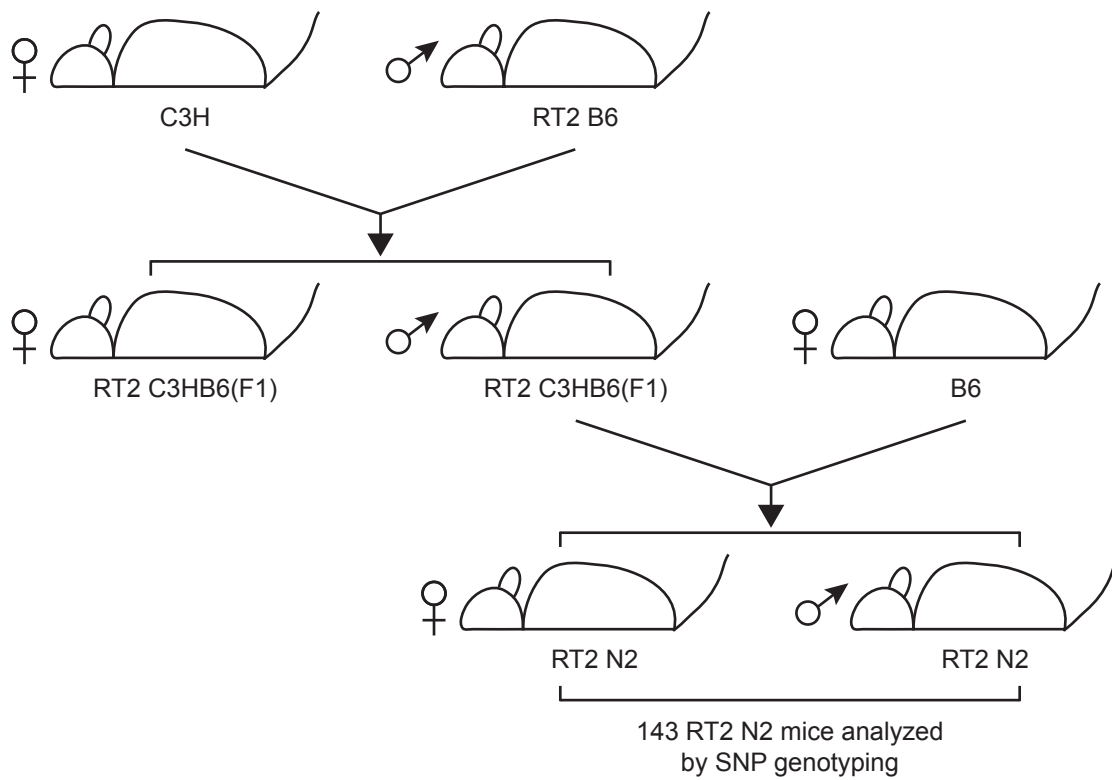
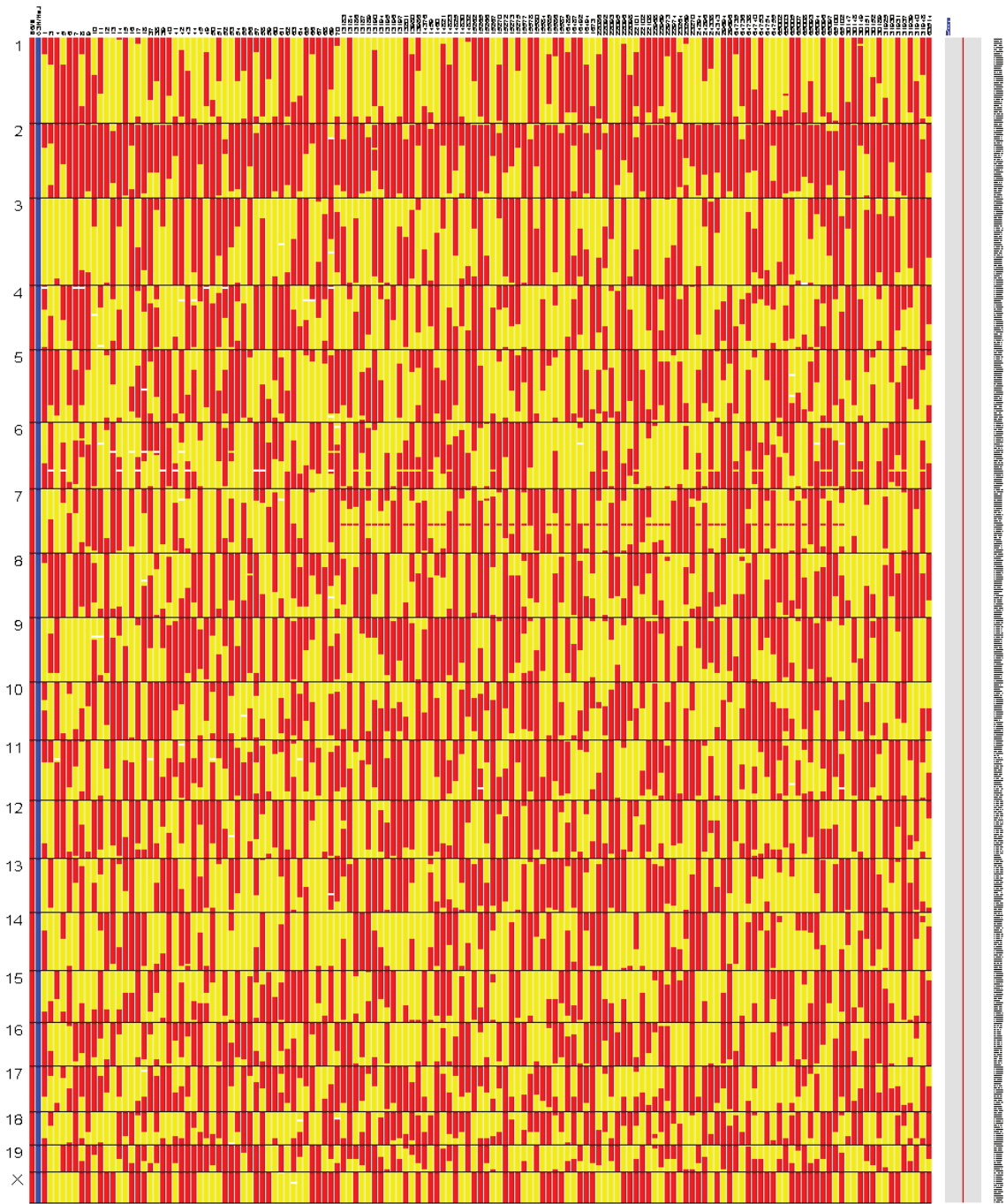


Figure 3.7. Schematic of breeding scheme for the generation of RT2 N2 mice.

RT2 B6 male mice were intercrossed with C3H female mice to produce RT2 F1 hybrid mice. RT2 F1 male mice were backcrossed once with B6 female mice to generate RT2 N2 mice. Constitutional tail DNA from 143 RT2 N2 mice was genotyped across 561 single nucleotide polymorphisms that cover the mouse genome and that discriminate between the B6 and C3H genetic backgrounds.

Figure 3.8



[2.0, 2.0]

Figure 3.8. SNP genotyping results for RT2 N2 mice.

Heat map of genotyping results for 561 single nucleotide polymorphisms (SNP) across the mouse genome for 143 RT2 N2 backcross mice. Red indicates homozygosity for the C57Bl/6 genetic background. Yellow indicates heterozygosity for the C57Bl/6 and C3HeB/Fe genetic backgrounds. White indicates a failed SNP call. Individual mice are arranged along the X-axis. SNPs are arranged along the Y-axis in chromosomal order (from mouse chromosome 1 through 19 and the X chromosome).

Figure 3.9

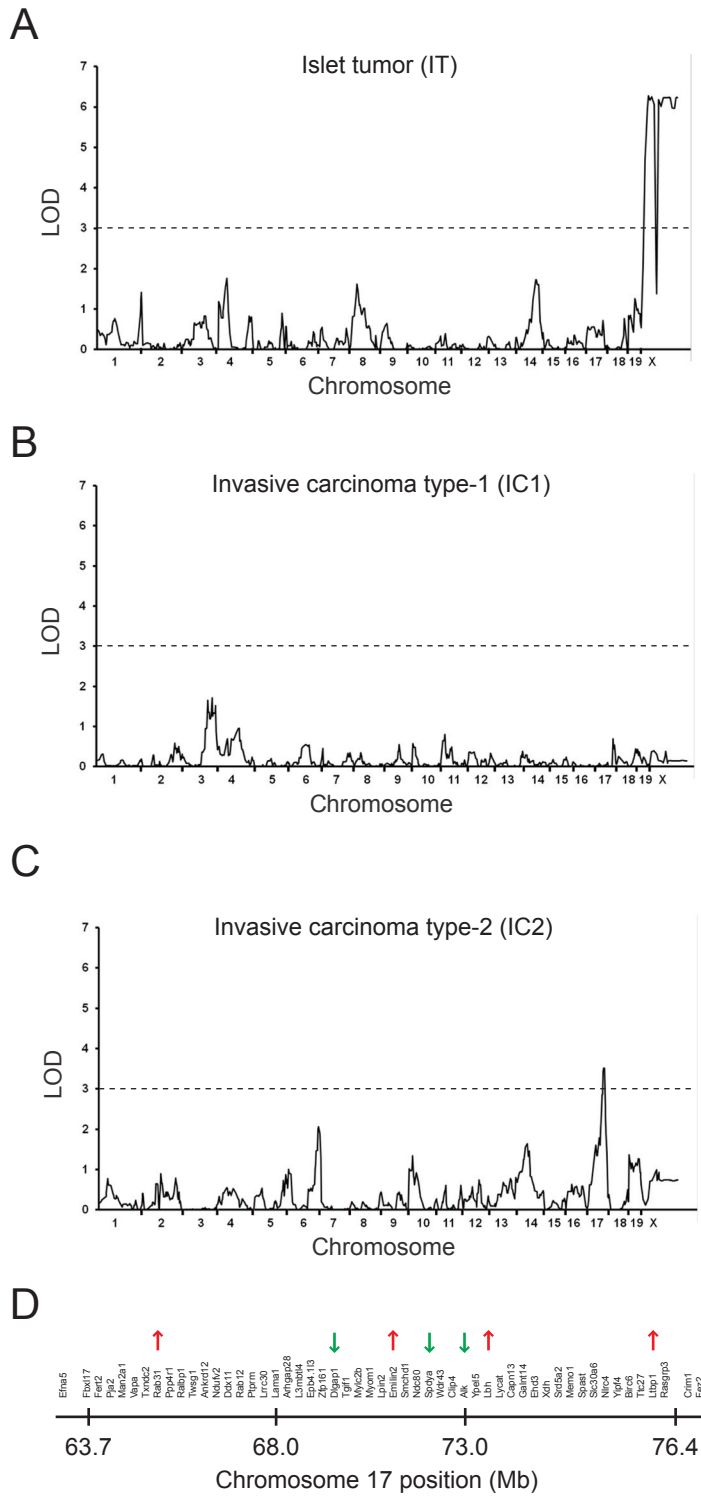


Figure 3.9. The IC2 tumor phenotype is linked to a region on chromosome 17.

(A) LOD scores for the IT phenotype across the mouse genome. The IT phenotype shows significant linkage ($\text{LOD} \geq 3.0$) to a region on chromosome X. (B) LOD scores for the IC1 phenotype across the mouse genome. (C) LOD scores for the IC2 phenotype across the mouse genome. The IC2 phenotype shows significant linkage ($\text{LOD} \geq 3.0$) to a region on chromosome 17. Dashed lines demarcate LOD-3.0 significance cutoff. (D) The physical map of the 95% confidence interval on chromosome 17. The map was constructed using data from the UCSC Genome Browser (<http://genome.ucsc.edu/>) and the NCBI MapViewer (<http://www.ncbi.nlm.nih.gov/projects/mapview/>) for the mouse genome. Red and green arrows indicate genes that are expressed at significantly higher and lower levels respectively in tumors isolated from RT2 C3H mice as compared to RT2 B6 mice.

Figure 3.10

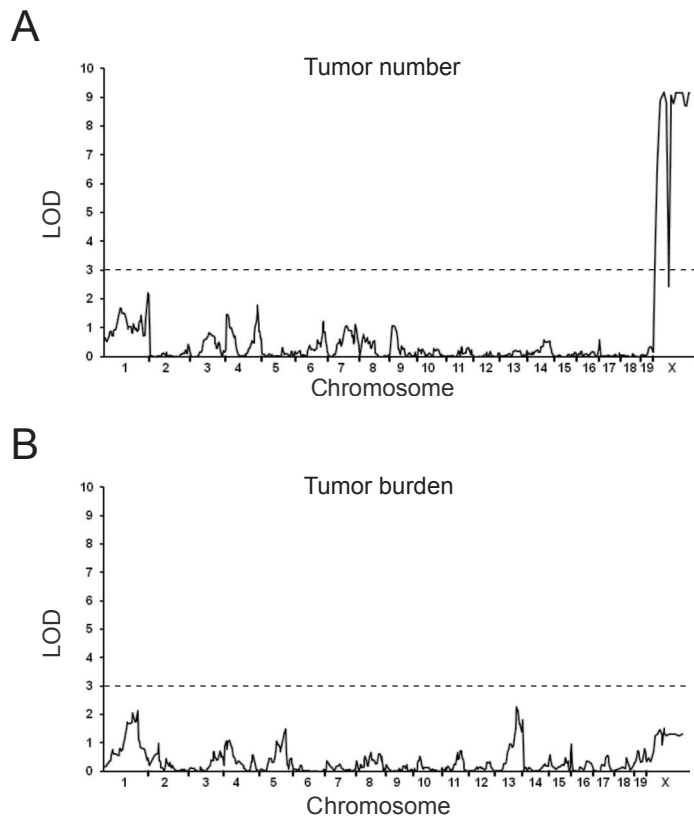


Figure 3.10. RT2 tumor number phenotype shows significant linkage to a region on chromosome X.

(A) LOD scores for the tumor number phenotype across the mouse genome. The tumor number phenotype shows significant linkage ($\text{LOD} \geq 3.0$) to a region on chromosome X. (B) LOD scores for the tumor burden phenotype across the mouse genome. Dashed lines demarcate LOD-3.0 significance cutoff.

Figure 3.11

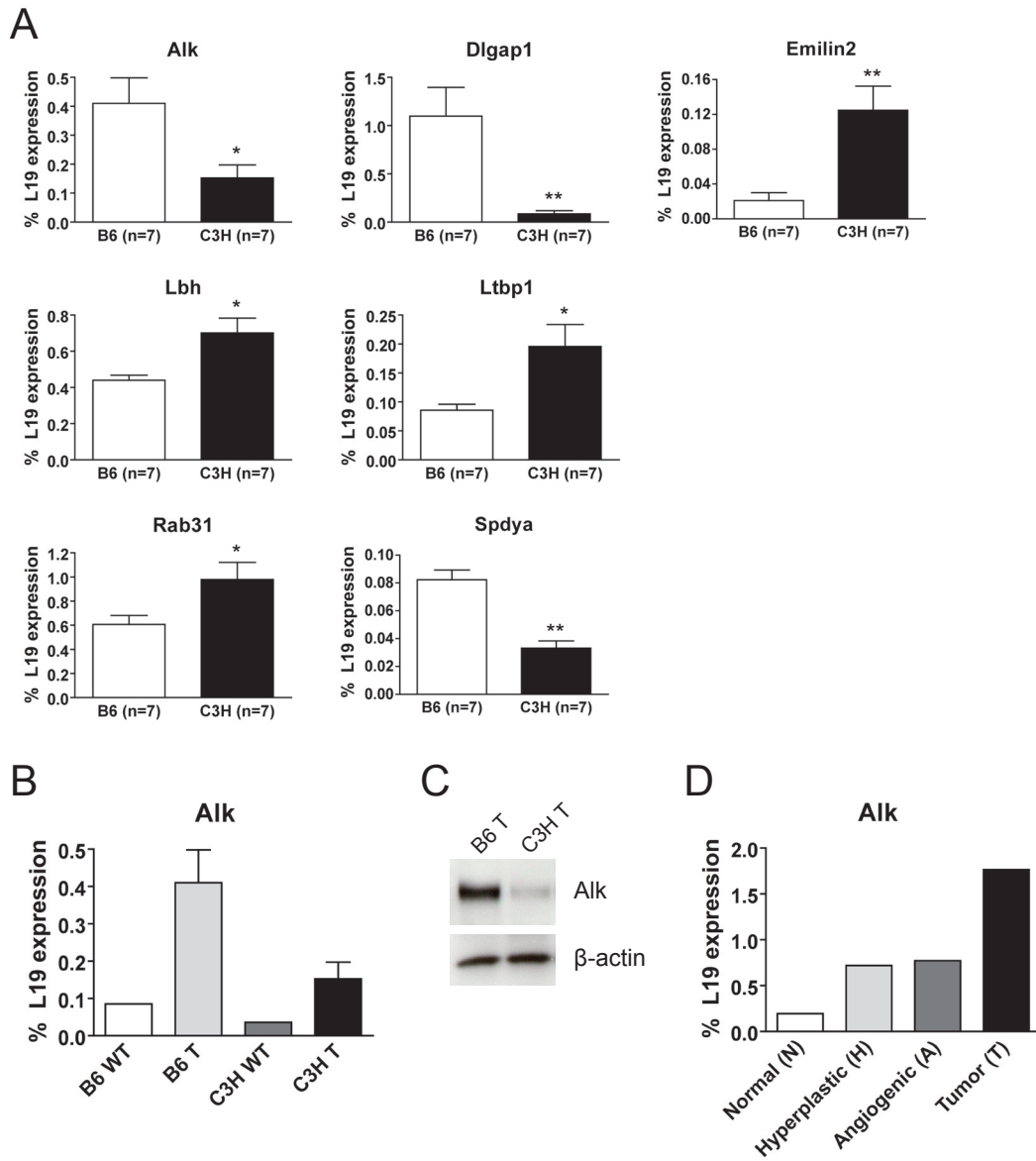


Figure 3.11. The anaplastic lymphoma kinase (Alk) is differentially expressed in the B6 and C3H genetic backgrounds.

(A) Real-time quantitative PCR values for Alk, Dlgap1, Emilin2, Lbh, Ltbp1, Rab31, and Spdya for tumors isolated from RT2 mice on the B6 and C3H backgrounds. Seven independent tumors per genotype were analyzed in triplicate. Data shown are mean plus standard error, and values are shown as the percent expression of the ribosomal protein L19 (L19). * $p < 0.05$ and ** $p < 0.01$ by the Mann-Whitney test. (B) Real-time quantitative PCR values for Alk in a pool of islets isolated from normal wild-type (WT) B6 or C3H mice or in tumors (T) isolated from RT2 mice on either the B6 or C3H backgrounds as in (A). Values are shown as the percent expression of L19. (C) Western analysis on tumor pool lysates (T) from RT2 B6 and RT2 C3H mice for Alk and β -actin. (D) Real time quantitative PCR values for Alk during the stages of RT2 tumorigenesis (normal wild-type [N], hyperplastic [H], angiogenic [A], tumor [T]) on the B6 genetic background. Values are shown as the percent expression of L19.

Figure 3.12

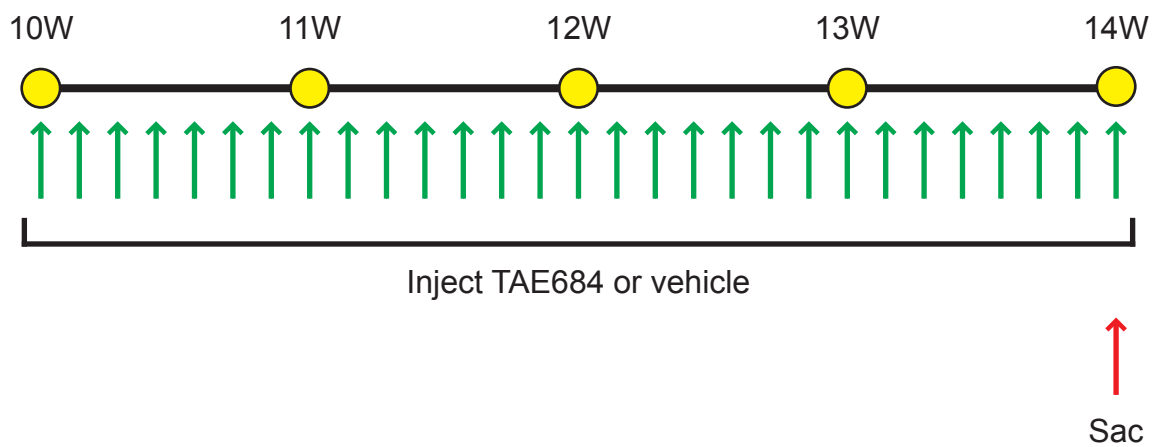
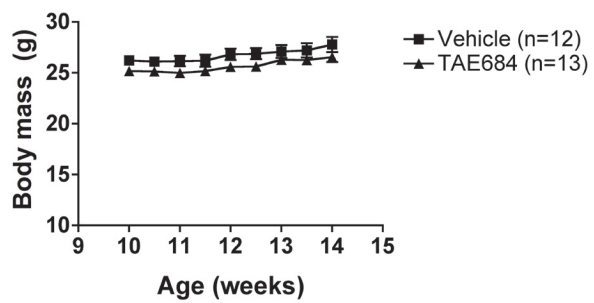


Figure 3.12. NVP-TAE684 dose regimen used to inhibit Alk kinase activity.

Male RIP1-Tag2 (RT2) mice on the C57Bl/6 genetic background were given a daily dose of NVP-TAE684 (TAE684), a small molecule inhibitor that specifically inhibits the kinase activity of the anaplastic lymphoma kinase (Alk) (Galkin et al. 2007), or vehicle control by oral gavage. The experimental therapeutic trial was of the intervention format and lasted from 10–14 weeks of age at which point the mice were sacrificed and analyzed.

Figure 3.13

A



B

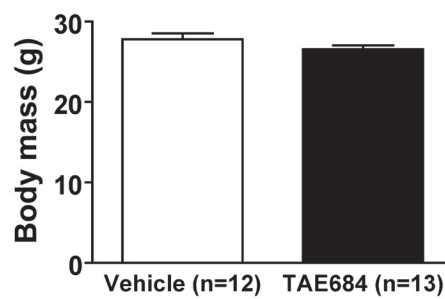


Figure 3.13. The Alk inhibitor TAE684 is well tolerated in RT2 mice in an experimental therapeutic trial.

(A) Longitudinal body mass for RT2 B6 mice treated with TAE684 or vehicle from 10–14 weeks of age. Data shown are mean plus standard error. Groups are not statistically different at any time point. (B) Body mass at time of sacrifice in RT2 B6 mice treated with TAE684 or vehicle from 10–14 weeks of age. Data shown are mean plus standard error. Groups are not statistically different.

Figure 3.14

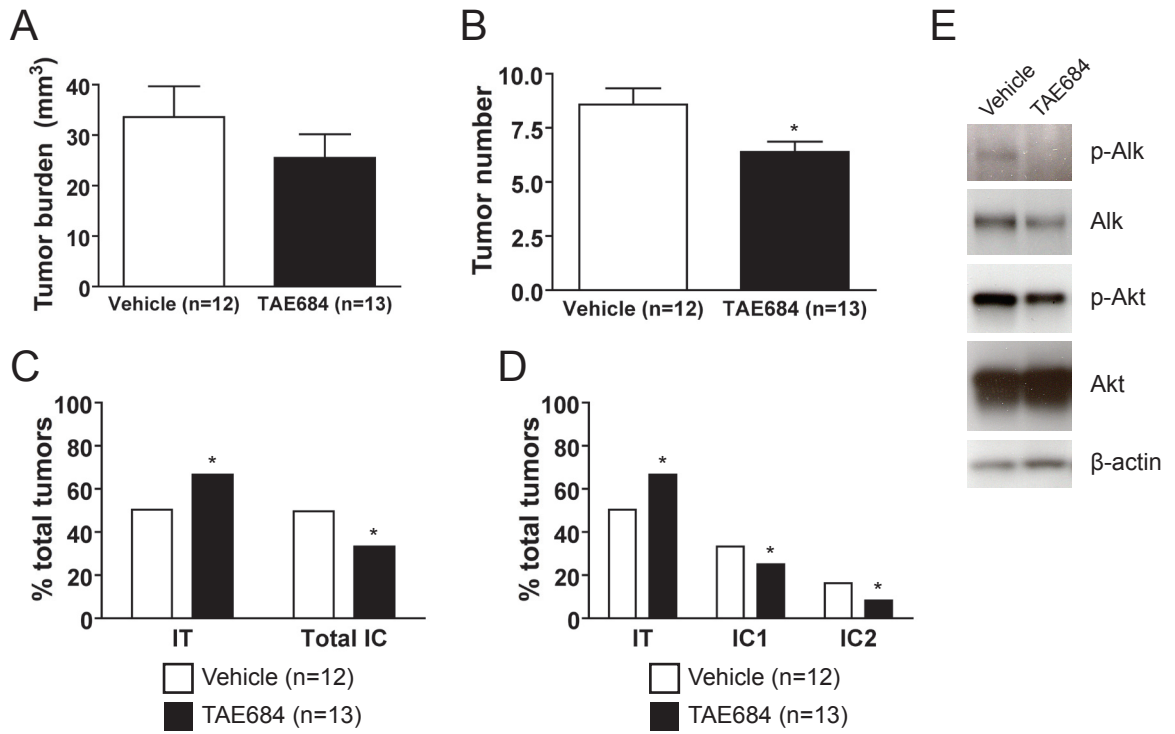


Figure 3.14. The Alk inhibitor NVP-TAE684 (TAE684) reduces tumor invasiveness in RT2 mice in an experimental therapeutic trial.

(A) Tumor burden for RT2 B6 mice treated with TAE684 or vehicle from 10–14 weeks of age. Data shown are mean plus standard error. Data are not statistically different. (B) Tumor number for RT2 B6 mice treated with TAE684 or vehicle from 10–14 weeks of age. Data shown are mean plus standard error. * $p < 0.05$ by the Mann-Whitney test. (C) Quantification of tumor invasiveness represented as the percentage of IT tumors or total IC tumors (IC1+IC2) in RT2 B6 mice treated with TAE684 or vehicle from 10–14 weeks of age. A minimum of 83 tumors per group was graded. * $p < 0.05$ by Fisher's exact test. (D) Same as C except IC tumors are separated into the IC1 and IC2 subclasses. * $p < 0.01$ by the Chi-square test. (E) Western analysis on tumor pool lysates from TAE684- or vehicle-treated RT2 B6 mice for phospho-Alk, total Alk, phospho-Akt, total Akt, and β -actin.

Chapter 4.

Conclusions and future directions

Progression to an invasive growth state is multifactorial

The progression of a tumor to an invasive growth state is governed by a complex and dynamic interaction of factors at multiple levels, as revealed in an extensive body of prior research (Christofori 2006) that is now extended with the new knowledge resulting from my thesis research, as described in the preceding chapters (Figure 2.18). Using the RIP1-Tag2 (RT2) mouse model of pancreatic neuroendocrine tumorigenesis (PNET), I demonstrated that alterations at the molecular and genetic levels can influence the development of an invasive phenotype. While I present compelling data describing how desmosomal adhesion can act as a barrier to the development of an invasive phenotype and how signaling from the Alk molecule can promote tumor invasiveness, several questions remain unresolved, and I discuss them here in further detail.

Desmosomes and invasion: conclusions, unresolved questions, and future directions

It is clear from the work presented in Chapter 2 of this dissertation as well as from other studies (Perl et al. 1998; Cavallaro and Christofori 2004) that cell-cell adhesion serves as one barrier to the development of an invasive growth phenotype. The importance of this cellular feature is exemplified by the number of distinct cellular structures, including desmosomes and adherens junctions (AJ), whose primary function is to maintain cell-cell adhesion (Garrod and Chidgey 2008; Hartsock and Nelson 2008). By genetically deleting one component of desmosomes, desmoplakin (Dsp), in the developing PNETs of RT2 mice, I observed that there was an increased incidence of invasive carcinomas, likely due to disrupted/ablated desmosomal adhesion. Interestingly, as previously noted, I only observed an increase in the incidence of focally invasive

carcinomas (IC1 lesions) while the incidence of widely invasive carcinomas (IC2 lesions) remained unchanged, and the reason for this result remains unknown. As has already been discussed, the persistence of cadherin 1 (Cdh1) expression and presumably of adherens junction adhesion following Dsp deletion may explain why only the IC1 but not IC2 fraction of invasive RT2 PNETs was impacted. Alternatively, as was also previously discussed in Chapter 2, it is possible that the genetic deletion of a different desmosomal component could lead to a more severe phenotype. For example, targeting a dominant-negative Cdh1 molecule, the transmembrane component of AJs, to the β cells of RT2 mice led to widespread tumor invasion as well as lymph node metastasis (Perl et al. 1998); thus, targeting one of the desmosomal cadherins, such as Dsc2 or Dsg2, might have a similar effect.

However, an alternative explanation for the differential impact of Dsp deletion on IC1 versus IC2 development has to do with the time at which the Dsp gene was deleted. In the experiments presented in Chapter 2, I genetically deleted Dsp in 10 week-old RT2 mice, the stage of RT2 tumorigenesis when angiogenic islet dysplasias are already present and when tumors are just forming. It is formally possible that I failed to see any impact on IC2 lesions because the four-week time period between genetic deletion of Dsp and time of sacrifice was insufficient to allow IC2 tumors to develop. Thus, it is possible that genetically deleting Dsp at an earlier time point in RT2 mice, either by inducing Pdx1-Cre^{ER} activity at an earlier time point or by using a different Cre line such as the RIP-Cre allele (Gannon et al. 2000), could lead to a more severe invasive phenotype. However, it should be noted that my attempts to delete Dsp at six weeks using the Pdx1-Cre^{ER} allele and during embryogenesis using the RIP-Cre allele were unsuccessful. In

the case of the Pdx1-Cre^{ER} allele, the tumors that developed underwent incomplete deletion of the Dsp gene while I failed to recover any Dsp knockouts, either in the presence or absence of the RIP-Tag transgene, when using the RIP-Cre allele (data not shown). The reasons for these experimental outcomes are unknown at this time.

An additional outstanding question is how Dsp deletion promotes tumor invasion. Clearly, loss of Dsp leads to disrupted/impaired desmosomal adhesion. However, it is also possible that Dsp actively signals to downstream targets that could impact invasion, and recent data have suggested that Dsp can indeed act as a signaling center (Wan et al. 2007). However, it is worth noting that I did not observe any impact on any parameter of tumor growth following deletion of the Dsp gene in the incipient tumors of RT2 mice, which is in accordance with a previous study examining the role of Dsp in the skin (Vasioukhin et al. 2001). Thus, if the deletion of Dsp does in fact alter downstream signals to promote invasion, it does not appear that these changes in signaling have any growth advantage, at least in the context of RIP-Tag tumorigenesis.

As my work demonstrates, the expression of multiple desmosomal genes was significantly decreased in the invasive IC2 class of RT2 PNETs as compared to the non-invasive IT class of RT2 PNETs at the RNA level, which was also reflected at the protein level. Additionally, genetically deleting Dsp in the incipient tumors of RT2 mice, which phenocopies the transcriptional downregulation of this particular desmosomal gene, resulted in an increased incidence of invasive tumors. Thus, it is clear that decreased expression of desmosomal genes promotes an invasive growth phenotype. However, the exact mechanism of how this downregulation occurs in the RT2 model remains unclear. Given that multiple desmosomal genes showed simultaneous downregulation, it is

tempting to speculate that these genes are coordinately regulated by a common factor such as one of the transcription factors involved in epithelial-to-mesenchymal transition (Peinado et al. 2007). Although overexpression of one such factor, *Zeb1*, in a cell line derived from a RT2 tumor failed to affect the expression of various desmosomal genes (data not shown), there are many other related transcription factors, like the Snail and Twist family of transcription factors, and some of these molecules have been shown to modulate the expression levels of desmosomal genes in other contexts (Aigner et al. 2007).

Given that the alterations in expression occurred at the RNA level, it is also possible that these genes undergo a euchromatin-to-heterochromatin shift in the invasive IC2 tumors such that these genes become inaccessible to the transcriptional machinery; it is also formally possible that the promoter regions of these genes are subject to hypermethylation, which would also inhibit transcription. It is worth noting that some of the desmosomal genes are found in clusters on the same chromosome, which may lend itself to coordinated regulation of at least some of these genes. In the case of the desmocollin and desmoglein genes (*Dsc1–3* and *Dsg1–4*), all of the genes are arrayed next to each other on mouse chromosome 18 (Garrod and Chidgey 2008). In contrast, the plakophilin genes (*Pkp1–4*) are located on independent chromosomes (mouse chromosomes 1, 16, 7, and 2 respectively), while the gene encoding desmoplakin is found on mouse chromosome 13.

It is interesting to speculate whether any of the desmosomal genes are mutated or deleted in human cancers. To date, much of the work on desmosomes has focused on their role in the skin and the heart, where mutations that lead to dysfunctional or non-

functional desmosomal components or to mislocalization of these molecules are known to contribute to skin blistering conditions and cardiomyopathies (Bazzi and Christiano 2007). However, such mutations have not been associated with human cancers, either in terms of susceptibility or progression, although it is certainly possible that such an association will be identified in the future. If so, it would be interesting to determine whether such mutations would have different outcomes on tumor phenotypes as compared to decreased or loss of expression. Indeed, it is important to ask whether the information obtained from this study can impact our understanding of human cancers. It seems clear from earlier pathology reports (Hiraki et al. 1996; Shinohara et al. 1998; Papagerakis et al. 2009) and the bioinformatic analysis presented in Chapter 2 that desmosomal components are altered in human cancers. It would be interesting to ask whether the status of these components can be used as prognostic markers, for example looking at the levels of expression of these genes to predict such things as the future degree of tumor malignancy or overall survival, which could in turn inform early decisions on patient treatment. Such information would have clear benefits in the clinic since the odds of survival from cancer are significantly increased when it is detected and diagnosed at an early stage.

Genetic modifiers of invasion: conclusions, unresolved questions, and future directions

As demonstrated by the data presented in Chapter 3 of this dissertation, genetic background can significantly impact tumor invasiveness in the RT2 model. I determined that the C3HeB/Fe (C3H) genetic background is largely resistant to the development of

invasive carcinomas while the C57Bl/6 (B6) genetic background is permissive to the development of invasive carcinomas in the RT2 mouse model. Using linkage analysis, I identified a region on mouse chromosome 17 that shows significant linkage to the development of the highly invasive IC2 class of RT2 PNETs. One gene residing in this locus, the anaplastic lymphoma kinase (Alk) was expressed at much lower levels at both the RNA and protein levels in tumors from RT2 C3H mice versus RT2 B6 mice. Additionally, pharmacological inhibition of Alk kinase activity significantly reduced tumor invasiveness in an experimental therapeutic trial in RT2 B6 mice, suggesting that Alk expression levels and presumably Alk signaling levels are one determinant of an invasive phenotype in RT2 mice.

There are several unresolved questions as to how the genetic modifier and Alk specifically impact tumor invasiveness. One outstanding question is centered on the mechanism behind the different levels of Alk expression observed in the B6 and C3H backgrounds. I did not identify any polymorphism between the two strains in any of the coding regions of the Alk gene (data not shown). Thus, it seems likely that polymorphisms in the non-coding regions of the Alk gene are responsible for the observed differences in expression, and several such polymorphisms exist between the B6 and C3H backgrounds. Polymorphisms located in the promoter region, which could impact initial transcription due to differential transcription factor binding, or polymorphisms found in the intronic regions that affected RNA splicing could both affect gene expression levels.

Furthermore, with regards to the Alk molecule, it remains to be determined how it ultimately promotes invasion. In my analysis using the Alk kinase inhibitor TAE684, I

observed that the levels of phosphorylated Akt, one downstream target of Alk, were decreased in the tumors of TAE684-treated RT2 mice. However, Akt is downstream of a number of signaling molecules that are activated in the RT2 model, including the epidermal growth factor receptor (Egfr), the type-1 insulin-like growth factor receptor (Igf1r) (Lopez and Hanahan 2002), and the insulin receptor (IR) (Ulanet et al. 2010), and it would seem likely that this common signaling node is not solely responsible for transmitting the pro-invasive signals. Interestingly, I did not observe any obvious differences in the levels of phosphorylated Erk 1/2 or phosphorylated Stat3, two additional downstream targets of the Alk molecule (data not shown). Thus, it seems likely that there are additional Alk targets yet to be identified that mediate Alk's pro-invasive signals, and identification of these molecules may offer additional therapeutic opportunities, if they are expressed and active in other cancers. Regardless, my data demonstrate that inhibiting Alk kinase activity is a viable method of inhibiting progression to an invasive growth state as well as some aspects of tumor growth, even when Alk acts as a progression factor and not as an initiating factor. These results support the notion of identifying additional cancers where Alk inhibition could provide some therapeutic benefit even when it is not the driving oncogenic factor.

While my research demonstrates that Alk contributes to the differences in the invasive phenotypes of RT2 B6 and RT2 C3H mice, it was not the only gene that showed significant differential expression between the two genetic backgrounds. Indeed, six other genes – *Dlgap1*, *Emilin2*, *Lbh*, *Ltbp1*, *Rab31*, and *Spdy* – all showed significant differential expression at the RNA level in tumors from RT2 B6 and RT2 C3H mice. Additionally, *Ltbp1* apparently contains a non-synonymous change in the coding region

of the gene (data not shown). Thus, it is possible that one or more of these genes, in addition to *Alk*, also contributes to the differences in invasive phenotypes, and it may be that the full invasive difference observed between the B6 and C3H genetic backgrounds is due to the interaction of multiple genes in this region. In this vein, it would be interesting to determine whether this region undergoes chromosomal loss in the IC2 tumors that develop in RT2 N2 and RT2 F1 mice, which are heterozygous for the B6 and C3H alleles at this locus, with loss of the C3H allele representing the predicted outcome. While the vast majority of RT2 N2 mice that developed an IC2 tumor were B6 homozygous at the linked chromosome 17 locus, a small fraction were B6/C3H heterozygous. My attempts to profile the IC2 tumors that developed in these particular RT2 N2 mice for genomic loss at the linked chromosome 17 locus were unsuccessful, and it remains undetermined at this time whether this region experiences genomic loss of this region, specifically of the invasion-suppressive C3H allele. However, it is worth noting that RT2 mice do not normally experience genomic gains or losses on chromosome 17 in the B6, C3H, or FVB/N genetic backgrounds when whole, ungraded PNETs are analyzed by comparative genomic hybridization (Hodgson et al. 2001; Hager et al. 2004).

As was previously discussed in Chapter 3, it does not appear that the genetic modifier identified in this particular study operates via cells originating from the bone marrow derived tissue compartment, members of which are known to affect tumor invasiveness in the RT2 model (Joyce et al. 2005; Gocheva et al. 2010). It seems most likely that this invasive modifier operates in the cancer cells themselves, although I cannot rule out the possibility that it mediates its effects through other cell types of the

stroma. However, with regards to Alk, it is tempting to speculate that Alk functions in the cancer cell itself given that previous studies have demonstrated that mutations or chromosomal translocations that result in aberrant Alk signaling and that serve as initiating oncogenic events (Morris et al. 1994; George et al. 2008; Mosse et al. 2008) occur in the cells that ultimately develop into the cancer.

Lastly, the idea that genetic polymorphisms can impact multiple aspects of tumorigenesis has been validated by a number of studies (Nagase et al. 1995; Lifsted et al. 1998; Park et al. 2005). Most notable are those studies that demonstrated how polymorphisms in the Egfr gene can influence a person's response to small molecule based therapies used to treat lung cancers (Sequist et al. 2007). That progression to an invasive growth state might similarly be subject to genetic modification, as I suggest in Chapter 3 of this dissertation, is clearly provocative. It seems likely, given that large-scale sequencing is rapidly becoming more efficient and affordable, that characterizing a person's constitutional DNA to identify genetic features in their pre-existing genetic makeup will become a standard requirement during cancer treatment, in addition to characterizing the molecular and genetic signature of the tumor itself, in order to predict tumor progression and to better tailor therapies for individual patients.

Concluding perspectives

Tumorigenesis is governed by an intricate and complex interaction of factors at the genetic, molecular, and cellular levels, and my thesis research provides new insights into the mechanisms by which a tumor can acquire or develop an invasive phenotype. The work presented in this dissertation is likely to have significant impact on future

investigations into this important area of cancer research and may lay the groundwork for the development of new diagnostics and therapeutics aimed at treating malignant and invasive cancers.

References.

Adams, T.E., Alpert, S., and Hanahan, D. 1987. Non-tolerance and autoantibodies to a transgenic self antigen expressed in pancreatic beta cells. *Nature* **325**(6101): 223-228.

Aigner, K., Dampier, B., Descovich, L., Mikula, M., Sultan, A., Schreiber, M., Mikulits, W., Brabletz, T., Strand, D., Obrist, P., Sommergruber, W., Schweifer, N., Wernitznig, A., Beug, H., Foisner, R., and Eger, A. 2007. The transcription factor ZEB1 (deltaEF1) promotes tumour cell dedifferentiation by repressing master regulators of epithelial polarity. *Oncogene* **26**(49): 6979-6988.

Ali, S.H. and DeCaprio, J.A. 2001. Cellular transformation by SV40 large T antigen: interaction with host proteins. *Semin Cancer Biol* **11**(1): 15-23.

Alpert, S., Hanahan, D., and Teitelman, G. 1988. Hybrid insulin genes reveal a developmental lineage for pancreatic endocrine cells and imply a relationship with neurons. *Cell* **53**(2): 295-308.

Arroyo, J.D. and Hahn, W.C. 2005. Involvement of PP2A in viral and cellular transformation. *Oncogene* **24**(52): 7746-7755.

Balmain, A., Gray, J., and Ponder, B. 2003. The genetics and genomics of cancer. *Nat Genet* **33 Suppl**: 238-244.

Bazzi, H. and Christiano, A.M. 2007. Broken hearts, woolly hair, and tattered skin: when desmosomal adhesion goes awry. *Curr Opin Cell Biol* **19**(5): 515-520.

Bergers, G., Javaherian, K., Lo, K.M., Folkman, J., and Hanahan, D. 1999. Effects of angiogenesis inhibitors on multistage carcinogenesis in mice. *Science* **284**(5415): 808-812.

Bergers, G., Brekken, R., McMahon, G., Vu, T.H., Itoh, T., Tamaki, K., Tanzawa, K., Thorpe, P., Itohara, S., Werb, Z., and Hanahan, D. 2000. Matrix metalloproteinase-9 triggers the angiogenic switch during carcinogenesis. *Nat Cell Biol* **2**(10): 737-744.

Brindle, K. 2008. New approaches for imaging tumour responses to treatment. *Nat Rev Cancer* **8**(2): 94-107.

Casanovas, O., Hager, J.H., Chun, M.G., and Hanahan, D. 2005a. Incomplete inhibition of the Rb tumor suppressor pathway in the context of inactivated p53 is sufficient for pancreatic islet tumorigenesis. *Oncogene* **24**(44): 6597-6604.

Casanovas, O., Hicklin, D.J., Bergers, G., and Hanahan, D. 2005b. Drug resistance by evasion of antiangiogenic targeting of VEGF signaling in late-stage pancreatic islet tumors. *Cancer Cell* **8**(4): 299-309.

Cavallaro, U. and Christofori, G. 2004. Cell adhesion and signalling by cadherins and Ig-CAMs in cancer. *Nat Rev Cancer* **4**(2): 118-132.

Chiarle, R., Voena, C., Ambrogio, C., Piva, R., and Inghirami, G. 2008. The anaplastic lymphoma kinase in the pathogenesis of cancer. *Nat Rev Cancer* **8**(1): 11-23.

Chidgey, M. and Dawson, C. 2007. Desmosomes: a role in cancer? *Br J Cancer* **96**(12): 1783-1787.

Christofori, G., Naik, P., and Hanahan, D. 1994. A second signal supplied by insulin-like growth factor II in oncogene-induced tumorigenesis. *Nature* **369**(6479): 414-418.

Christofori, G. 2006. New signals from the invasive front. *Nature* **441**(7092): 444-450.

Coussens, L.M., Hanahan, D., and Arbeit, J.M. 1996. Genetic predisposition and parameters of malignant progression in K14-HPV16 transgenic mice. *Am J Pathol* **149**(6): 1899-1917.

Demant, P. 2003. Cancer susceptibility in the mouse: genetics, biology and implications for human cancer. *Nat Rev Genet* **4**(9): 721-734.

Easton, D.F. Pooley, K.A. Dunning, A.M. Pharoah, P.D. Thompson, D. Ballinger, D.G. Struwing, J.P. Morrison, J. Field, H. Luben, R. Wareham, N. Ahmed, S. Healey, C.S.

Bowman, R. Meyer, K.B. Haiman, C.A. Kolonel, L.K. Henderson, B.E. Le Marchand, L. Brennan, P. Sangrajrang, S. Gaborieau, V. Odefrey, F. Shen, C.Y. Wu, P.E. Wang, H.C. Eccles, D. Evans, D.G. Peto, J. Fletcher, O. Johnson, N. Seal, S. Stratton, M.R. Rahman, N. Chenevix-Trench, G. Bojesen, S.E. Nordestgaard, B.G. Axelsson, C.K. Garcia-Closas, M. Brinton, L. Chanock, S. Lissowska, J. Peplonska, B. Nevanlinna, H. Fagerholm, R. Eerola, H. Kang, D. Yoo, K.Y. Noh, D.Y. Ahn, S.H. Hunter, D.J. Hankinson, S.E. Cox, D.G. Hall, P. Wedren, S. Liu, J. Low, Y.L. Bogdanova, N. Schurmann, P. Dork, T. Tollenaar, R.A. Jacobi, C.E. Devilee, P. Klijn, J.G. Sigurdson, A.J. Doody, M.M. Alexander, B.H. Zhang, J. Cox, A. Brock, I.W. MacPherson, G. Reed, M.W. Couch, F.J. Goode, E.L. Olson, J.E. Meijers-Heijboer, H. van den Ouweland, A. Uitterlinden, A. Rivadeneira, F. Milne, R.L. Ribas, G. Gonzalez-Neira, A. Benitez, J. Hopper, J.L. McCredie, M. Southey, M. Giles, G.G. Schroen, C. Justenhoven, C. Brauch, H. Hamann, U. Ko, Y.D. Spurdle, A.B. Beesley, J. Chen, X. Mannermaa, A. Kosma, V.M. Kataja, V. Hartikainen, J. Day, N.E. Cox, D.R. and Ponder, B.A. 2007. Genome-wide association study identifies novel breast cancer susceptibility loci. *Nature* **447**(7148): 1087-1093.

Edlund, H. 2002. Pancreatic organogenesis--developmental mechanisms and implications for therapy. *Nat Rev Genet* **3**(7): 524-532.

Forster, I., Hirose, R., Arbeit, J.M., Clausen, B.E., and Hanahan, D. 1995. Limited capacity for tolerization of CD4+ T cells specific for a pancreatic beta cell neo-antigen. *Immunity* **2**(6): 573-585.

Frese, K.K. and Tuveson, D.A. 2007. Maximizing mouse cancer models. *Nat Rev Cancer* **7**(9): 645-658.

Galkin, A.V., Melnick, J.S., Kim, S., Hood, T.L., Li, N., Li, L., Xia, G., Steensma, R., Chopiuk, G., Jiang, J., Wan, Y., Ding, P., Liu, Y., Sun, F., Schultz, P.G., Gray, N.S., and Warmuth, M. 2007. Identification of NVP-TAE684, a potent, selective, and efficacious inhibitor of NPM-ALK. *Proc Natl Acad Sci U S A* **104**(1): 270-275.

Gallicano, G.I., Kouklis, P., Bauer, C., Yin, M., Vasioukhin, V., Degenstein, L., and Fuchs, E. 1998. Desmoplakin is required early in development for assembly of desmosomes and cytoskeletal linkage. *J Cell Biol* **143**(7): 2009-2022.

Gannon, M., Shiota, C., Postic, C., Wright, C.V., and Magnuson, M. 2000. Analysis of the Cre-mediated recombination driven by rat insulin promoter in embryonic and adult mouse pancreas. *Genesis* **26**(2): 139-142.

Garrod, D. and Chidgey, M. 2008. Desmosome structure, composition and function. *Biochim Biophys Acta* **1778**(3): 572-587.

Geiger, T., Gooding, L.R., and Flavell, R.A. 1992. T-cell responsiveness to an oncogenic peripheral protein and spontaneous autoimmunity in transgenic mice. *Proc Natl Acad Sci U S A* **89**(7): 2985-2989.

Geiger, T., Soldevila, G., and Flavell, R.A. 1993. T cells are responsive to the simian virus 40 large tumor antigen transgenically expressed in pancreatic islets. *J Immunol* **151**(12): 7030-7037.

George, R.E., Sanda, T., Hanna, M., Frohling, S., Luther, W., 2nd, Zhang, J., Ahn, Y., Zhou, W., London, W.B., McGrady, P., Xue, L., Zozulya, S., Gregor, V.E., Webb, T.R., Gray, N.S., Gilliland, D.G., Diller, L., Greulich, H., Morris, S.W., Meyerson, M., and Look, A.T. 2008. Activating mutations in ALK provide a therapeutic target in neuroblastoma. *Nature* **455**(7215): 975-978.

Gidekel Friedlander, S.Y., Chu, G.C., Snyder, E.L., Girnius, N., Dibelius, G., Crowley, D., Vasile, E., DePinho, R.A., and Jacks, T. 2009. Context-dependent transformation of adult pancreatic cells by oncogenic K-Ras. *Cancer Cell* **16**(5): 379-389.

Gocheva, V., Zeng, W., Ke, D., Klimstra, D., Reinheckel, T., Peters, C., Hanahan, D., and Joyce, J.A. 2006. Distinct roles for cysteine cathepsin genes in multistage tumorigenesis. *Genes Dev* **20**(5): 543-556.

Gocheva, V., Wang, H.W., Gadea, B.B., Shree, T., Hunter, K.E., Garfall, A.L., Berman, T., and Joyce, J.A. 2010. IL-4 induces cathepsin protease activity in tumor-associated macrophages to promote cancer growth and invasion. *Genes Dev* **24**(3): 241-255.

Gu, G., Dubauskaite, J., and Melton, D.A. 2002. Direct evidence for the pancreatic lineage: NGN3+ cells are islet progenitors and are distinct from duct progenitors. *Development* **129**(10): 2447-2457.

Hager, J.H., Hodgson, J.G., Fridlyand, J., Hariono, S., Gray, J.W., and Hanahan, D. 2004. Oncogene expression and genetic background influence the frequency of DNA copy number abnormalities in mouse pancreatic islet cell carcinomas. *Cancer Res* **64**(7): 2406-2410.

Halbleib, J.M. and Nelson, W.J. 2006. Cadherins in development: cell adhesion, sorting, and tissue morphogenesis. *Genes Dev* **20**(23): 3199-3214.

Hanahan, D. 1985. Heritable formation of pancreatic beta-cell tumours in transgenic mice expressing recombinant insulin/simian virus 40 oncogenes. *Nature* **315**(6015): 115-122.

Hanahan, D. and Weinberg, R.A. 2000. The hallmarks of cancer. *Cell* **100**(1): 57-70.

Hartsock, A. and Nelson, W.J. 2008. Adherens and tight junctions: structure, function and connections to the actin cytoskeleton. *Biochim Biophys Acta* **1778**(3): 660-669.

Hennings, H., Glick, A.B., Lowry, D.T., Krsmanovic, L.S., Sly, L.M., and Yuspa, S.H. 1993. FVB/N mice: an inbred strain sensitive to the chemical induction of squamous cell carcinomas in the skin. *Carcinogenesis* **14**(11): 2353-2358.

Herzig, M., Savarese, F., Novatchkova, M., Semb, H., and Christofori, G. 2007. Tumor progression induced by the loss of E-cadherin independent of beta-catenin/Tcf-mediated Wnt signaling. *Oncogene* **26**(16): 2290-2298.

Hiraki, A., Shinohara, M., Ikebe, T., Nakamura, S., Kurahara, S., and Garrod, D.R. 1996. Immunohistochemical staining of desmosomal components in oral squamous cell carcinomas and its association with tumour behaviour. *Br J Cancer* **73**(12): 1491-1497.

Hirohashi, S. 1998. Inactivation of the E-cadherin-mediated cell adhesion system in human cancers. *Am J Pathol* **153**(2): 333-339.

Hodgson, G., Hager, J.H., Volik, S., Hariono, S., Wernick, M., Moore, D., Nowak, N., Albertson, D.G., Pinkel, D., Collins, C., Hanahan, D., and Gray, J.W. 2001. Genome scanning with array CGH delineates regional alterations in mouse islet carcinomas. *Nat Genet* **29**(4): 459-464.

Hsieh, S.M., Look, M.P., Sieuwerts, A.M., Foekens, J.A., and Hunter, K.W. 2009. Distinct inherited metastasis susceptibility exists for different breast cancer subtypes: a prognosis study. *Breast Cancer Res* **11**(5): R75.

Hubner, N., Wallace, C.A., Zimdahl, H., Petretto, E., Schulz, H., Maciver, F., Mueller, M., Hummel, O., Monti, J., Zidek, V., Musilova, A., Kren, V., Causton, H., Game, L.,

Born, G., Schmidt, S., Muller, A., Cook, S.A., Kurtz, T.W., Whittaker, J., Pravenec, M., and Aitman, T.J. 2005. Integrated transcriptional profiling and linkage analysis for identification of genes underlying disease. *Nat Genet* **37**(3): 243-253.

Inoue, M., Hager, J.H., Ferrara, N., Gerber, H.P., and Hanahan, D. 2002. VEGF-A has a critical, nonredundant role in angiogenic switching and pancreatic beta cell carcinogenesis. *Cancer Cell* **1**(2): 193-202.

Jeanes, A., Gottardi, C.J., and Yap, A.S. 2008. Cadherins and cancer: how does cadherin dysfunction promote tumor progression? *Oncogene* **27**(55): 6920-6929.

Jolicoeur, C., Hanahan, D., and Smith, K.M. 1994. T-cell tolerance toward a transgenic beta-cell antigen and transcription of endogenous pancreatic genes in thymus. *Proc Natl Acad Sci U S A* **91**(14): 6707-6711.

Joyce, J.A., Freeman, C., Meyer-Morse, N., Parish, C.R., and Hanahan, D. 2005. A functional heparan sulfate mimetic implicates both heparanase and heparan sulfate in tumor angiogenesis and invasion in a mouse model of multistage cancer. *Oncogene* **24**(25): 4037-4051.

Lander, E. and Kruglyak, L. 1995. Genetic dissection of complex traits: guidelines for interpreting and reporting linkage results. *Nat Genet* **11**(3): 241-247.

Lawlor, E.R., Soucek, L., Brown-Swigart, L., Shchors, K., Bialucha, C.U., and Evan, G.I. 2006. Reversible kinetic analysis of Myc targets in vivo provides novel insights into Myc-mediated tumorigenesis. *Cancer Res* **66**(9): 4591-4601.

Levine, A.J. 1997. p53, the cellular gatekeeper for growth and division. *Cell* **88**(3): 323-331.

Lewis, J.E., Jensen, P.J., and Wheelock, M.J. 1994. Cadherin function is required for human keratinocytes to assemble desmosomes and stratify in response to calcium. *J Invest Dermatol* **102**(6): 870-877.

Lewis, J.E., Wahl, J.K., 3rd, Sass, K.M., Jensen, P.J., Johnson, K.R., and Wheelock, M.J. 1997. Cross-talk between adherens junctions and desmosomes depends on plakoglobin. *J Cell Biol* **136**(4): 919-934.

Li, R. and Morris, S.W. 2008. Development of anaplastic lymphoma kinase (ALK) small-molecule inhibitors for cancer therapy. *Med Res Rev* **28**(3): 372-412.

Lifsted, T., Le Voyer, T., Williams, M., Muller, W., Klein-Szanto, A., Buetow, K.H., and Hunter, K.W. 1998. Identification of inbred mouse strains harboring genetic modifiers of mammary tumor age of onset and metastatic progression. *Int J Cancer* **77**(4): 640-644.

Lopez, T. and Hanahan, D. 2002. Elevated levels of IGF-1 receptor convey invasive and metastatic capability in a mouse model of pancreatic islet tumorigenesis. *Cancer Cell* **1**(4): 339-353.

Morris, S.W., Kirstein, M.N., Valentine, M.B., Dittmer, K.G., Shapiro, D.N., Saltman, D.L., and Look, A.T. 1994. Fusion of a kinase gene, ALK, to a nucleolar protein gene, NPM, in non-Hodgkin's lymphoma. *Science* **263**(5151): 1281-1284.

Mosse, Y.P., Laudenslager, M., Longo, L., Cole, K.A., Wood, A., Attiyeh, E.F., Laquaglia, M.J., Sennett, R., Lynch, J.E., Perri, P., Laureys, G., Speleman, F., Kim, C., Hou, C., Hakonarson, H., Torkamani, A., Schork, N.J., Brodeur, G.M., Tonini, G.P., Rappaport, E., Devoto, M., and Maris, J.M. 2008. Identification of ALK as a major familial neuroblastoma predisposition gene. *Nature* **455**(7215): 930-935.

Nagase, H., Bryson, S., Cordell, H., Kemp, C.J., Fee, F., and Balmain, A. 1995. Distinct genetic loci control development of benign and malignant skin tumours in mice. *Nat Genet* **10**(4): 424-429.

Nava, P., Laukoetter, M.G., Hopkins, A.M., Laur, O., Gerner-Smidt, K., Green, K.J., Parkos, C.A., and Nusrat, A. 2007. Desmoglein-2: a novel regulator of apoptosis in the intestinal epithelium. *Mol Biol Cell* **18**(11): 4565-4578.

Offield, M.F., Jetton, T.L., Labosky, P.A., Ray, M., Stein, R.W., Magnuson, M.A., Hogan, B.L., and Wright, C.V. 1996. PDX-1 is required for pancreatic outgrowth and differentiation of the rostral duodenum. *Development* **122**(3): 983-995.

Olson, P., Lu, J., Zhang, H., Shai, A., Chun, M.G., Wang, Y., Libutti, S.K., Nakakura, E.K., Golub, T.R., and Hanahan, D. 2009. MicroRNA dynamics in the stages of tumorigenesis correlate with hallmark capabilities of cancer. *Genes Dev* **23**(18): 2152-2165.

Paez-Ribes, M., Allen, E., Hudock, J., Takeda, T., Okuyama, H., Vinals, F., Inoue, M., Bergers, G., Hanahan, D., and Casanovas, O. 2009. Antiangiogenic therapy elicits malignant progression of tumors to increased local invasion and distant metastasis. *Cancer Cell* **15**(3): 220-231.

Papagerakis, S., Shabana, A.H., Pollock, B.H., Papagerakis, P., Depondt, J., and Berdal, A. 2009. Altered desmoplakin expression at transcriptional and protein levels provides prognostic information in human oropharyngeal cancer. *Hum Pathol* **40**(9): 1320-1329.

Parangi, S., Dietrich, W., Christofori, G., Lander, E.S., and Hanahan, D. 1995. Tumor suppressor loci on mouse chromosomes 9 and 16 are lost at distinct stages of tumorigenesis in a transgenic model of islet cell carcinoma. *Cancer Res* **55**(24): 6071-6076.

Park, Y.G., Zhao, X., Lesueur, F., Lowy, D.R., Lancaster, M., Pharoah, P., Qian, X., and Hunter, K.W. 2005. Sipal is a candidate for underlying the metastasis efficiency modifier locus Mtes1. *Nat Genet* **37**(10): 1055-1062.

Peinado, H., Olmeda, D., and Cano, A. 2007. Snail, Zeb and bHLH factors in tumour progression: an alliance against the epithelial phenotype? *Nat Rev Cancer* **7**(6): 415-428.

Perl, A.K., Wilgenbus, P., Dahl, U., Semb, H., and Christofori, G. 1998. A causal role for E-cadherin in the transition from adenoma to carcinoma. *Nature* **392**(6672): 190-193.

Piva, R., Chiarle, R., Manazza, A.D., Taulli, R., Simmons, W., Ambrogio, C., D'Escamard, V., Pellegrino, E., Ponzetto, C., Palestro, G., and Inghirami, G. 2006. Ablation of oncogenic ALK is a viable therapeutic approach for anaplastic large-cell lymphomas. *Blood* **107**(2): 689-697.

Quan, L., Hutson, A., and Demant, P. 2010. A locus on chromosome 8 controlling tumor regional diversity—a new type of tumor diversity in the mouse lung. *Int J Cancer* **126**(11): 2603-2613.

Quigley, D.A., To, M.D., Perez-Losada, J., Pelorosso, F.G., Mao, J.H., Nagase, H., Ginzinger, D.G., and Balmain, A. 2009. Genetic architecture of mouse skin inflammation and tumour susceptibility. *Nature* **458**(7237): 505-508.

Runswick, S.K., O'Hare, M.J., Jones, L., Streuli, C.H., and Garrod, D.R. 2001. Desmosomal adhesion regulates epithelial morphogenesis and cell positioning. *Nat Cell Biol* **3**(9): 823-830.

Sambrook, J. and Russell, D.W. 2001. *Molecular cloning : a laboratory manual*. Cold Spring Harbor Laboratory Press, Cold Spring Harbor, N.Y.

Sequist, L.V., Bell, D.W., Lynch, T.J., and Haber, D.A. 2007. Molecular predictors of response to epidermal growth factor receptor antagonists in non-small-cell lung cancer. *J Clin Oncol* **25**(5): 587-595.

Shinohara, M., Hiraki, A., Ikebe, T., Nakamura, S., Kurahara, S., Shirasuna, K., and Garrod, D.R. 1998. Immunohistochemical study of desmosomes in oral squamous cell carcinoma: correlation with cytokeratin and E-cadherin staining, and with tumour behaviour. *J Pathol* **184**(4): 369-381.

Skowronski, J., Jolicoeur, C., Alpert, S., and Hanahan, D. 1990. Determinants of the B-cell response against a transgenic autoantigen. *Proc Natl Acad Sci U S A* **87**(19): 7487-7491.

Smith, K.M., Olson, D.C., Hirose, R., and Hanahan, D. 1997. Pancreatic gene expression in rare cells of thymic medulla: evidence for functional contribution to T cell tolerance. *Int Immunol* **9**(9): 1355-1365.

Stylianou, D.C., Auf der Maur, A., Kodack, D.P., Henke, R.T., Hohn, S., Toretsky, J.A., Riegel, A.T., and Wellstein, A. 2009. Effect of single-chain antibody targeting of the ligand-binding domain in the anaplastic lymphoma kinase receptor. *Oncogene* **28**(37): 3296-3306.

Tomlinson, I.P., Webb, E., Carvajal-Carmona, L., Broderick, P., Howarth, K., Pittman, A.M., Spain, S., Lubbe, S., Walther, A., Sullivan, K., Jaeger, E., Fielding, S., Rowan, A., Vijayakrishnan, J., Domingo, E., Chandler, I., Kemp, Z., Qureshi, M., Farrington, S.M., Tenesa, A., Prendergast, J.G., Barnetson, R.A., Penegar, S., Barclay, E., Wood, W., Martin, L., Gorman, M., Thomas, H., Peto, J., Bishop, D.T., Gray, R., Maher, E.R., Lucassen, A., Kerr, D., Evans, D.G., Schafmayer, C., Buch, S., Volzke, H., Hampe, J., Schreiber, S., John, U., Koessler, T., Pharoah, P., van Wezel, T., Morreau, H., Wijnen, J.T., Hopper, J.L., Southey, M.C., Giles, G.G., Severi, G., Castellvi-Bel, S., Ruiz-Ponte, C., Carracedo, A., Castells, A., Forsti, A., Hemminki, K., Vodicka, P., Naccarati, A., Lipton, L., Ho, J.W., Cheng, K.K., Sham, P.C., Luk, J., Agundez, J.A., Ladero, J.M., de la Hoya, M., Caldes, T., Niittymaki, I., Tuupanen, S., Karhu, A., Aaltonen, L., Cazier, J.B., Campbell, H., Dunlop, M.G., and Houlston, R.S. 2008. A genome-wide association study identifies colorectal cancer susceptibility loci on chromosomes 10p14 and 8q23.3. *Nat Genet* **40**(5): 623-630.

Tselepis, C., Chidgey, M., North, A., and Garrod, D. 1998. Desmosomal adhesion inhibits invasive behavior. *Proc Natl Acad Sci U S A* **95**(14): 8064-8069.

Tuveson, D.A. and Jacks, T. 2002. Technologically advanced cancer modeling in mice. *Curr Opin Genet Dev* **12**(1): 105-110.

Ulanet, D.B., Ludwig, D.L., Kahn, C.R., and Hanahan, D. 2010. Insulin receptor functionally enhances multistage tumor progression and conveys intrinsic resistance to IGF-1R targeted therapy. *Proc Natl Acad Sci U S A* **107**(24): 10791-10798.

Vasioukhin, V., Bauer, C., Degenstein, L., Wise, B., and Fuchs, E. 2001a. Hyperproliferation and defects in epithelial polarity upon conditional ablation of alpha-catenin in skin. *Cell* **104**(4): 605-617.

Vasioukhin, V., Bowers, E., Bauer, C., Degenstein, L., and Fuchs, E. 2001b. Desmoplakin is essential in epidermal sheet formation. *Nat Cell Biol* **3**(12): 1076-1085.

Vleminckx, K., Vakaet, L., Jr., Mareel, M., Fiers, W., and van Roy, F. 1991. Genetic manipulation of E-cadherin expression by epithelial tumor cells reveals an invasion suppressor role. *Cell* **66**(1): 107-119.

Wakabayashi, Y., Mao, J.H., Brown, K., Girardi, M., and Balmain, A. 2007. Promotion of Hras-induced squamous carcinomas by a polymorphic variant of the Patched gene in FVB mice. *Nature* **445**(7129): 761-765.

Wan, H., South, A.P., and Hart, I.R. 2007. Increased keratinocyte proliferation initiated through downregulation of desmoplakin by RNA interference. *Exp Cell Res* **313**(11): 2336-2344.

Weinberg, R.A. 1995. The retinoblastoma protein and cell cycle control. *Cell* **81**(3): 323-330.

Winter, S.F. and Hunter, K.W. 2008. Mouse modifier genes in mammary tumorigenesis and metastasis. *J Mammary Gland Biol Neoplasia* **13**(3): 337-342.

Appendix.

Legends for datasets

Dataset 2.1. Microarray analysis of non-invasive IT tumors and highly invasive IC2 tumors from RT2 mice.

Dataset contains the complete microarray analysis profiling the non-invasive islet tumor (IT) class and highly invasive type-2 carcinoma (IC2) class of RIP-Tag pancreatic neuroendocrine tumors (PNET), which were isolated from end-stage RIP1-Tag2 (RT2) mice. Three arrays per tumor class were run using Affymetrix 430 2.0 Mouse Genome microarrays.

Dataset 3.1. Phenotype and SNP genotyping results for RT2 N2 mice.

Dataset contains the complete phenotype and genotype data for 143 RT2 N2 mice. Phenotype data include the number of IT lesions per animal, the number of IC1 lesions per animal, the number of IC2 lesions per animal, the tumor burden per animal, and the tumor number per animal. Genotype data include genotyping results examining 561 single nucleotide polymorphisms (SNP) that distinguish between the C57Bl/6 (B6) and the C3HeB/Fe (C3H) genetic backgrounds across the mouse genome.

Dataset 3.2. Linkage analysis for the IT, IC1, IC2, tumor number, and tumor burden metrics.

Dataset contains the complete LOD scores for the entire mouse genome for the IT, IC1, IC2, tumor number, and tumor burden metrics. A LOD score is given for each position in the mouse genome corresponding to one of the 561 single nucleotide polymorphisms (SNP) that were genotyped and that distinguish between the C57Bl/6 (B6) and C3HeB/Fe (C3H) genetic backgrounds.

Dataset 3.3. Quantitative PCR results for the genes residing in the linked chromosome 17 locus.

Dataset contains the complete quantitative PCR analysis profiling pancreatic neuroendocrine tumors (PNET) isolated from end-stage RIP1-Tag2 (RT2) mice and normal islets isolated from wild-type mice on the C57Bl/6 (B6) and C3HeB/Fe (C3H) genetic backgrounds. Seven independent PNETs and one pool of wild-type islets per genetic background were profiled. All 50 genes located within the chromosome 17 locus that showed significant linkage to the development of IC2 tumors were profiled. The genes *Nudt12*, *Efna5*, *Crim1*, *Fez2*, *Vit*, and *Strn*, which flank the linked chromosome 17 locus, as well as *Cdh1*, *Dsp*, *Igf2*, and *Zeb1* were also profiled. Additionally, the housekeeping genes *Rpl19*, *Ppia*, and *Gusb* as well as the ribosomal RNA 18S were analyzed, and all values are shown as the percent expression of *Rpl19*. Data were generated using a low-density TaqMan array.

Publishing Agreement

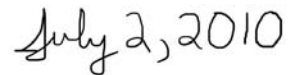
It is the policy of the University to encourage the distribution of all theses, dissertations, and manuscripts. Copies of all UCSF theses, dissertations, and manuscripts will be routed to the library via the Graduate Division. The library will make all theses, dissertations, and manuscripts accessible to the public and will preserve these to the best of their abilities, in perpetuity.

Please sign the following statement:

I hereby grant permission to the Graduate Division of the University of California, San Francisco to release copies of my thesis, dissertation, or manuscript to the Campus Library to provide access and preservation, in whole or in part, in perpetuity.



Author Signature



Date